BERGISCHE
UNIVERSITÄT
WUPPERTAL

Dissertation

Aspects of quark mass dependence in lattice QCD

Lukas Varnhorst

Major: Physics
Supervisor: Prof. Dr. Z. Fodor

The PhD thesis can be quoted as follows:

urn:nbn:de:hbz:468-20200903-103412-9
[http://nbn-resolving.de/urn/resolver.pl?urn=urn%3Anbn%3Ade%3Ahbz%3A468-20200903-103412-9]

DOI: 10.25926/vrwh-6t66
[https://doi.org/10.25926/vrwh-6t66]

Acknowledgement

First of all, I want to thank my adviser, Prof. Dr. Zoltán Fodor, for the opportunity to work on such interesting projects, for his continuing support during my work on this thesis and for the comments on the manuscript.

I also would like to thank Dr. Christian Hölbling for his helpful input, and for reading the manuscript of this thesis.

I am especially grateful to all my coauthors of the papers this thesis is based on.

I very grateful to the entire lattice group at the University of Wuppertal for providing the nice working atmosphere.

I am deeply grateful to my girlfriend Jana Günther for all her support while this thesis has been created. I also would like to thank her for her comments on the unfinished manuscript of this text.

Furthermore, I want to thank my entire family for all the support during my work on this thesis.

*Computations were performed using the JUGENE and JURECA installations of Forschungszentrum (FZ) Jülich and HPC resources provided by the "Grand équipement national de calcul intensif" (GENCI) at the "Institut du développement et des ressources en informatique scientifique" (IDRIS) (GENCI-IDRIS Grant No.52275), on further resources at FZ Jülich, on clusters at Wuppertal and CPT, on SuperMUC at Leibniz Supercomputing Centre in München and on HazelHen at the High Performance Computing Center in Stuttgart. This work was supported in part by the OCEVU Labex (ANR-11-LABX-0060) and the A*MIDEX project (ANR-11-IDEX-0001-02) which are funded by the "Investissements d'Avenir" French government program and managed by the "Agence nationale de la recherche" (ANR), by CNRS Grants No. GDR No. 2921 and PICS No. 4707, by EU Grants FP7/2007-2013/ERC No. 208740, MRTN-CT-2006-035482 (FLAVIAnet), by DFG Grants No. FO 502/2, SFB TRR-55, by UK STFC Grants No.ST/L000296/1 and ST/L000458/1m, by the Gauss Centre for Supercomputing e.V, by the GENCI-IDRIS supercomputing Grant No. 52275, and by a GSI grant.*

Contents

List of Figures

List of Tables

Chapter 1

Introduction

The strong interaction — one of the four fundamental forces of nature — is described by a quantum field theory of non abelian [4] $SU(3)$ gauge fields. It is mediated by gluons, excitations of these gauge fields. The strong interaction differs from all other fundamental interactions within the standard model of particle physics, the theory that describes the strong, weak and electromagnetic interactions of particles, in the its low and high energy behavior; a very prominent feature of the strong interaction is asymptotic freedom [5–8]. Couplings in quantum field theories often depend on the energy scales of the processes considered. The term asymptotic freedom describes the fact the strong coupling becomes arbitrarily small if processes with very high energy scales are considered. Consequently, in processes with very low energy scales the coupling becomes large and perturbative methods are inapplicable [9]. Even the asymptotic degrees of freedom are different from the degrees of freedom in the Lagrangian. [9]

In the standard model the only fundamental matter degrees of freedoms which interact with the gluons are fermions referred to as quarks. Considering only the gluons and quarks alone, and thereby ignoring all other interactions, would lead to a Yang-Mills theory [4] coupled to six massless fermions. Such a theory has no free continuous parameter and exhibits an additional chiral symmetry which is not observed in nature. [9] Therefore, such a theory is not a good description of nature. At energy scales well above the QCD scale, where the theory of quarks and gluons becomes non-perturbative, the electroweak symmetry breaking via the Higgs mechanism [10] takes place. [9] As a consequence, a massive scalar degree of freedom — the Higgs boson [10] — appears. At the same time, some of the gauge bosons carrying the electroweak force and the fundamental fermions of the standard model acquire masses [10]. More precisely phrased, well below the electroweak transition scale the fundamental fermion and gauge degrees of freedoms are replaced by compound states containing also the Higgs field. These states behave like fundamental particles with a mass. The strongly interacting sector of the standard model is therefore well approximated by a $SU(3)$-Yang-Mills theory with six massive quarks. [9]

The masses of quarks appearing in this theory span, one may say somewhat surprisingly, many orders of magnitude. They range from a few MeV in the cases of the up and the down quark to hundreds of GeV in the case of the top quark. The masses of the quarks are illustrated in figure 1.1. [9] Accepting the differences in magnitudes as they are, an immediate question is: Would changes in the quark masses by small amounts change physics in any notable way? Would physics be almost the same, qualitatively similar or even qualitatively different? To answer these questions the framework of lattice QCD [11] is almost ideally suited. Because the quark masses can not be varied in nature, it is hard do answer these questions purely phenomenological.

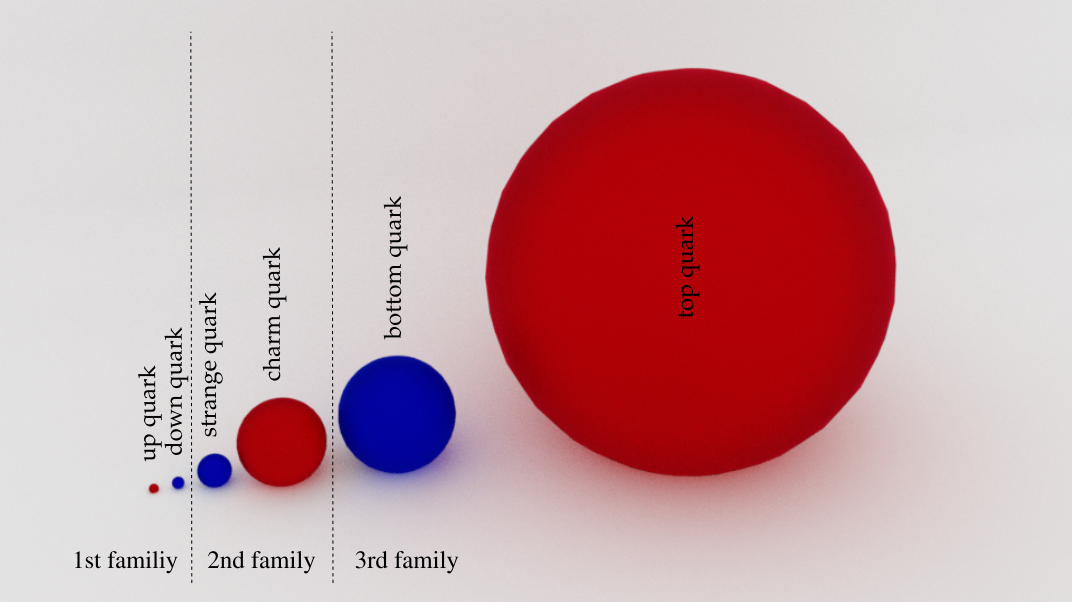

Figure 1.1 – *Spheres with constant density and sizes that approximately reproduce the ratio between quark masses. The spheres are ordered in ascending order with respect to their masses. Up type quarks are colored in red and down type quarks are colored in blue. The three families of quarks are indicated. Notably the ordering of the up and down type quarks are reversed in the first family. (Masses from [9])*

Lattice QCD, on the other hand, allows naturally for calculations with unphysical quark masses.

One may ask whether questions about quark mass dependencies are purely academic: For theorists working on QCD it is of course interesting to understand the behavior of the theory in its full parameter space. But one might be tempted to think that knowing the predictions of the theory for the quark masses realized in nature is sufficient. While this is true in principle, there are areas where interesting insights can be gained by studying the quark mass dependence of certain observables. One such case is is the dependence of bound state masses in QCD on the masses of the quarks. A well know theorem, the Feynman-Hellmann theorem [12–15], relates this dependency to scalar quark density matrix elements of the bound states considered. These matrix elements are true observables of the theory with physical quark masses and play an important role in, for example, dark matter detection experiments. [16] Studying the quark mass dependence of the proton and neuron masses allows to answer the question: How strongly couples the Higgs boson, or any other particle that interacts with scalar quark condensates, to the nucleon? The answer to this question is non-trivial since the majority of the masses of the nucleons are due to the energy stored in the fluctuating quantum fields inside them. [17] This is markedly different then in weakly interacting field theories. There, the majority of the masses of the propagating degrees of freedoms are generated either by explicit mass terms in the Lagrangian or by particle-Higgs interactions. [18]

The dependence of the nucleon mass on the quark masses is conventionally described by the nucleon sigma terms. They are properly normalized derivatives of the nucleon mass with respect

to quark masses. They encode how strongly a particle that couples to scalar quark densities couples to a nucleon. Besides the Higgs boson, many candidates for dark matter, the elusive, large part of the energy density of our universe that gravitates like matter but the origin of which is largly unknown, share this feature [9]. Many experiments [9] aim to exclude regions of the parameter spaces of theories predicting dark matter candidates, or at finding a direct signal for dark matter interacting with nucleons. For them, the knowledge of the nucleon sigma terms is important to interpret their findings [16]. Consequently, a determination of all nucleon sigma terms with sufficient precision clearly has immediate experimental consequence [16].

These dependencies are also important because quark masses them self can not be directly measured, i.e. one can not put quarks on a — possibly sophisticated — scale or study their free propagation outside of bound states, except at very high energies. Quark masses are merely parameters of QCD and on their own do not carry any physical meaning. As common for parameters of an interacting quantum field theory, the values of them change as a function of the energy scale considered. Therefore, the quark masses have to be determined, at a certain scale, by tuning them and comparing predictions of the theory which depend on them with measurements. Once the measurements are reproduced, the physical quark masses have been found. [19]

The small contributions that hadron masses receive because the masses of the up quark and the down quark are not equal, is of the same order then the contribution from the electromagnetic charges of the quarks. Therefore, the electromagnetic interaction must be included in any computation that is supposed to be sensitive to the difference between the masses of the two lightest quark flavors. [19] Including the electromagnetic interaction in a lattice calculation is challenging. That is the case mainly because photons are massless and therefore finite volume correction, that can not be avoided on a finite lattice, are much more pronounced than in the case of QCD. In addition, conceptual and numerical challenges on top of those found in pure QCD calculations exist. Nevertheless, calculations in QCD+QED are possible (see e.g. [20] and references therein).

The aim of this thesis is twofold: The nucleon sigma terms and the the scalar quark contents of the nucleons are to be determined. Also, the difference between the light quark masses is to be determined.

The thesis proceeds as follows: First, the standard model of particle physics is briefly introduced. Then, the lattice formulation of QCD and QED are described. In the following part the numerical methods and techniques required for the calculations in this thesis are briefly discussed. This is followed by a description of the calculation of the nucleon sigma terms. Then, the extraction of the difference between the light quark masses is discussed. Finally, the results are summarized and the thesis concludes.

1.1 Declaration of individual contributions

The work described in this thesis was carried out within the Budapest-Marseille-Wuppertal (BMW) collaboration. Below, I indicate my individual contributions to the projects:

2hex analysis of nucleon sigma terms: I performed an independent analysis. Compared to the main analysis, my analysis used some techniques that where later used for the 3hex analysis. In my analysis all the pion, kaon, nucleon and omega masses where fitted separately and the individual effects and qualities of the fits where studied.

3hex analysis of nucleon sigma terms: I developed the strategy to split the analysis into a part dealing with mesonic sigma terms and a part dealing with a mixing matrix. Furthermore, I developed the renormalization scheme employed. I implemented several fitting codes that performed both fully correlated fits as well as separate fits to the Wilson data. The code used for the final analysis was crosschecked to be exactly equivalent to my code even on the level of individual fits. I also performed the staggered parts of the analysis with code independently developed by myself.

Light quark mass difference and violation of Dashen's theorem: I performed one of several independent analyses of the data.

Chapter 2

Aspects of the standard model of particle physics and dark matter

In this chapter I introduce some aspects of the standard model of particle physics and some aspects of dark matter. First, I describe the general structure of the standard model. Then, I introduce dark matter. I explain the gauge part of the strong interaction followed by a discussion of the coupling to fermions. In the following paragraph, I introduce symmetries of the Lagrangian of the strong interaction. Afterwards, I explain aspects of the renormalization of the strong interaction. Finally, I discuss heavy quark effective field theories with an emphasis on the results required for the subjects of this thesis.

2.1 Structure of the standard model

The standard model of particle physics describes the strong, weak, and electromagnetic interactions observed in nature. It is a gauge theory with a $SU(3) \times SU(2) \times U(1)$ gauge group coupled to fermions and scalar fields. The $SU(2) \times U(1)$ part of the gauge group describes the electroweak part [21–24] of the standard model and the $SU(3)$ part describes the strongly interacting part. [9]

The fermions in the standard model come in three identical copies called families. Each family consists of a charged lepton, a neutrino, and two quarks. The leptons are called electron, muon and tau. The neutrinos are the electron-neutrino, the muon-neutrino and the tau-neutrino. In each family there is one up-type quark and one down-type quark. The up-type quarks are the up, charm and top quarks and the down-type quarks are the down, strange and bottom quarks. The down-type quarks are not mass eigenstates but linear combinations of them. These linear combinations are determined by the Cabibo-Kobayashi-Maskawa (CKM) matrix [9, 25]. [18]

The electroweak interaction is a chiral gauge theory, i.e. it treats left handed and right handed fermions differently. The left handed particles form doublets under the $SU(2)$ gauge group while the right handed ones form singlets. Because of the group structure of $SU(2)$, the fermions can be characterized by the weak isospin T and its third component T_3. The left handed particles have $T = 1/2$. The third component T_3 of the weak isospin is $1/2$ for neutrinos and up-type quarks and $-1/2$ for leptons and down-type quarks. The right handed electrons and quarks have $T = T_3 = 0$ and do not take part in the weak interaction. Right handed neutrinos are not part of the standard model. The coupling to the $U(1)$ part of the electroweak interaction is described by the hypercharge Y. Table 2.1 lists the electroweak charges of the fermions in the standard model. [26]

Table 2.1 *– Table of the weak isospin and hypercharges of the fermions in the standard model. The table is based on a table in [26]. ν refers to the neutrinos, $l^-_{L/R}$ to the left/righthanded, charged leptons, $(u/d)_{L/R}$ to the left and righthanded up and down type quarks.*

Particle	T	T_3	Y
ν	$\frac{1}{2}$	$\frac{1}{2}$	-1
l^-_L	$\frac{1}{2}$	$-\frac{1}{2}$	-1
l^-_R	0	0	-2
u_L	$\frac{1}{2}$	$\frac{1}{2}$	$\frac{1}{3}$
d^-_L	$\frac{1}{2}$	$-\frac{1}{2}$	$\frac{1}{3}$
u_R	0	0	$\frac{4}{3}$
d^-_R	0	0	$-\frac{2}{3}$

In addition, the standard model contains scalar Higgs fields [10]. These give the gauge bosons their masses and generate masses for the fundamental fermions. The Higgs fields are subject to a potential that is shaped like a sombrero-hat and is often called Mexican hat potential. It leads to a spontaneous symmetry breaking[1]. This mechanism breaks the fundamental $SU(2) \times U(1)$ gauge symmetry in a particular way. After symmetry breaking, there are three massive gauge bosons in the spectrum of the theory: Two charged ones ($W^{\pm}$) and one neural one (Z^0). In addition, there remains one massless gauge boson, the photon, corresponding to a $U(1)$ symmetry. The photon couples to the electric charge $Q = T_3 + Y/2$. The Higgs mechanism also predicts the existence of a massive scalar boson, the Higgs boson. It has recently been observed [28, 29]. [9]

The strong interaction takes place purely between quarks and gluons. The $SU(3)$ charge of quarks is referred to as color charge. [9] A peculiar feature of the strong interaction is asymptotic freedom [5–8]. Some of the theoretical foundations of the strong interaction are discussed in later chapters. The structure of the standard model is visualized in figure 2.1.

2.2 Dark matter

The standard model of particle physics describes only a a small fraction of the energy in the universe. The majority of the universe's energy is made up by dark matter and dark energy. The exact nature of these important contributions is not yet understood. See the dark matter section of [9] for a review. This section is based upon this review.

The evidence for dark matter is large: Here, I mention three experimental arguments for its existence following the more in depth discussion in [9]:

- The bullet cluster: A galaxy cluster has passed through another cluster. Astronomers have used gravitational lensing to deduce the distribution of gravitating matter and found it to be different than the distribution of visible matter. It was also found that the majority of the gravitating mass, the dark matter, was weakly interacting.
- The cosmic microwave background (CMB): Fits to the power spectrum of the CMB have

[1] It can be debated in light of Elizurs theorem whether the term "breaking" is a misnomer for the phase transition between the "symmetric" phase and the "Higgs phase". To conform with the usual terminology, I will nevertheless refer to this transition as the electroweak symmetry breaking transition. For more details see [27] and references therein

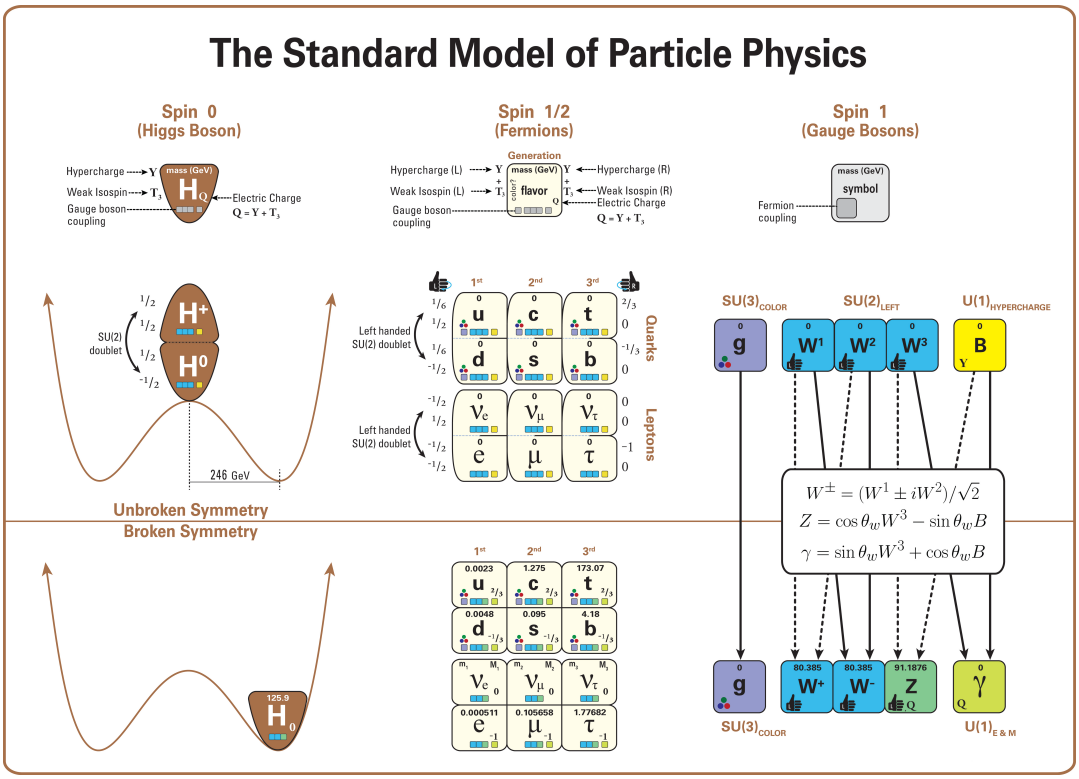

Figure 2.1 – *The structure of the standard model. The picture is unmodified from [30] where it was published under the CC BY-SA 4.0 license (*`https://creativecommons.org/licenses/by-sa/4.0/`*) The top half of the diagram shows the structure of the standard model before the electroweak symmetry breaking. The lower half shows the structure after the symmetry breaking. The left side visualizes how the Higgs field acquires a vacuum expectation value. The middle part shows the fermions and their coupling to gauges bosons and the Higgs field before and after symmetry breaking. The right part visualizes the gauge bosons and their properties before and after the symmetry breaking.*

been used to calculate the contribution of baryonic matter, dark matter, and dark energy to the mass density of the universe.

- The rotation of galaxies: The velocity of the rotations of stars around centers of galaxies have been measured. It was found that stars far away from the centers rotate faster around them than they should based on the distribution of visible matter in these galaxies. This can be explained by additional dark matter present in these galaxies.

There are alternative theories proposed that do not feature dark matter, e.g. theories that modify the laws of gravity, called MOND (modified Newtonian dynamics) [31].

Many particle physics models where proposed to explain dark matter. Heavily studied candidates are models including weakly interacting massive particles (WIMPs). WIMPs appear in many beyond the standard model theories. Notably, many supersymmetric models provide for a natural WIMP candidate, the lightest supersymmetric particle. [9].

Large experimental efforts are undertaken to constrain the properties of the WIMPs, should they exits. If WIMPs make up at least part of the dark matter, there must be a cloud of WIMPs in our galaxy, the milky way, through which the earth moves. WIMPs are supposed to scatter of nuclei in detectors. An observation of a statistically significant number of such events would allow for a direct detection of dark matter. The described interactions would happen very infrequently because of the weakness of the interactions between WIMPs and standard model particles. A very good suppression of the background is therefore key to these measurements. This is why many of these experiments are operated in underground laboratories. An important signature for WIMP dark matter would be a directional asymmetry of the detector signal provided that the direction changes with the daily rotation of earth. Also, the flux should be modulated annually because of the earth's movement changes direction with respect to the sun's movement in the galaxy over the course of a year. [9]

In figure 2.2 current experimental limits for the WIMP mass and the cross sections of spin-independent WIMP-nucleon scatterings are shown. The experimental sources for this plot are described in [9] and references therein. See also [32] for a review of the experimental efforts.

2.3 $SU(3)$ gauge theory

The strong interaction is locally symmetric under $SU(3)$ rotations of the matter fields. Yang and Mills laid the theoretical foundations for theories with such a local, non-abelian gauge symmetry. In their original work [4] they did not consider the $SU(3)$ symmetry of QCD, which was not know at that time. Instead, they considered the isospin symmetry between protons and neutrons as gauge symmetry. However, their arguments are equally valid for the $SU(3)$ symmetry of the strong interaction. To assign any meaning to spatial and temporal changes in the matter fields in a Yang-Mills theory, a measure to compare fields at different points in spacetime has to be specified. Comparing two values of matter fields at points x and y requires a $SU(3)$ matrix $U_{\mathscr{C}}(x, y)$ that describes the rotation between the two coordinate choices at these points. This matrix is given by the parallel transporter [1]

$$U_{\mathscr{C}}(x, y) = \mathscr{P} \exp\left[\mathrm{i}g \int_{\mathscr{C}} \mathrm{d}x^{\mu} A_{\mu}\right]. \tag{2.1}$$

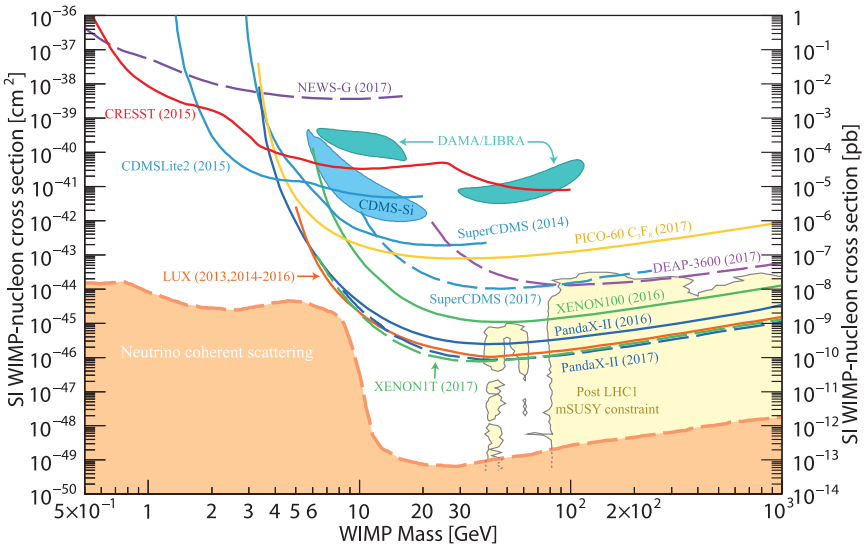

Figure 2.2 – *Limit on the WIMP mass and nucleon-WIMP-crosssections via spin-independent scattering. Regions on top of the colored bands are excluded by experiments. The orange region can not be reached by experiments because they can not distinguish the WIMP scattering signal from the background originating in neutrino coherent scattering. The yellow region shows a parameter range of typical SUSY models. The figure is from [9] where more details and references to the experiments can be found.*

In this equation, $\mathscr{C}$ is a path between the two points x and y. The A_μ are the gauge potentials and are elements of the Lie algebra $\mathfrak{su}(3)$. The symbol $\mathscr{P}$ is the path ordering operator. It ensures that the factors in this expression are evaluated in the right order along the path. [1] The expression simplifies to

$$U(x + \epsilon n, x) = 1 - \mathrm{i}g\epsilon n^\mu A^a_\mu t^a + \mathcal{O}(\epsilon^2), \tag{2.2}$$

a single $SU(3)$ matrix close to unity, if only infinitesimally separated points are considered. [1] Here, n is a unit fourvector, ϵ is a small real number, and t^a are the generators of $SU(3)$. The covariant derivative, a generalization of the derivative that takes coordinate transformations mediated by gauge fields into account, is defined as [1]

$$D_\mu = \partial_\mu - \mathrm{i}gA^a_\mu t^a. \tag{2.3}$$

The first term describes the change in the function values on which D_μ is applied. The second term describes the change of the internal coordinate system.

In order to construct the field strength tensor, it is useful to look at repeated applications of covariant derivatives. Two covariant derivatives successively applied on a matter field ψ yield [1]

$$\begin{aligned} D_\mu D_\nu \psi &= \partial_\mu \partial_\nu \psi - \mathrm{i}g(t^b \partial_\mu A^b_\nu - t^a A^a_\mu \partial_\nu)\psi - g^2 A^a_\mu A^b_\nu t^a t^b \psi \\ &= \partial_\mu \partial_\nu \psi - \mathrm{i}g(t^b \partial_\mu A^b_\nu)\psi - g^2 A^a_\mu A^b_\nu t^a t^b \psi. \end{aligned} \tag{2.4}$$

The expression can be intuitively interpreted as walking an infinitesimal step in the μ direction followed by an infinitesimal step in the ν direction. The same procedure can repeated with the μ

and ν directions interchanged. The difference between these two operations, the commutator of the covariant derivatives, is [1]

$$[D_\mu, D_\nu] = D_\mu D_\nu - D_\nu D_\mu = \mathrm{i}g t^a(\partial_\mu A^a_\nu - \partial_\nu A^a_\mu) + g^2 A^b_\nu A^a_\mu [t^a, t^b]. \tag{2.5}$$

The field strength tensor $F_{\mu\nu}$ is defined as

$$F_{\mu\nu} = t^a(\partial_\mu A^a_\nu - \partial_\nu A^a_\mu) - \mathrm{i}g A^b_\nu A^a_\mu [t^a, t^b] = t^a(\partial_\mu A^a_\nu - \partial_\nu A^a_\mu) + g A^b_\nu A^a_\mu f^{abc} t^c \tag{2.6}$$

such that

$$[D_\mu, D_\nu] = \mathrm{i}g F_{\mu\nu}. \tag{2.7}$$

Here, f^{abc} are the structure constants of $SU(3)$ which fulfill $[t^a, t^b] = \mathrm{i} f^{abc} t^c$.

The field strength tensor can also be constructed in a different way that is closely related to the construction of the Wilson gauge action. This construction is quickly reviewed here. The gauge transporter $U(x, x)$ around a small square with side length ϵ located in the $\mu\nu$ plane is considered. [1, 26] At leading order in ϵ it is [1]

$$U(x, x) = 1 + \mathrm{i}g\epsilon^2 F^a{}_{\mu\nu}(x) t^a + \mathcal{O}(\epsilon^3). \tag{2.8}$$

This is not gauge invariant as the t^a are matrices in color space. [1] It can be made gauge invariant by taking the trace in color space. The t^a are traceless and therefore the only non-trivial terms contributing to the trace of $U(x, x)$ must be of higher order in ϵ. Any $SU(3)$ matrix close to unity can be written as [1]

$$1 + \mathrm{i}(\epsilon' \beta^a + \epsilon'^2 \gamma^a + \ldots) t^a - \frac{1}{2}(\epsilon'^2 \beta^a \beta^b + \ldots) t^a t^b + \ldots \tag{2.9}$$

When taking the trace, the terms proportional to t^a vanish. However, $t^a t^b$-terms remain. Their coefficient is determined by β^a, the first coefficient in the ϵ expansion of the coefficient of the t^a-term. Substituting $\epsilon' = \epsilon^2$ one finds [1]

$$\operatorname{tr} U(x, x) = 1 - \frac{1}{2}\epsilon^4 g^2 F^a{}_{\mu\nu} F^b{}_{\mu\nu} \delta^{ab} + \mathcal{O}(\epsilon^6). \tag{2.10}$$

This shows that the first non-vanishing, gauge invariant contribution to the trace is $F^a_{\mu\nu} F^a_{\mu\nu}$. Note that μ and ν specify the orientation of the small square and no summation over them is implied at this point. On the lattice one uses this relation to define the Wilson gauge action [33, 34].

The discussion is closed by remarking that there is a deep connection to the formalism used in general relativity. Because of this analogy, $F_{\mu\nu}$ is also called the curvature of the gauge field. [26]

Requiring Lorentz invariance and renormalizability, the number of possible terms in the Lagrangian can be further reduced: Only the terms

$$F^a{}_{\mu\nu} F^{a\mu\nu} \quad \text{and} \quad \epsilon^{\mu\nu\rho\sigma} F^a{}_{\mu\nu} F^a{}_{\rho\sigma} \tag{2.11}$$

are admissible. The latter term, however, is CP odd. It turns out that the coefficient of it is constrained to be tiny by measurements of the neutron electric dipole moment. Why this coefficient is so small is not fully understood. This puzzle is called the strong CP problem [1].

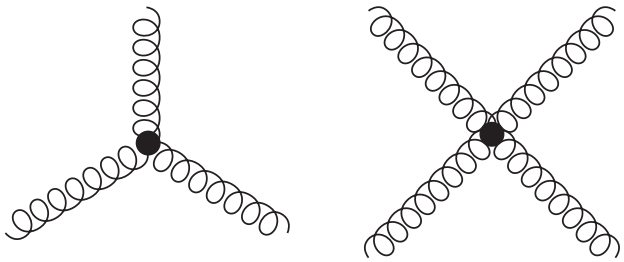

Figure 2.3 *– The self-interaction vertices of Yang-Mills theory (after [1]).*

Conventionally, this term is not considered to be part of QCD. Putting everything together, the pure gauge Lagrangian of QCD is [1]

$$\mathscr{L}_{YM} = -\frac{1}{4}\,\mathrm{tr}[F_{\mu\nu}F^{\mu\nu}] = -\frac{1}{4}F^{a}{}_{\mu\nu}F^{a\mu\nu}. \tag{2.12}$$

One important feature of Yang-Mills theory is that it predicts a self-interaction between the bosons carrying the force [1, 4]. This can be seen by writing down $F^{a}{}_{\mu\nu}F^{a\mu\nu}$ explicitly:

$$\begin{aligned} F^{a}{}_{\mu\nu}F^{a\mu\nu} &= ((\partial^{\mu}A^{a\nu} - \partial^{\nu}A^{a\mu}) + gA^{c\nu}A^{b\mu}f^{bca})((\partial_{\mu}A^{a}_{\nu} - \partial_{\nu}A^{a}_{\mu}) + gA^{e}_{\nu}A^{d}_{\mu}f^{eda}) \\ &= 2(\partial^{\mu}A^{a\nu})(\partial_{\mu}A^{a}_{\nu}) - 2(\partial^{\mu}A^{a\nu})(\partial_{\nu}A^{a}_{\mu}) \\ &\quad + 4gA^{c\nu}A^{b\mu}f^{bca}\partial_{\mu}A^{a}_{\nu} + g^{2}A^{c\nu}A^{b\mu}A^{e}_{\nu}A^{d}_{\mu}f^{bca}f^{eda} \end{aligned} \tag{2.13}$$

The first two terms are quadratic in the fields. They describe the free propagation of the gauge bosons. The remaining terms contain three or four gauge fields and hence describe interactions. The vertices corresponding to these self interactions are shown in figure 2.3. All self interaction terms contain one or more factors of f^{abc}. The structure constants, defined by the commutators of generators, vanish for abelian gauge groups. This is why self interactions are absent in QED which has the abelian gauge group $U(1)$.

2.4 The Lagrangian including quarks

Quarks can be introduced to the action as Grassmann valued fields $\bar{\psi}(x)$ and $\psi(x)$. They transform in the fundamental representation of $SU(3)$ and are minimally coupled to the gluon fields. Free fermion fields are described by the Dirac Lagrangian [1, 35]

$$\mathscr{L}_{\mathrm{Dirac}} = \bar{\psi}(x)(\mathrm{i}\gamma^{\mu}\partial_{\mu} - m)\psi(x). \tag{2.14}$$

In a gauge theory each instance of a partial derivative has to be replaced by a covariant derivative. This results in the Lagrangian [1]

$$\mathscr{L} = \bar{\psi}(x)(\mathrm{i}\gamma^{\mu}D_{\mu} - m)\psi(x) - \frac{1}{4}\,\mathrm{tr}[F_{\mu\nu}F^{\mu\nu}] \tag{2.15}$$

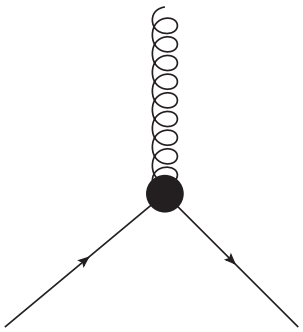

Figure 2.4 *– The interaction vertices beween quarks and gluons.*

that describes one quark flavor coupled to gluons. The covariant derivative automatically introduces interactions between quarks and gluons. This can be seen by writing out the covariant derivative:

$$\bar{\psi}(x)\gamma^{\mu}D_{\mu}\psi(x) = \bar{\psi}(x)\gamma^{\mu}\partial_{\mu}\psi(x) - \mathrm{i}g\bar{\psi}(x)\gamma^{\mu}A_{\mu}(x)\psi(x) \tag{2.16}$$

The first term describes the dynamics of free quarks and the second one describes interactions. These are of the type depicted in figure 2.4. The diagrams in figures 2.3 and 2.4 are the only fundamental interactions in QCD. The full Lagrangian of QCD is obtained by adding the five additional quark flavors to eqn. (2.15). [1]

2.5 Symmetries of QCD

There are a number of interesting global symmetries of the Lagrangian in eqn. (2.15), especially in the limits of degenerate or massless quarks. Not all of these symmetries survive quantization. Some of them are spontaneously [36] or anomalously [37, 38] broken. Both cases lead to interesting phenomena.

In the case of N_f degenerate quark flavors, there are the $SU(N_f)_V$ vector symmetries [34]

$$\psi \rightarrow \exp(\mathrm{i}\alpha T_i)\psi \quad \text{and} \quad \bar{\psi} \rightarrow \bar{\psi}\exp(-\mathrm{i}\alpha T_i). \tag{2.17}$$

Here, the T_i are the generators of the $SU(N_f)$ group in flavor space. Independent of the quark masses, there is an additional $U(1)_V$ vector symmetry [34]

$$\psi \rightarrow \exp(\mathrm{i}\alpha \mathbb{1})\psi \quad \text{and} \quad \bar{\psi} \rightarrow \bar{\psi}\exp(-\mathrm{i}\alpha \mathbb{1}). \tag{2.18}$$

Eqn. (2.17) is the generalization of isospin to an arbitrary number of flavors and eqn. (2.18) is responsible for the baryon number conservation. [34]

The left and right handed components of the quark fields are [34]:

$$\psi_L = \frac{1-\gamma_5}{2}\psi \quad \text{and} \quad \psi_R = \frac{1+\gamma_5}{2}\psi \tag{2.19}$$

Plugging these definitions in the Dirac Lagrangian yields

$$\mathscr{L}_{\text{Dirac}} = \mathrm{i}(\bar{\psi}_L \gamma^\mu \partial_\mu \psi_L + \bar{\psi}_R \gamma^\mu \partial_\mu \psi_R) - m(\bar{\psi}_L \psi_R + \bar{\psi}_R \psi_L) \tag{2.20}$$

It can be shown that in the classical, massless case, in which the second term is absent, there are additional axial $SU(N_f)_A$

$$\psi \to \exp(\mathrm{i}\alpha\gamma_5 T_i)\psi \quad \text{and} \quad \bar{\psi} \to \bar{\psi}\exp(-\mathrm{i}\alpha\gamma_5 T_i). \tag{2.21}$$

and $U(1)_A$

$$\psi \to \exp(\mathrm{i}\alpha\gamma_5 \mathbb{1})\psi \quad \text{and} \quad \bar{\psi} \to \bar{\psi}\exp(-\mathrm{i}\alpha\gamma_5 \mathbb{1}). \tag{2.22}$$

symmetries because γ_5 mixes left handed with right handed fields. [34] These symmetries are explicitly broken by the quark mass term. [34] Altogether, the massless QCD Lagrangian is symmetric under a

$$SU(N_f)_V \times SU(N_f)_A \times U(1)_V \times U(1)_A \tag{2.23}$$

global symmetry. [34] The axial part of this symmetry can not be found in the spectrum of QCD. One could attribute this to the non-vanishing quark masses. However, at least the masses of the two lightest quarks are so small compared to the characteristic QCD scale, that, if they would be the only source of symmetry breaking, an approximate symmetry should be visible. [34] Instead, the $U(1)_A$ symmetry is anomalously broken. [37, 38] The reason is that every possible gauge invariant regulator breaks this symmetry. A simple way to understand this was found by the authors of [39, 40]. They noted that, while at the classical level the Lagrangian is invariant under the $U(1)_A$ symmetry, the regulated path integral measure is not. [1, 41]. The remaining $SU(3)_A$ axial symmetries are spontaneously broken. [1, 36, 41]

2.6 Aspects of the renormalization of QCD

Renormalization is required for the calculation of many quantities in most interesting quantum field theories. [1] The need for it can be motivated using the following analogy [42] with classical electrodynamics: Consider an infinitely heavy particle with charge q_0 in a polarizable medium composed of electrical dipoles. The dipoles in the medium will orient them self in such a way that the charge q_0 is screened; the charge seen from far away will be smaller then the original charge q_0. In a quantum field theory, the vacuum state itself is polarizable: Due to quantum fluctuations, charge-anticharge pairs can be created from the vacuum. These pairs act like the dipoles of a medium and screen part of the charge q_0. This screening is such that the effective charge that can be seen is the smaller the farther away one is from the charge. Since, even in principle, one can not separate the particles from the vacuum, the question arises whether the charge q_0 is fundamental. Therefore, it is quite natural to consider not the charge q_0 but the the $q(d)$ measured at a certain distance d. Since in scattering experiments small distances correspond to large momentum transfers and long distances correspond small momentum transfers, one considers in this setting a charge that depends on a momentum scale of the process. [42]

To correctly implement renormalization in the context of a quantum field theory, a two step procedure is employed. In a first step a regularization scheme is introduced that removes

spurious infinities from the calculations. Usually, this regularization introduces a scale at which the parameters of the theory are given. In a second step the regulator is removed in such a way that physical observables remain finite and approach values that are independent of the regulator. [1]

One choice for a regulator is a discrete space-time lattice of points at which the fields of the theory are defined. Such a lattice comes with a lattice spacing a defining the scale of the regulator. The action can be expressed in terms of the fields at the lattice points. At at fixed lattice spacing a, the parameters of the action can be tuned such that certain long distance observables have the same values that are observed in experiments. To remove the regulator, the lattice spacing a is successively decreased. While doing so, the values of the parameters of the action have to be adjusted such that the long distance observables remain the same. Ultimately, by taking the limit $a \longrightarrow 0$, the regulator is removed. Then, all observables approach their continuum values. The parameters of the action may even diverge in that limit without posing a problem since they are not observables. [34]

Many of the calculations in this thesis are done in such a scheme. While it is well suited for numerical calculations, in many analytic, perturbative calculations a different scheme is used. This is the modified minimal subtraction scheme ($\overline{\text{MS}}$). In that scheme, regularization is achieved in a very different way: Whenever a certain process is to be calculated in perturbation theory, a number of space-time integrals, corresponding to Feynman diagrams, have to be evaluated. These integrals depend explicitly on the number of dimensions of space time. If they diverge, they can be made finite by formally changing the number of dimensions to a non-integer value. When taking the limit in which the number of space time dimensions approaches the correct integer number, the integrals diverge again. These divergences must be canceled prior to taking this limit by putting the divergent part — and, out of convention, some certain finite part — into counterterms added to the Lagrangian. These counterterms effectively change the values of the parameters of the theory from bare ones to renormalized ones. [1] The integrals appearing in the calculations of the Feynman diagrams are usually not dimensionless. In order for the dimension of the result to stay the same, even when the number of dimensions of space-time is changed to a fractional value, one has to introduce an artificial and arbitrary scale μ. It often appears in a logarithm of a ratio with the momentum that is transferred in the process in question. If this logarithm is large, then the perturbative expansion frequently converges slower then if it where small. Therefore, it is desirable to choose μ to be of the order of the momentum transfered. [1] At a finite order of the perturbative expansion the values of the counter terms depend on the choice of the scale μ. Consequently, all parameters of the theory depend on the value of this scale; couplings or other parameters of the theory are always specified as a function of the renormalization scale μ when using the $\overline{\text{MS}}$ scheme. [1]

The coupling and masses specified at a given scale μ are called running coupling and running masses. Their evolutions with the scale μ are described by the renormalization group equations. In a gauge theory with fermions, like QED or QCD, the relevant parameters are the coupling constant α (or specifically α_s in the case of QCD) and the masses of the fermions. The renormalization group equation for the couping constant is [9]

$$\mu^2 \frac{\partial \alpha}{\partial \mu^2} = \beta(\alpha) = -b_0\alpha^2 - b_1\alpha^3 - b_2\alpha^4 - \dots . \tag{2.24}$$

where the right hand side is called beta-function. The first two coefficients in this expansion are the same in all renormalization schemes. In the case of QCD they are $b_0 = (33 - 2N_f)/(12\pi)$ and $b_1 = (153 - 19N_f)/(24\pi^2)$ where N_f is the number of quark flavors. [9] The higher order coefficients depend on the renormalization scheme and can be found for the $\overline{\text{MS}}$ scheme in [43–47]. The runnings of the mass parameters of the fermions are described by the equation [9]

$$\mu^2 \frac{\partial m(\mu)}{\partial \mu^2} = -\gamma_m(\alpha(\mu))m(\mu) = m(\mu)(\gamma_1\alpha + \gamma_2\alpha^2 + \gamma_3\alpha^3 + \ldots)$$

where $m(\mu)$ is the running mass of one fermion and γ_m is the anomalous dimension of the fermion mass. The two leading contributions to the anomalous dimension are $\gamma_1 = 1/\pi$ and $\gamma_2 = 202/(36\pi^2) - 20N_f/(108\pi^2)$ and higher orders can be found in [9, 48, 49].

A consequence of eqn. (2.24) is that for $\mu \longrightarrow \infty$ the coupling becomes arbitrary small and the theory is almost a free theory. This phenomenon is called asymptotic freedom. [5–8] On the other hand, if μ becomes small the coupling constant, calculated in perturbation theory, becomes bigger and eventually diverges. The scale at which the coupling diverges is referred to as Λ_{QCD} and is of the same order of magnitude as the masses of typical QCD bound states. Of cause, perturbation theory has already ceased to give meaningful results long before μ reaches Λ_{QCD}.

The classical field theory corresponding to the QCD Lagrangian with all quarks taken to be massless is scale invariant. The quantum effects that are responsible for the running of the coupling break this scale invariance and lead to the appearance of a characteristic scale. This mechanism is referred to as dimensional transmutation and is the origin of Λ_{QCD}. It is an example of an anomalous breaking of a symmetry, in this case the rescaling symmetry. In this sense, the anomalous breaking of the scale invariance is responsible for a sizeable fraction of the masses of most QCD bound states. [1]

It is a widespread convention not to consider the running of the coupling constant in a theory that contains all flavors of quarks but in a series of effective field theories (EFTs). The reason, as described in more detail in [50], is the following: The decoupling theorem [51] ensures that physics at a low scale is, to a good approximation, decoupled from the effects of quarks with masses much heavier then this scale. The small effects of these heavy quarks are well described by an expansion in $1/M$ where M is the mass of the heavy quark. However, eqn. (2.24) clearly shows that the running of the coupling constant depends on the number of quark flavors in the theory. At first this seems to be in direct contradiction with the decoupling theorem. The solution to this apparent contradiction is that α_s is not a measurable quantity; every quantity that can be measured, e.g. a cross section, will show the decoupling. This implies that in the calculation of these observables the effects of the heavy quarks have to be included, only for them to be canceled by the effects of the heavy quarks on the running of the coupling constant. Clearly, this is inconvenient. It is easier to introduce a tower of effective field theories with the heavy quark effects being integrated out: In addition to the fundamental $N_f = 6$ theory, effective $N_f = 5, 4, 3$ theories are introduced. The parameters of the effective field theories are calculated by matching at a given scale. It turns out that logarithmic corrections to the matchings are small if the matching scales are taken to be close to the masses of the quark flavors to be integrated out. Conventionally, the matching scales are taken to be the running quark mass of the quark flavor to be integrated out at the scale where μ is equal to this mass. These scales, at which the

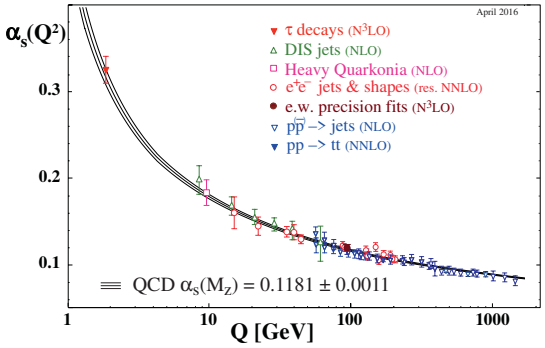

Figure 2.5 *– Running of the strong coupling constant α_s. (Figure from [9]) The value of the strong coupling constant α_s is shown as a function of the energy scale Q.*

matching is performed, are called quark thresholds. Schematically the matching has the form

$$N_f = 6 \text{ theory} \xrightarrow{\text{matching at } \mu = m_t(m_t)} N_f = 5 \text{ theory} \xrightarrow{\text{matching at } \mu = m_b(m_b)} N_f = 4 \text{ theory} \xrightarrow{\text{matching at } \mu = m_c(m_c)} N_f = 3 \text{ theory} \quad (2.25)$$

Details can be found in [50] on which the above discussion of the matching procedure and the EFTs is based. The precise matching conditions can be found in [9].

The running of the coupling constant, as determined by the QCD beta function, the matching conditions, and a multitude of experimental measurements, can be found in figure 2.5.

2.7 Heavy flavor effective theories and quark contents

The renormalization pattern of the nucleon quark contents $f_{qN} = m_q(\langle N \mid \bar{q}q \mid N\rangle - \langle 0 \mid \bar{q}q \mid 0\rangle)$ are important for this thesis. In this expression, $\mid N\rangle$ is a normalized nucleon state, $\mid 0\rangle$ is the vacuum sate, m_q is the mass of the quark flavor q, and $\bar{q}q$ is the scalar combination of quark field operators. Firstly, the quark contents are renormalization group invariants in a theory where the number of quark flavors is constant. As explained in the last section, it is customary to integrate out heavy quark flavors at the quark thresholds. Hence, in the resulting EFTs the corresponding quark contents of the integrated out quark flavors must vanish. The contribution to the Higgs coupling of the integrated out flavors, however, does not vanish but is absorbed into an effective gluon-Higgs coupling. This is related to the well known mixing of these two operators that also leads to gluon-gluon fusion. [52] The corresponding Feynman diagrams can be found in figure 2.6.

The quark contents are related to the nucleon mass via a sum rule involving the expectation value of the trace of the energy momentum tensor: [2, 53, 54]

$$\langle \theta_\mu{}^\mu \rangle_N = \langle N \mid (1+\gamma_m) \sum_f m_f \bar{q}_f q_f + \frac{\beta}{2g} G^2 \mid N\rangle - \langle 0 \mid \ldots \mid 0\rangle = M_N \quad (2.26)$$

Here, γ_m is the mass anomalous dimension of QCD, β is the β-function, g the gauge coupling, G is the gluon field strength, and the operator between the vacuum state is the same then between

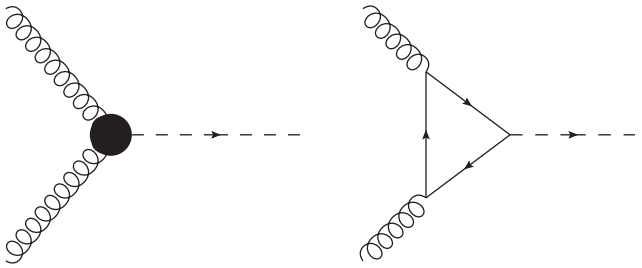

Figure 2.6 – *The mixing between a quark loop and an effective gluon-gluon-Higgs vertex. The right diagram contributes, if integrated out, to an effective gluon-gluon-Higgs vertex as depicted by the black dot in the left diagram.*

Table 2.2 – *The values of the coefficients b_i^n and c_i^n. [2, 3]*

i	b_i^3	c_i^3	b_i^4	c_i^4	b_i^5	c_i^5
0	0.0740741	0.0740741	0.08	0.08	0.0869565	0.0869565
1	0.0229236	0.0700806	0.0308124	0.081742	0.0412178	0.0965761
2	0.0412178	0.0534895	0.0157223	0.0664099	0.0246729	0.0846867
3	-0.012595	-0.0245554	-0.0218678	-0.0409409	-0.0334609	-0.0578502

the nucleon states. Using this, the quark content of the $(n+1)$-th flavor in an $N_f = n+1$ theory can be deduced form the knowledge of the quark content of the n flavors in an $N_f = n$ theory. To leading order the relation is [2, 3, 53]

$$f_{hN} = \frac{2}{3\beta_0}(1-\lambda) + \mathcal{O}\left(\frac{\Lambda_{\text{QCD}}}{m_h}, \alpha_s\right) \tag{2.27}$$

where h denotes the heavy $(n+1)$-th flavor and

$$\lambda = \sum_{q=1}^{n} f_{qN}. \tag{2.28}$$

In [2], corrections up to order $\mathcal{O}(\alpha_s^3)$ are calculated. They take the form

$$f_{hN} = \sum_{i=0}^{3}(b_i^n - c_i^n\lambda)\alpha_s^i.$$

The coefficients [2, 3] b_i^n and c_i^n can be found in table 2.2. This relation is true up to correction of order $\mathcal{O}(\alpha_s^4)$ and $\mathcal{O}(\Lambda_{\text{QCD}}^2/m_h^2)$.

Chapter 3

The lattice formulation of gauge theories

Almost all calculations in this thesis are performed by monte carlo simulations of lattice regularized gauge theories. The idea to study the interactions of quarks and gluons on a space-time-lattice was first proposed by Wilson in 1974 [11]. It was realized that this formulation of gauge theory is well suited for a numerical approach [55, 56]. I will present a short overview of some aspects the lattice regularization of QCD. The main focus will be on aspects relevant for this thesis. The discussion is largely based on [33, 34] for the lattice specific details and on [1] for continuum calculations.

3.1 The regularization

The lattice regularization is constructed by introducing a regular lattice Λ of space time points and by defining the matter and gauge fields at the lattice points and at the straight lines between nearest-neighbor points. The lattice Λ itself is defined by

$$\Lambda := \{\vec{n} = a(n_1, n_2, n_3, n_4) | n_{1\ldots3} < N_s \in \mathbb{N}_0, n_4 < N_t \in \mathbb{N}_0\}. \tag{3.1}$$

Here, N_s is the spatial extend [1] and N_t is the temporal extent of the lattice, both in units of the lattice spacing a. In the following, unit vectors with lengths of one lattice spacing will be denoted by $\hat{\mu} := a\vec{e}_\mu$. Lattice points are specified by a 4-component index $\vec{n}$. The four entries of them are integers ranging from 0 to N_t or N_s respectively. Attached to each lattice point there are a number of fields: Firstly, Grassmann-valued fields $\psi^a(\vec{n})$ and $\bar{\psi}^a(\vec{n})$ with the index a, called color index, running through the values 0 to 3 for $SU(3)$ gauge theory. These fields represent the quarks. Secondly, four matrix valued fields $U_\mu^{ab}(\vec{n})$ with μ running from 1 to 4, the four space time dimensions. These fields represent the gluons. Here, a and b are the matrix indices, which are in the same space then the color indices of the Grassmann-valued field. The $U_\mu^{ab}(\vec{n})$ are elements of $SU(3)$ for the case of QCD. Because $SU(3)$ has eight generators, the same number of independent real numbers uniquely characterizes each of the $U_\mu^{ab}(\vec{n})$. The $U_\mu^{ab}(\vec{n})$ act as discretized version of the parallel transporter between neighboring points; they provide the transformations between $\psi^a(\vec{n})$ and $\psi^b(\vec{n} + \hat{\mu})$. Therefore, $U_\mu^{ab}(\vec{n})$ is thought to reside at the link between the lattice sites $\vec{n}$ and $\vec{n} + \hat{\mu}$. A two dimensional sketch can be found in figure 3.1.

[1] It is possible to have different lattice sizes for the three spatial extents. To keep the notation compact here and in the following we discuss only the case with spatial dimensions of equal size. The extension to the general case is straight forward.

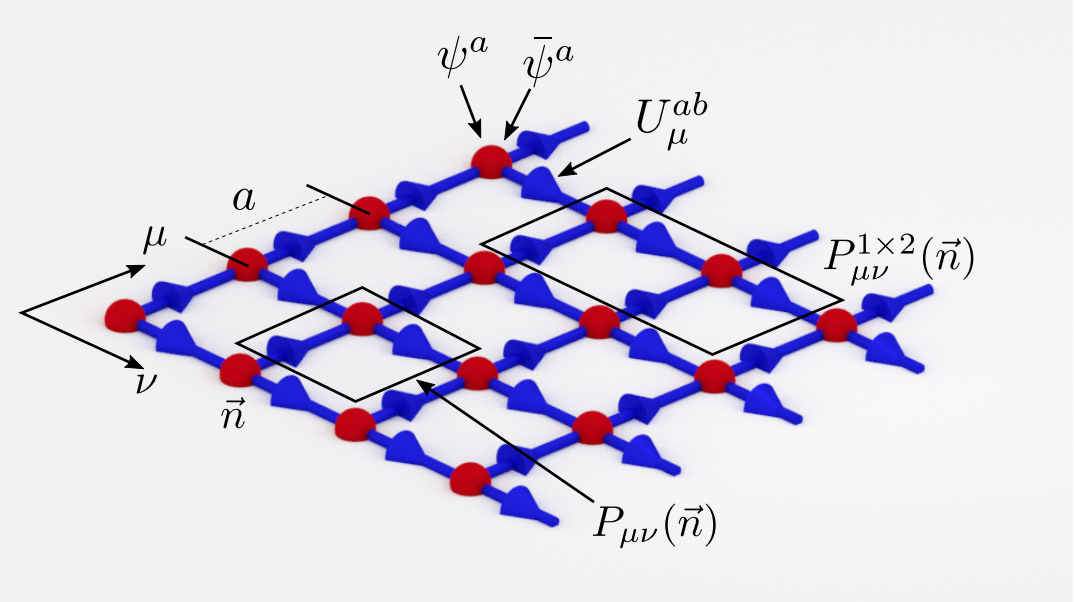

Figure 3.1 *– A two dimensional slice of the space-time lattice. The fermion fields ψ^a and $\bar{\psi}^a$ reside on the lattice points while the gauge fields U_μ^{ab} can be thought to be located on the lattice links. The smallest closed path on the lattice is called a plaquette $P_{\mu\nu}$. There are also larger loops for example $P_{\mu\nu}^{1\times 2}$.*

3.2 The gauge action of QCD

Before the lattice regulator can be employed in a practical calculation, an action must be formulated in terms of the discretized fields. The simplest gauge action of this type is the Wilson gauge action. In the continuum theory the euclidean gauge action is the integral over the Lagrangian density

$$\mathcal{L} = \frac{1}{4g_s^2}\,\mathrm{tr}[F_{\mu\nu}F_{\mu\nu}] \quad \text{with} \quad F_{\mu\nu} = \frac{1}{\mathrm{i}g_s}[D_\mu, D_\nu] = \partial_\mu A_\nu - \partial_\nu A_\mu + \mathrm{i}[A_\mu, A_\nu]. \tag{3.2}$$

For details see the previous chapter. At first, discretizing the derivatives of the type $\partial_\mu A_\nu$ appearing in the Lagrangian seem natural. However, it is more convenient do directly discretize $\mathrm{tr}[F_{\mu\nu}F_{\mu\nu}]$. This term corresponds, in the continuum, to a sum over infinitely small rectangles. Infinitesimal small paths, however, can not exist on a lattice. Instead, the smallest possible[2] closed paths are plaquettes $P_{\mu\nu}(\vec{n})$, products of four gauge links forming squares. The lattice plane in which such a plaquette is oriented is denoted by the indices μ and ν. A graphical representation of these plaquettes is shown in figure 3.1. The transformation in color space picked up along a plaquette is

$$P_{\mu\nu}(\vec{n}) = U_\mu(\vec{n})U_\nu(\vec{n}+\hat{\mu})U_\mu^\dagger(\vec{n}+\hat{\nu})U_\nu^\dagger(\vec{n}). \tag{3.3}$$

[2] For $N_S \leq 4$ or $N_t \leq 4$ and with periodic boundary conditions there are paths that wind around the lattice that are smaller or of the same size. Because we are interested in an action that reproduces the continuum case, such terms are not considered here.

and the Wilson gauge action, formulated in terms of these plaquettes, is

$$S_{\text{Wilson}} = \frac{2}{g_s^2} \sum_{\vec{n}\in\Lambda} \sum_{\mu<\nu} \text{Re}(3 - \text{tr}\, P_{\mu\nu}(\vec{n})). \tag{3.4}$$

The plaquettes can be Taylor expanded in the lattice spacing, as demonstrated e.g. in [33], so that

$$\text{tr}\, P_{\mu\nu}(\vec{n}) = 3 + \text{i}a^2\, \text{tr}[F_{\mu\nu}] - \frac{a^4}{2}\, \text{tr}[F_{\mu\nu}F_{\mu\nu}] + \mathcal{O}(a^6). \tag{3.5}$$

In the last term no sum over μ and ν implied. Inserting this result into eqn. (3.4) leads to

$$S_{\text{Wilson}} = a^4 \left(\frac{1}{g_s^2} \sum_{\vec{n}\in\Lambda} \sum_{\mu<\nu} \text{tr}[F_{\mu\nu}F_{\mu\nu}] + \mathcal{O}(a^2) \right) = a^4 \left(\frac{1}{2g_s^2} \sum_{\vec{n}\in\Lambda} \sum_{\mu,\nu} \text{tr}[F_{\mu\nu}F_{\mu\nu}] + \mathcal{O}(a^2) \right), \tag{3.6}$$

showing that classically S_{Wilson} is up to $\mathcal{O}(a^2)$ corrections equal to the continuum gauge action. It is a wide spread convention to define $\beta = {}^6/_{g_s^2}$ so that the Wilson gauge action is

$$S_{\text{Wilson}} = \frac{\beta}{2} \sum_{\vec{n}\in\Lambda} \sum_{\mu<\nu} \text{Re}(3 - \text{tr}\, P_{\mu\nu}(\vec{n})). \tag{3.7}$$

It is worthwhile to ask whether the $\mathcal{O}(a^2)$ contributions can be eliminated. This is useful, since numerical calculations are necessarily done at finite values of a. If the $\mathcal{O}(a^2)$ contributions can be eliminated, only much smaller $\mathcal{O}(a^4)$ corrections remain. [33] There is some freedom in constructing a lattice gauge action that can be leveraged to achieve this. In addition to plaquettes, larger loops like for example $P_{\mu\nu}^{1\times2}$, as shown in figure 3.1, can be used. Once the prefactor has been suitably chosen, the action has the same leading order behavior then the Wilson gauge action but different $\mathcal{O}(a^2)$ corrections. These correction can be calculated for both actions and the two actions can be combined into a linear combination such that the $\mathcal{O}(a^2)$ terms cancel. The resulting action, with the prefactors calculated perturbatively at tree level, is [33]

$$S_{\text{Wilson}} = \frac{\beta}{2} \sum_{\vec{n}\in\Lambda} \sum_{\mu<\nu} \text{Re} \left(3 - \frac{5}{3}\, \text{tr}\, P_{\mu\nu}(\vec{n}) + \frac{1}{12}\, \text{tr}\, P_{\mu\nu}^{1\times2} \right) \tag{3.8}$$

This action is called the Lüscher-Weisz action [57]. In the quantized theory the $\mathcal{O}(a^2)$ coefficients receive quantum corrections so that in the above action the $\mathcal{O}(a^2)$ terms cancel only at tree-level and corrections of order $\mathcal{O}(\alpha_s a^2)$ remain. [33]

3.3 The fermion action

A lattice fermion action can be constructed by discretizing the continuum fermion action. However, complications fundamentally different from those in the case of the gauge action, appear. The action for one species of free Dirac fermions in continuous euclidean space-time is [33]

$$S = \int \text{d}^4x \bar{\psi}(\gamma_\mu \partial_\mu + m)\psi. \tag{3.9}$$

The so called "naïve" discretization is constructed from it by replacing the partial derivative by a finite difference operator [33]

$$\partial_\mu f \to \Delta_\mu f := \frac{f(x+\hat{\mu}) - f(x-\hat{\mu})}{2a}. \tag{3.10}$$

The resulting fermion action is [11, 34]

$$S = a^4 \sum_{n\in\Lambda} \bar{\psi}(n) \left(\sum_{\mu=1}^{4} \gamma_\mu \frac{\psi(n+\hat{\mu}) - \psi(n-\hat{\mu})}{2a} + m\psi(n) \right). \tag{3.11}$$

It can be cast into the bilinear form

$$S = a^4 \sum_{m,n\in\Lambda} \sum_{\alpha,\beta} \bar{\psi}_\alpha(n) D_{\alpha\beta}(n,m) \psi_\beta(m) \tag{3.12}$$

where the Dirac indices are now explicitly written out. [34] Here, the fermion matrix $D_{\alpha\beta}(n,m)$ is [34]

$$D_{\alpha\beta}(n,m) = \sum_{\mu=1}^{4} [\gamma_\mu]_{\alpha\beta} \frac{\delta_{n+\hat{\mu},m} - \delta_{n-\hat{\mu},m}}{2a} + m\delta_{\alpha\beta}\delta_{m,n}. \tag{3.13}$$

Shortly after he published this action in [11], Wilson realized that it describes not one but 2^d degenerate fermions species, where d is the number of spacetime dimensions. [58] This can be understood by Fourier transforming the naïve fermion action. The Fourier transform of the fermion matrix is [34]

$$\tilde{D}_{\alpha\beta}(p) = \delta_{\alpha\beta} m + \frac{\mathrm{i}}{a} \sum_{\mu=1}^{4} [\gamma_\mu]_{\alpha\beta} \sin(a p_\mu) \tag{3.14}$$

The first term contributes to the diagonal part of the fermion operator. This term is constant and proportional to the mass of the fermions. The second term contributes to the offdiagonal part and has zeros at all corners of the Brillouine zone. A visualization can be found in figure 3.2. It has be shown, e.g. in [58], that in the low energy spectrum of the theory each of the zeros corresponds to a copy of the fermion one wants to describe. The additional species are called doublers.

A possible remedy is to add to the naïve fermion operator a discretization of the Laplace operator [33, 58]

$$\Box_\mu f = \frac{f(x+\hat{\mu}) - 2f(x) + f(x-\hat{\mu})}{2a^2}. \tag{3.15}$$

Then, the action reads [33]

$$S = a^4 \sum_{n\in\Lambda} \bar{\psi}(\gamma_\mu \Delta_\mu + m + ra \sum_\mu \Box_\mu)\psi, \tag{3.16}$$

where the parameter r is often set to 1. After writing out explicitly the discretized derivatives, the fermion matrix is [34, 58]

$$D_{\alpha\beta}(n,m) = \sum_{\mu=1}^{4} \frac{[\mathbb{1} - \gamma_\mu]_{\alpha\beta}\delta_{n+\hat{\mu},m} + [\mathbb{1} + \gamma_\mu]_{\alpha\beta}\delta_{n-\hat{\mu},m}}{2a} + \left(m + \frac{4}{a}\right)\delta_{\alpha\beta}\delta_{m,n}. \tag{3.17}$$

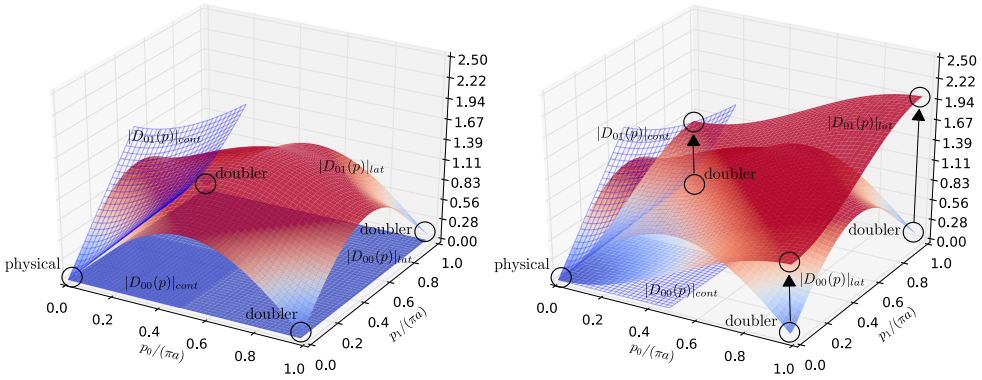

Figure 3.2 *– Doubler structure of the Wilson fermions in two dimensions. In the left picture the components of the massless naive fermion operator in momentum space is shown and compared to the continuum. It can be seen that the diagonal part is constant. This constant is proportinal to the quark mass. On the right hand side the naive fermion operator has been replaced by the Wilson fermion operator. The diagonal term has been modified by the Wilson term so that in three of the four corners it has a non-vansihing value with vanishing first derivatives. This genearates an effective fermion mass for thoose modes. The off-digaonal component has not been modified.*

The above operator is called Wilson operator. To see that it solves the doubling problem a Fourier transform is used again to arrive at [34]

$$\tilde{D}_{\alpha\beta}(p) = \delta_{\alpha\beta} m + \frac{\mathrm{i}}{a} \sum_{\mu=1}^{4} [\gamma_\mu]_{\alpha\beta} \sin(a p_\mu) + \frac{1}{a} \delta_{\alpha\beta} \sum_{\mu=1}^{4} (1 - \cos(a p_\mu)). \tag{3.18}$$

The second term is 0 for $p_\mu = 0$ but contributes $2l/a$ if l components of p are equal to π/a. [34] These contributions have the form of mass terms; a mass inversely proportional to the lattice spacing is added to each of the doublers. This decouples them in the continuum limit. The situation is visualized in figure 3.2. [34]

It should be noted that while the Wilson fermion operator decouples the doublers it also breaks chiral symmetry. [33] There is a no-go theorem by Nilesen and Ninomiya [59–61] which states that it is impossible to formulate a chiral lattice Dirac operator that avoids the fermion doubling and for which a reasonable set of conditions is fulfilled: It is impossible to have a fermion formulation that has a local, hermitian, translation invariant Hamiltonian on the lattice without either introducing an equal number of left handed and right handed species or violating continuum chiral symmetry on the lattice. [59]

To couple any of the fermion operators to gauge fields all terms in the operators have to be made gauge invariant. Terms in which all fermion fields are located at the same lattice site are already gauge invariant. Products of two fermion fields at different lattice sites can be made gauge invariant by inserting products of gauge links that connect both sites. [33] Since only couplings between two nearest neighbors appear in the free Wilson ferminon action, it is natural [3] to use for this purpose the single gauge link connecting the two neigbours. This procedure

[3] In principle any other path with the same start- and endpoint can be used. More extended paths are however not

results in [34]

$$D^{ab}_{\alpha\beta}(n,m) = \sum_{\mu=1}^{4} \frac{[\mathbb{1}-\gamma_\mu]_{\alpha\beta} U^{ab}_\mu \delta_{n+\hat{\mu},m} + [\mathbb{1}+\gamma_\mu]_{\alpha\beta} [U^\dagger_\mu]^{ab} \delta_{n-\hat{\mu},m}}{2a} + \left(m + \frac{4}{a}\right) \delta_{\alpha\beta}\delta^{ab}\delta_{m,n}. \quad (3.19)$$

The additional indices a and b compared to the free case are the color indices. Since the fermions transform according to the fundamental representation of $SU(3)$, on each lattice site and for each value of the Dirac indices there have to be 3 fermion fields labeled by a and b. [34]

Interacting Wilson fermions have cut-off effects of $\mathcal{O}(a)$. [33] These are significantly worse then the $\mathcal{O}(\alpha_s a^2)$ cutoff effects of the gauge action. The $\mathcal{O}(a)$ cutoff effects can be canceled by defining the clover-improved Wilson operator [33, 62]

$$D_{\boxplus} = D - a\frac{r c_{\boxplus}}{2}\sigma_{\mu\nu}F_{\mu\nu} \quad (3.20)$$

where $\sigma_{\mu\nu} = \frac{1}{2}\mathrm{i}[\gamma_\mu, \gamma_\nu]$, $c_{\boxplus}$ is an improvement coefficient and $F_{\mu\nu}$ is a suitably discretized version of the field strength tensor. [62] In section 3.2 it was motivated that $F_{\mu\nu}$ is related to the plaquette via eqn. (3.5):

$$P_{\mu\nu}(\vec{n}) = 1 + \mathrm{i}a^2 F_{\mu\nu} - \frac{a^4}{2}F_{\mu\nu}F_{\mu\nu} + \mathcal{O}(a^6) \quad (3.21)$$

Therefore, $\mathfrak{Im}\, P_{\mu\nu}(n)$ is a valid discretization of the field strength tensor. [33] However, this equation determines $F_{\mu\nu}$ at a point $n + \frac{1}{2}\hat{\mu} + \frac{1}{2}\hat{\nu}$. [33] It is advantageous to use a combination of four gauge field loops of minimal size located in the μ-ν plane and containing the point n. This combination in given by [62]

$$\begin{aligned}\boxplus_{\mu\nu}(n) = \frac{1}{4}\Big(& U_\mu(n)U_\nu(n+\hat{\mu})U^\dagger_\mu(n+\hat{\nu})U^\dagger_\mu(n-\hat{\mu}) \\ & - U^\dagger_\nu(n-\hat{\nu})U^\dagger_\mu(n-\hat{\mu}-\hat{\nu})U_\nu(x-\hat{\mu}-\hat{\nu})U_\mu(x-\hat{\mu}) \\ & + U_\nu(n)U^\dagger_\mu(n-\hat{\mu}+\hat{\nu})U^\dagger_\nu(n-\hat{\mu})U_\mu(n-\hat{\mu}) \\ & - U_\mu(n)U^\dagger_\nu(n+\hat{\nu}-\hat{\nu})U^\dagger_\mu(n-\hat{\nu})U_\nu(n-\hat{\nu})\Big). \end{aligned} \quad (3.22)$$

A graphical representation of this clover term can be found in figure 3.3. This expression determines $F_{\mu\nu}$ at a point n. Using this discretization of the field strength tensor one arrives at the clover improved Wilson fermion action [62]

$$D_{\boxplus} = D - a\frac{r c_{\boxplus}}{2}\sigma_{\mu\nu}\,\boxplus_{\mu\nu}\,. \quad (3.23)$$

The coefficient $c_{\boxplus}$ has to be tuned in such a way that the $\mathcal{O}(a)$ lattice artifacts cancel. The tree-level value of $c_{\boxplus}$ is 1 [33] and this value has been used for the Wilson fermion action in this work. In the quantized theory the coefficient $c_{\boxplus}$ receives quantum correction so that at leading order [63, 64]

$$c_{\boxplus} = 1 + \mathcal{O}(\alpha_s) \quad (3.24)$$

used in practice. The smearing techniques discussed in a later sections however have a similar effect.

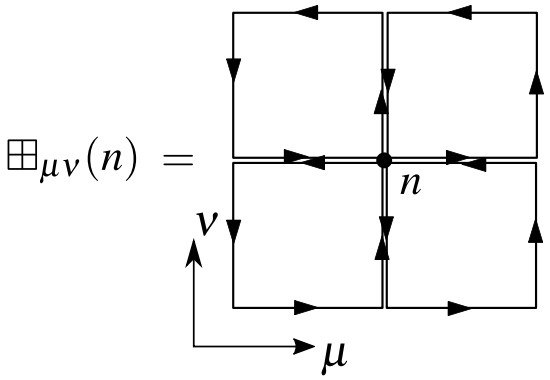

Figure 3.3 *– A graphical visualisation of the clover term $\boxplus_{\mu\nu}(b)$. It name is due to the similarity to four-leaved clover.*

where α_s is the strong coupling constant. Therefore, the tree-level improved action with $c_{\boxplus} = 1$ has lattice artifacts of order $\mathcal{O}(\alpha_s a)$. The quantum correction to $c_{\boxplus}$ can be computed either in a perturbative expansion [63, 64] or non-pertubatively [65] (vgl. [33]). It turns out, however, that the tree-level value of $c_{\boxplus}$ combined with a smearing procedure makes the $O(\alpha_s a)$ contributions very small and for many observables $\mathcal{O}(a^2)$ effects are numerically dominant. [66]

Apart from the Wilson fermion action, other fermion actions are in use. They get rid of (part of) the doublers in different ways. A very widespread alternative to Wilson fermions are staggered fermions, as introduced by Kogut and Susskind in [67] in a Hamiltonian setting and later extended in [68] to a Lagrangian setting. This formulation exploits the fact that the naïve Dirac operator has an exact d-fold degenerate spectrum. In the staggered formulation, this degeneracy is lifted, reducing the number of doublers. [33] A pedagogical introduction to staggered fermions can also be found in [34]. The staggered fermion operator has the form

$$D_{ab}(n,m) = a^4 \left(\sum_{\mu=1}^{4} \eta_\mu(n) \frac{U_\mu^{ab}(n+\hat{\mu})\delta_{m,n+\hat{\mu}} - U_\mu^{\dagger ab}(n-\hat{\mu})\delta_{m,n-\hat{\mu}}}{2a} + m\delta_{nm}\delta^{ab} \right). \tag{3.25}$$

The phases

$$\eta_\mu(n) = (-1)^{\sum_{\nu<\mu} n_\nu} \tag{3.26}$$

play a similar role then the γ-matrices appearing in the Wilson formulation. In figure 3.4 the staggered construction is illustrated. In the naïve fermion action the γ matrices result in a coupling of each spinor component on a given lattice site to exactly one spinor component on each neighboring site. This happens in such a way, that there are four disjoint set of spinor components containing one component per lattice site. These sets do not couple to each other and it turns out that they are described by the same action. Hence they describe four identical copies of the same fermion. Only one of the four copies is used in the staggered formulation. Therefore, the number of doublers is reduced by a factor of four as compared to the naïve case and the staggered operator in four dimensions describes four flavors of quarks. However, in contrast to the Wilson formulation, the Dirac components of the different quark flavors are

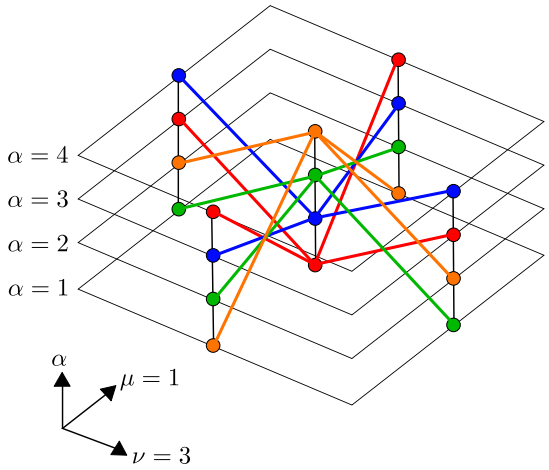

Figure 3.4 – *The construction of staggered fermions.*

distributed among the lattice sites; one flavor can be constructed from the fermion fields on one lattice hypercube.

Gauge fields can be smeared, before beeing used in the construction of the Direc operator, to decrease the numerical size of the cutoff effects [33]. Such smearing procedures aim at smoothing out short range fluctuations of the gauge fields which are strongly affected by the cutoff. [33] The simplest form of smearing, APE smearing, is to replace any gauge link $U_\mu(n)$ by a sum of itself and a staple $S_\mu(n)$, which is defined as [33]

$$S_\mu(n) = \sum_{\nu \neq \mu} U_\nu(n) U_\mu(n+\hat{\nu}) U_\nu^\dagger(n+\hat{\mu}) + U_\nu^\dagger(n-\nu) U_\mu(n-\nu) U_\nu(n-\nu+\mu). \tag{3.27}$$

The smeared link variables $U_\mu^{(\mathrm{APE})}(n)$ are defined as

$$U_\mu^{(\mathrm{APE})}(n) = (\alpha - 1) U_\mu(n) + \frac{\alpha}{d-1} S_\mu(\nu) \tag{3.28}$$

where d is the space-time dimension and α is a free parameter. [33] This procedure was originally proposed in [69]. The APE smearing has the drawback that the smeared links are not elements of $SU(3)$. [33] This can be alleviated by projecting the links back into $SU(3)$: First a unitary matrix

$$U'^{(\mathrm{APE})}_\mu(n) = \frac{U_\mu^{(\mathrm{APE})}(n)}{\sqrt{U_\mu^{(\mathrm{APE})\dagger}(n) U_\mu^{(\mathrm{APE})}(n)}} \tag{3.29}$$

which lies in $U(3)$ is constructed. Then the phase of the determinant is removed, so that

$$\hat{U}_\mu^{(\mathrm{APE})}(n) = U'^{(\mathrm{APE})}_\mu(n) \det{}^{-1/3} U'^{(\mathrm{APE})}_\mu(n) \tag{3.30}$$

is an element of $SU(3)$. [33] The main drawback of this procedure is that the back projection step is not not a differentiable operation. [33] Many update algorithms, including the HMC algorithm

used in most modern lattice QCD calculations, require differentiability. One possible remedy is to apply stout-smearing as proposed in [70]. In this procedure the staple $A_\mu(n)$ is combined with the gauge link $U_\mu(n)$ to form the combination[4] [70]

$$\Omega_\mu(n) = \rho S_\mu(n) U_\mu^\dagger(n). \tag{3.31}$$

This matrix is used to construct a hermitian and traceless matrix $Q_\mu(n)$ via [70]

$$Q_\mu(n) = \frac{\mathrm{i}}{2}(\Omega_\mu^\dagger(n) - \Omega_\mu(n)) - \frac{\mathrm{i}}{6}\,\mathrm{tr}(\Omega_\mu^\dagger(n) - \Omega_\mu(n)). \tag{3.32}$$

Since by definition $Q_\mu(n) \in \mathfrak{su}(3)$, it is possible to construct a new $SU(3)$ link variable by multiplying the old link variable with the exponential of $\mathrm{i}Q_\mu(n)$ so that [70]

$$U_\mu^{(\mathrm{stout})}(n) = \exp(\mathrm{i}Q_\mu(n)) U_\mu(n). \tag{3.33}$$

This method produces new gauge links in a differentiable fashion. Expanding each of the new link variables in terms of ρ reveals that, to leading order, the contributing terms are the same as the ones appearing in APE smearing. [70] To tune the amount of smearing, one can vary the value of ρ and/or apply several steps of smearing. [70] A possible problem arising with repeated application of smearing is that the radius of smearing in lattice units may potentially become large [71]. After one step of APE or stout smearing only links which are neighboring links of $U_\mu(n)$ appear in the smeared link $U_\mu^{(\mathrm{APE/stout})}(n)$. After two steps already next-to-neighbor links appear and so forth. In [71], a new method termed HYP smearing was proposed that allows, in a multi step procedure, a high level of smearing while still using only links residing inside the hypercubes that share the link $U_\mu(n)$. [71] An Illustration of HYP smearing can be found in figure 3.5. HYP smearing, again, is not a differentiable procedure since it uses projected sums of links and staples much like APE smearing. [33, 69, 71] A possible remedy is to use analytic projection as in stout smearing for the individual steps of HYP smearing. [72]. This form of smearing is called HEX smearing.

Combining clover improvement and smearing dramatically reduces the cut-off effects of fermions. [33] The effect of both measures on the Wilson operator can be seen in figure 3.6. In blue the original Wilson operator is shown. The fact that the eigenvalues do not touch the imaginary axis indicates additive mass renormalization. [33] Also one can see that the would-be chiral mode on the real axis in the non-doubler sector is not located close to where the low-lying eigenvalues pinch the real axis. [33] Both these defects are helped with smearing and clover improvement. [33] However, combining both procedures is much better then using any one of the two methods alone. [33]

3.4 The gauge action for QED

Some of the calculations in this thesis required a formulation of QED on the lattice, which is described in this section. The discussion in this section is base on [20]. In the case of QCD it is useful to formulate the theory in terms of the gauge fields $U_\mu(n)$ instead of the gauge potentials

[4] The method also works if ρ takes a different value for each summand in 3.27.

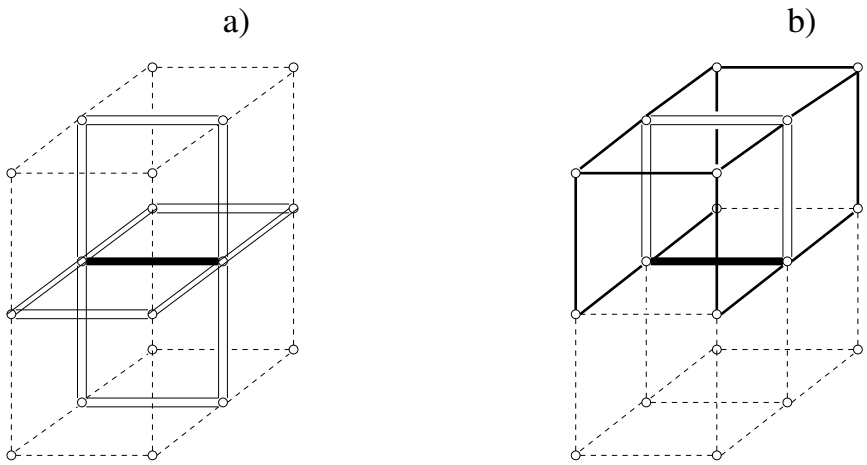

Figure 3.5 *– Illustration of the HYP smearing. The final smeared link which is the fat line in a) is constructed from the original link and staples depicted by double lines in a). These staples are again constructed from the original link and staples shown with solid lines in b). (Figure from [71])*

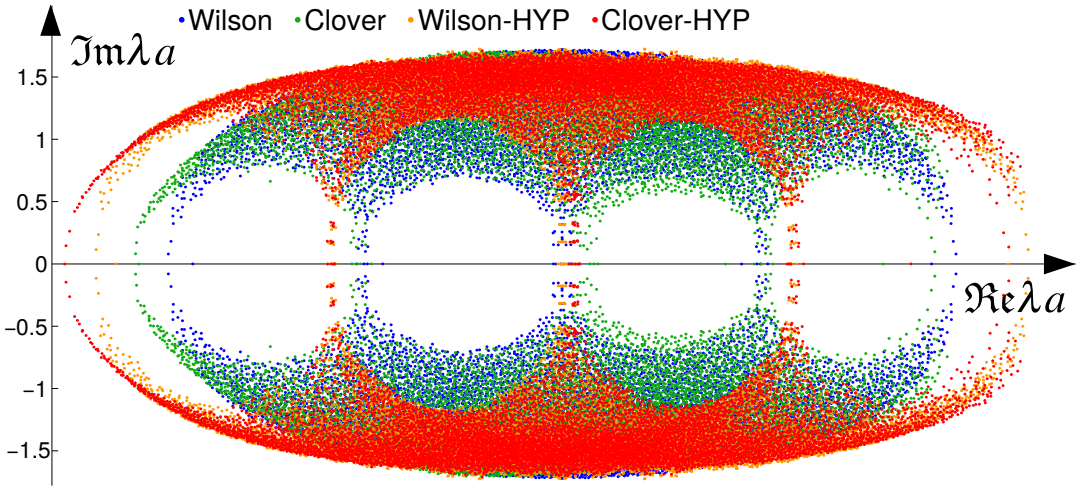

Figure 3.6 *– The effect of smearing and clover-improvement on the spectrum of the Wilson operator on a gauge configuration with topological charge one. (Quelle: [33], with modifications)*

$A_\mu(n)$. The reason for this is it allows to maintain exact gauge invariance even at finite lattice spacing, which was not possible in a formulation based on gauge potentials. In the case of QED, the gauge symmetry is abelian and no such complications arise that would prevent the usage of the gauge potentials. [20] Such a formulation based on the gauge potentials is called non-compact formulation.

Naïvely, one could use a discretization of the the action

$$S_\gamma^{\text{naive}} = \int \mathrm{d}^4x \sum_{\mu,\nu} (\partial_\mu A_\nu - \partial_\nu A_\mu)^2 \tag{3.34}$$

to define QED on a lattice. This is the usual action for the gauge part of QED in a infinite volume as it can be found in many textbooks (e.g. [1]), rotated to the euclidean case. QED in the continuum is symmetric under gauge transformations, which have the form

$$A_\mu(x) \longrightarrow A_\mu(x) - \partial_\mu \phi(x). \tag{3.35}$$

This, especially, includes transformations of the form

$$A_\mu(x) \longrightarrow A_\mu(x) - \partial_\mu c_\nu x_\nu \tag{3.36}$$

with a constant four-vector c. They shift the four components of the gauge field by a space-time independent amount c_μ, so that

$$A_\mu(x) \longrightarrow A_\mu(x) - c_\mu. \tag{3.37}$$

The lattice calculations described in this thesis are necessarily done in a finite volume, which is implemented by using periodic boundary conditions for the gauge potentials. The transformation in eqn. (3.37) remains a symmetry of the theory. In a finite volume it can, however, not be written as a gauge symmetry. From eqn. (3.36) follows that one would need to set $\phi(x) = c_\nu x_\nu$. Such a function is not compatible with the periodic boundary conditions. This peculiar symmetry needs special attention before one can add QED to a lattice computation. [73]

That this symmetry poses a problem can also be seen by rewriting the action in terms of the Fourier components $\tilde{A}_\mu(k)$ of the gauge potentials. By a standard computation (see e.g. [1]) it can be shown that the contribution of the momentum k to the action is

$$S(k) = \tilde{A}_\mu(k)(-k^2\delta_{\mu\nu} + k_\mu k_\nu)\tilde{A}^*_\nu(k). \tag{3.38}$$

This is a quadratic form defined by a 4×4 matrix per momentum k. These matrices are not invertible since

$$(-k^2\delta_{\mu\nu} + k_\mu k_\nu)k_\nu = 0. \tag{3.39}$$

This completely standard problem can be solved by gauge fixing. For example, in a ξ-gauge the analog to eqn. (3.38) reads [1]

$$S(k) = \tilde{A}_\mu(k)\left(-k^2\delta_{\mu\nu} + \left(1 - \frac{1}{\xi}\right)k_\mu k_\nu\right)\tilde{A}^*_\nu(k). \tag{3.40}$$

The matrices are now invertible with one notable exception: In the $k = 0$ case the matrix becomes the 0-matrix. It follows that the contribution of the momentum mode $k = 0$ is independent

form the value of $\tilde{A}_\mu(k)$. Since a constant shift is absorbed in the $k = 0$ mode, this is exactly the problematic contribution. Note that in the infinite volume the action can be written as

$$S = \int \frac{\mathrm{d}^4 k}{(2\pi)^4} S(k). \tag{3.41}$$

with $S(k)$ being the contribution of momentum k. The case $k = 0$ is a set of measure zero and therefore poses no problem. In a finite volume the allowed momenta are discrete and the action is a discrete sum of the form

$$S = \sum_k \frac{1}{(2\pi a)^4} S(k). \tag{3.42}$$

The case $k = 0$ is one of the terms contributing to this sum and hence can not be ignored. The modes of A_μ causing this problem are referred as zero modes.

From an intuitive perspective the problem arises because Gauss's law implies that it is impossible to have a periodic electric field of a point particle with a net charge that is continuous everywhere except at the location of the charge. [73, 74] The net charge Q in a volume Λ can be calculated via

$$Q = \int_\Lambda \mathrm{d}^3 x \, \vec{\nabla} \cdot \vec{E} = \int_{\partial\Delta} \mathrm{d}\vec{n} \cdot \vec{E} \tag{3.43}$$

assuming the field $\vec{E}$ is continuously differentiable. Because of periodicity the rightmost integral has to vanish. Consequently, the net charge in a box with periodic boundary is 0. [73, 74] The situation is illustrated in figure 3.7.

One approach to deal with the zero modes is not to integrate over them in the path integral. Following the notation in [20], this choice, applied in the Coulomb gauge, will be denoted as $\mathrm{QCD}_{\mathrm{TL}}$. It is implemented by forcing $\tilde{A}_\mu(0) = 0$. One should note that this is a modification of the path integral that is non-local both in space and time since it can be enforced by adding the term [20]

$$-\frac{1}{\xi^2} \sum_\mu \left(\sum_n A_\mu(n) \right)^2 \tag{3.44}$$

to the action. In the limit $\xi \to \infty$ this results in $\tilde{A}_\mu(0) = 0$. This term couples gauge fields at arbitrary distances and times and reflection positivity is violated. [20] In this theory the finite volume corrections to masses can be worked out [20]. An explicit formula for the finite volume mass correction of charged meson reads

$$\frac{M(L)}{M(\infty)} - 1 = -q^2 \alpha \frac{\varkappa}{M(\infty)L} \left[1 + \frac{1}{M(\infty)L} \left(1 - \frac{\pi}{2\varkappa} \frac{T}{L} \right) \right] + \mathcal{O}(1/L^3). \tag{3.45}$$

Here, $M(L)$ is the mesons mass at spatial lattice extend L, q is the meson's charge and α is the QED coupling constant. Formulas for other particles are given in [20]. The above formula does not only depend on the dimensionless combination ML but also on T/L which is also dimensionless and divergent in the $L \to \infty$ limit. In figure 3.8 the behavior of the finite volume correction for several values of T/L is shown. It is evident that at small L the corrections are large and strongly depend on T/L. In fact, for $L \to \infty$ with fixed T, a situation commonly arising when taking the

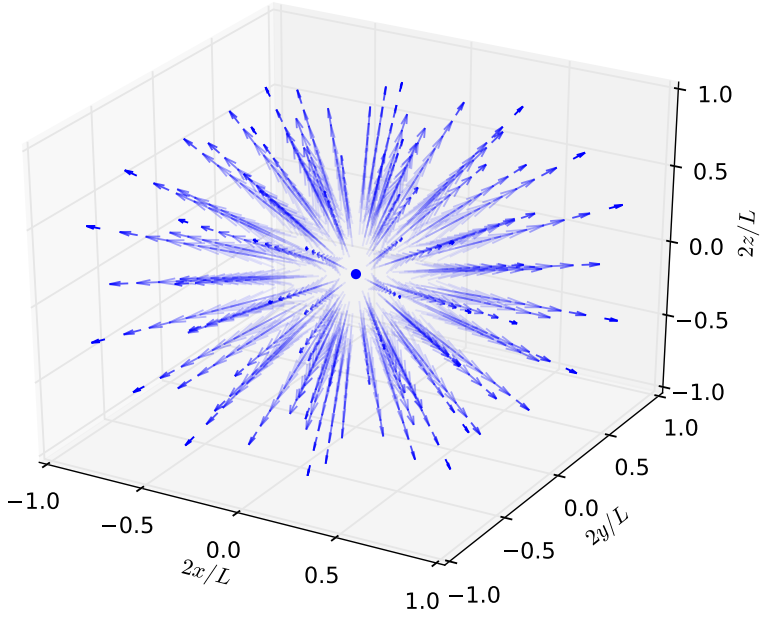

Figure 3.7 *– Electromagentic field of an electric point charge. It is impossible to make the electric field of a charged particle periodic and continous. A simple periodic continuation would make the field non-differentiable at the boundary. [73]*

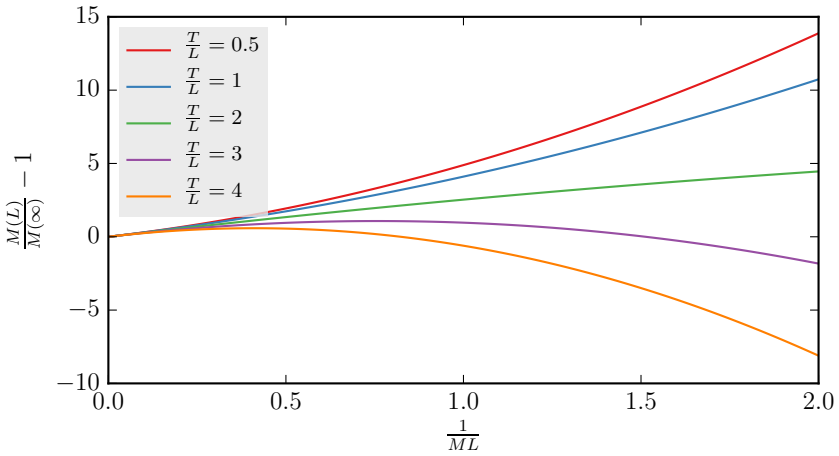

Figure 3.8 *– Finite volume correction to a scalar boson of initfinite-volume mass $M(\infty)$ in QCD_{TL} to order $\mathcal{O}(1/L^2)$ for $\alpha q^2 = 1$. The finite volume correction depends on the two dimensionless numbers ML and T/L.*

continuum limit in finite volume, they diverge. However, in practical lattice calculations T/L is of order $\mathcal{O}(1)$ and one can nevertheless perform a proper infinite volume limit. [20]

Hawakaya and Uno have proposed a different way to deal with the problem posed by zero modes. They suggested to remove the zero modes on all time slices separately. [74] This is done by enforcing [20]

$$\sum_{\vec{x}} A_\mu(t, \vec{x}) \text{ for all } t. \tag{3.46}$$

Again following the notation of [20], the resulting theory is called $\mathrm{QED_L}$. Eqn. (3.46) does only couple gauge fields at the same time slices. The finite volume correction for various particles have been worked out [20] and for the case of a scalar boson it reads

$$\frac{M(L)}{M(\infty)} - 1 = -q^2\alpha \frac{\kappa}{M(\infty)L}\left[1 + \frac{2}{M(\infty)L}\right] + \mathcal{O}(1/L^3). \tag{3.47}$$

The problematic term featuring T/L is absent in this expression.

Chapter 4

Numerical techniques

In this chapter I will briefly summarize some numerical techniques that where used for generating the gauge configurations used in this thesis. First, I will explain how the Grassman valued fermion fields are integrated out so that the path integral can be calculated with important sampling. Then, I will introduce the Metropolis algorithm. Afterwards, I will describe the hybrid monte carlo algorithm.

4.1 Integration of fermionic fields

The path integral for calculating $\langle O \rangle$ for an observable O in QCD, after regularization by a lattice, can be written as

$$\langle O \rangle = \frac{1}{Z} \int \mathcal{D}U \mathcal{D}\bar{\psi} \mathcal{D}\psi \; O \; \exp(-S_{\text{gauge}}(U) - \bar{\psi} D(U) \psi). \tag{4.1}$$

Here, $S_{\text{gauge}}(U)$ is a gauge action of choice, for example the Luescher-Weissz-action from eqn. (3.8) and $D(U)$ is a Dirac operator, for example the clover improved Wilson operator from eqn. (3.23). The partition function Z is defined as

$$Z = \int \mathcal{D}U \mathcal{D}\bar{\psi} \mathcal{D}\psi \; \exp(-S_{\text{gauge}}(U) - \bar{\psi} D(U) \psi), \tag{4.2}$$

the same integral as in eqn. (4.1) except that the observable in the integrand is missing. The symbol $\mathcal{D}\phi$ means

$$\mathcal{D}\phi = \prod_{n \in \Lambda} \mathrm{d}\phi(n) \tag{4.3}$$

for any field ϕ. The gauge fields $U_\mu(n)$ are elements of $SU(3)$ and $\mathrm{d}U(n)$ is the Haar measure. The fermion fields $\bar{\psi}$ and ψ are Grassmann numbers. Two Grassmann numbers θ_1 and θ_2 fulfill

$$\{\theta_1, \theta_2\} = 0 \,, \quad \theta_i^2 = 0 \tag{4.4}$$

and commute with any complex number. The concepts of differentation and integration can also be generalized to Grassmann numbers. [34]

Efficiently representing many Grassmann numbers on a Computer is difficult except in certain special cases. However, since the integrand in eqn. (4.1) is quadratic in the Grassmann valued fields, the integral can be carried out analytically. Doing so results in the expression

$$\langle O \rangle = \frac{1}{Z} \int \mathcal{D}U \; O \; \det D(U) \; \exp(-S_{\text{gauge}}(U)). \tag{4.5}$$

This path integral, containing only bosonic fields, is amendable to a numerical treatment by monte carlo methods. [34]

Historically, the evaluation of the determinant was challenging and calculations where done in the quenched approximation where $\det D(U)$ was neglected. [34] Within that approximation local update algorithms are reasonably efficient. In the following sections, in a first step the simplest such algorithm, the Metropolis algorithm, is explained. Then, the HMC algorithm, which allows to efficiently include the determinant and which builds on the Metropolis algorithm, will be introduced. The discussion is largely based on [34, 75].

4.2 The Metropolis algorithm and importance sampling

The path integrals of interest have the form

$$\langle O \rangle = \frac{1}{Z} \int \mathcal{D}U \, O \, \exp(-S(U)) \tag{4.6}$$

where $S(U)$ is real valued for every configuration of gauge fields U. The gauge fields have to be integrated over at every point of the lattice. A direct evaluation of the integral by a high-dimensional quadrature rule is not feasible. $1/Z \exp(-S(U))$, however, can be interpreted as a multivariate probability density function. If one can construct a process which samples gauge field configurations with this probability density, then the observable O can be calculated by

$$\langle O \rangle = \frac{1}{N} \sum_{i=1}^{N} O_i. \tag{4.7}$$

Here, N is the number of samples drawn from the distribution and O_i is the value of the observable O on the i-th sample. This method, which is called importance sampling, can be very efficient. The effectiveness of this methods curucially depends on the positivity of $\exp(-S)$ that gaurantees that no cancellations can occur. [34]

To sample from the correct distribution, Marcov chain monte carlo (MCMC) methods are often used. A given configuration U_i of gauge fields is evolved into a new configuration U_{i+1} by a process that depends only on U_i but not on the previous configurations $U_{i-1}, U_{i-2}, \ldots$. [34, 75]

A particularly simple MCMC algorithm is the Metropolis algorithm. In its most often used form it consists of the following steps:

i. Based on a configuration U_i, propose a new configuration U_i' which differs from U_i by a small modification. This proposal must be reversible, which means that the likelihood to propose U_i if U_i' would have been the initial configuration must be the same then the likelihood to propose U_i' given U_i as initial configuration. Furthermore, every configuration must be reachable in principle after many proposals.
ii. Calculate $S(U_i)$ and $S(U_i')$.
iii. Draw a random number r between 0 and 1. If $r < \exp(-S(U_i') + S(U_i))$, set $U_{i+1} = U_i'$ (accept), otherwise set $U_{i+1} = U_i$ (reject).

The above procedure is repeated to build up a chain of configurations $(U_1, U_2, \ldots, U_N)$. There is a large freedom in how to generate the proposals in step i. While in principle every procedure

that fullfills the mentioned conditions is admissible, the acceptance rate may depend strongly on the details of the procedure. If the proposals are badly choosen, the acceptance rate may be very low and the algorithm is very inefficient, as it gets stuck at one configuration for a long time. [34]

While the Metropolis algorithm is relatively easy to understand and imlpement, it is not very often used in lattice QCD calculations nowadays. For full QCD, local update algorithms like the Metroplois are not efficient because of the presence of the fermion determinant. A suitable algorithm will be explained in the next section. [34]

4.3 The hybrid monte carlo algorithm

Modern lattice QCD calculations make use of the hybrid monte carlo (HMC) algorithm. Here, for each real parameter in the configuration U a conjugate variable Π called momentum is defined. One also defines a fictitious Hamiltonian

$$\mathrm{H} = \frac{1}{2}\Pi^2 + S(U) \tag{4.8}$$

not to be confused with the physical Hamiltonian. The expectation value of an observable O can be written as

$$\langle O \rangle = \frac{\int \mathcal{D}U\, O\, \exp(-S)}{\int \mathcal{D}U\, \exp(-S)} = \frac{\int \mathcal{D}U \mathcal{D}\Pi\, O\, \exp(-\frac{1}{2}\Pi - S)}{\int \mathcal{D}U \mathcal{D}\Pi\, \exp(-\frac{1}{2}\Pi - S)} = \frac{\int \mathcal{D}U \mathcal{D}\Pi\, O\, \exp(-\beta \mathrm{H})}{\int \mathcal{D}U \mathcal{D}\Pi\, \exp(-\beta \mathrm{H})} \tag{4.9}$$

with $\beta = 1$. The last expression is the expectation value of O in a canonical ensemble with the Hamiltonian H. The HMC algorithm consists of the following steps:

i. Generate new momenta distributed according to the probability density function $\exp(-\frac{1}{2}\Pi^2)$.

ii. Evolve the fields U and momenta Π according to Hamilton's equations

$$\dot{U} = \frac{\partial \mathrm{H}}{\partial \Pi} \quad \text{and} \quad \dot{\Pi} = -\frac{\partial \mathrm{H}}{\partial U} \tag{4.10}$$

for a fixed time interval Δt.

iii. Calculate the change in the energy ΔE along the trajectory. Accept the new configuration with probability $\exp(-\Delta E)$

Step ii. evolves the system in an microcanonical ensamble with a fixed energy E. Carrying out this step exactly would in principle be enough. [76]. However, in practice, the time evolution is performed using some numerical integrator that produces a small error. Therefore, the integration is embedded in a MCMC sampling of a canonical ensemble. For this procedure to be correct, it is acceptable that the numerical integration is inexact as long as it is exactly reversible. [34]

One important advantage of the HMC algorithm over local monte carlo algorithms, like the plain Metropolis agorithm, is that it allows to make large non-local steps in in the proposal step. In the case of pure gauge theory this is not beneficial because the action is local. However, if fermions are present, the det D-factor is non-local. Therefore, after a local update one would need to calculate a large determinant. If this non-loacl calculation is necessay, it is much more efficient to have the proposal change the field configuration globally. [34]

Even with global proposals, it is still prohibitvely expensive to calculate the entire fermion determinant for every update. This motivates the introduction of pseudofermions. These are based on the similarity between the Gaussian integrals over complex and Grassmann valued fields. Namely, it has been shown that [34]

$$\int d^N\bar{\psi}d^N\psi \exp(-\bar{\psi}M\psi) = \det M, \tag{4.11a}$$

$$\int d^N\phi^\dagger d^N\phi \exp(-\phi^\dagger M\phi) = \pi^N |\det M|^{-1}. \tag{4.11b}$$

Here $\bar{\psi}$ and ψ are Grassmann variables and ϕ are complex numbers. In the case of QCD with two generate flavors the Grassmann integration over the fermion fields produces a factor $\det D$ for each flavor. To calculate $\langle O\rangle$

$$\langle O\rangle = \frac{1}{Z}\int \mathcal{D}U\, O \det{}^2 D(U)\ \exp(-S_{\text{gauge}}(U)). \tag{4.12}$$

has to be evaluated. The square of the determinant can be rewritten as

$$\det{}^2 D(U) = \det D(U) \det D(U) = \det D(U) \det D^\dagger(U) = \det(D(U)D^\dagger(U)). \tag{4.13}$$

Using this identity and the analogy between bosonic and fermionic Gaussian integrals from eqns. (4.11a) and (4.11a), the path integral can be rewritten as

$$\langle O\rangle = \frac{1}{Z}\int \mathcal{D}U\mathcal{D}\phi\mathcal{D}\phi^\dagger\, O \exp(-S_{\text{gauge}}(U) - \phi^\dagger(D(U)D^\dagger(U))^{-1}\phi). \tag{4.14}$$

The advantage of this formulation is that there is no need to calculate a determinant. Instead one only has to compute $(DD^\dagger)^{-1}\phi$ which is much cheaper. [34]

The hybrid monte carlo algorithm must be modified slightly to include the psudofermion fields [34]:

i. Randomly generate pseudofermion fields ϕ distributed according to the probability density

$$\exp(-\phi^\dagger(D(U)D^\dagger(U))^{-1}\phi) \tag{4.15}$$

on the initial gauge field configuration.

ii. Randomly generate new momenta distributed according to the probability density function $\exp(-\frac{1}{2}\Pi^2)$.

iii. Evolve the fields U and momenta Π according to Hamilton's equations

$$\dot{U} = \frac{\partial \mathrm{H}}{\partial \Pi} \quad \text{and} \quad \dot{\Pi} = -\frac{\partial \mathrm{H}}{\partial U} \tag{4.16}$$

for a fixed time interval Δt with the Hamiltonian

$$\mathrm{H} = \frac{1}{2}\Pi^2 + S(U) + \phi^\dagger(D(U)D^\dagger(U))^{-1}\phi. \tag{4.17}$$

iv. Calculate the change in the Energy ΔE along the trajectory. Accept the new configuration with probability $\exp(-\Delta E)$.

The algorithm described above is applicable only for an even number of degenerate quark flavors. This restriction can be circumvented by the rational hybrid monte carlo (RHMC) algorithm. [77] It makes use of the fact that a powerlaw function in a given range can be well approximated by a sum of rational functions

$$x^{\gamma} \approx \alpha_0 + \sum_{i=1}^{k} \frac{\alpha_i}{x + \beta_i} \tag{4.18}$$

where α_i and β_i depend on γ, the order of the approximation, and the approximation range. There are algorithms [78] to determine appropriate α_i and β_i so that the approximation is accurate up to a certain error. Using this approximation, a single fermion species can be realized by employing

$$\phi^{\dagger}(D(U)D^{\dagger}(U))^{-1/2}\phi \approx \alpha_0\phi^{\dagger}\phi + \sum_{i=1}^{k} \alpha_i\phi^{\dagger}(D(U)D^{\dagger}(U) + \beta_i)^{-1}\phi. \tag{4.19}$$

The inversion of the shiftet operator $(D(U)D^{\dagger}(U) + \beta_i$ can be efficienty done for multiple values of β_i using a multishift algorithm. [79, 80] The method above is also used to reduce the number of flavors in the case of staggered fermions from four to one. There is ample evidence that this is procedure is correct. [81–98][1] Some authors disagree with this, see e.g. [99–101].

[1] Collection of references from [33], see there for a discussion.

Chapter 5

Analysis strategies

In this chapter I will explain common analysis methods that where used in several projects described in this thesis. Firstly, I will explain the statistical treatment and the estimation of statistical uncertainties. Then, I will describe how systematic uncertainties have been estimated. This is followed by a discussion of the spectral decomposition of correlation functions. After that, the results are applied to derive the Feynman-Hellman theorem which was used to extract matrix elements from two-point functions. Then, I describe the use of the Kolmogorov-Smirnov test to determine optimal fitranges. Finally, I will explain the method used for correlated fits that takes uncertainties on independent variables into account.

5.1 Statistical treatment

This section explains the statistical treatment of monte carlo data. A overview on the topic can be found in [75, 102] on which this section is based. The mean value of an observable O can be calculated via the sample average

$$\langle O \rangle = \frac{1}{N} \sum_{i=1}^{N} O_i + \mathcal{O}(1/N) \tag{5.1}$$

where O_i is the measured value of the observable on each configuration and N is the number of configurations. The sample average, the right hand side of eqn. (5.1) without the $\mathcal{O}(1/N)$ terms, will be denoted as $\bar{O}$. Due to the nature of the calculations, the expectation value is determined only up to an statistical uncertainty ΔO. The magnitude of this uncertainty scales proportional to $\sqrt{1/N}$. However, the error can not simply be estimated by the sample standard deviation. This would be the correct procedure if all individual samples O_i would be completely independend. [102] One of the features of MCMC is, however, that a new configuration is always based on a previous one. Therefore, the measurements are not independent and the naïve estimate of the uncertainty fails. [33, 75, 102]

Configurations that are separated from each other by a large number of updates are almost independent. The characteristic timescale after which configurations become independent is called autocorrelation time. To determine it, the sample autocorrelation function

$$C(t) = \frac{1}{N} \sum_{k=1}^{N-t} (O_k - \overline{O})(O_{k+t} - \overline{O}) \tag{5.2}$$

and its normalized version

$$\Gamma(t) = \frac{C(t)}{C(0)} \tag{5.3}$$

can be used. In [102], a formula for the estimation of the error of the auto correlation function is presented:

$$(\Delta\Gamma)^2 \approx \sum_{k=1}^{k_{\max}} (\Gamma(k+t) + \Gamma(k-t) - 2\Gamma(k)\Gamma(t)), \tag{5.4}$$

Here, $t_{\max}$ has to be sufficiently high. The asymptotic late time behavior of the autocorrelation function is expected to behave as

$$\Gamma(t) \propto \exp(-t/\tau_{\exp}). \tag{5.5}$$

The autocorrelation function at late time is difficult to estimate; it is compatible with zero after very few autocorrelation times in almost all cases. Frequently, at early times the deviation from the exponential behavior is significant and a reliable extraction of $t_{\exp}$ is not possible. It is therefore useful to define a closely related quantity, the integrated autocorrelation time τ_{int}. It can be estimated by the sum

$$\tau_{\text{int}}^{W} = \frac{1}{2} + \sum_{t=1}^{W} \Gamma(t). \tag{5.6}$$

If the autocorrelation function decays purely exponentialy with a decay constant $\tau_{\exp}$, it can be shown that

$$\tau_{\text{int}} = \int_0^{+\infty} \mathrm{d}t \ \exp(-t/\tau_{\exp}) \tag{5.7}$$

where

$$\tau_{\text{int}} = \lim_{W\to\infty} \tau_{\text{int}}^{W}. \tag{5.8}$$

When the integral is cut off at a time W, eqn. (5.6) can be seen as the Riemann sum approximating[1] this integral. In practice this limit is seldom taken as the contributions from late times to the sum in eqn. (5.6) would be exponentially small and would introduce large statistical noise. A optimal value for W is complicated to obtain; a sophisticated autowindowing procedure was proposed in [102]. Often, however, it suffices to cut of the sum at the first instance where the estimate of $\Gamma(t)$ becomes negative. It can be shown that the correct formula for $(\Delta O)^2$ is

$$(\Delta O)^2 = \frac{2\tau_{\text{int}} + 1}{N-1}(\overline{O^2} - \overline{O}^2) \tag{5.9}$$

This means that a large autocorrelation time decreases the effective number of independent configurations. [102]

Eqn. (5.9) is only applicable to quantities that can be directly measured on each configuration, although related formulae for derived quantities exist. However, there is a general method with which errors can be calculated in these cases. It is known as the statistical bootstrap [103]. When performing a monte carlo calculation, configurations are sampled from a certain target

[1] However this sum converges only if the time increments become small compared to the characteristic timescale τ. Therefore convergence is only reached if $\tau \to \infty$. This is neither the case nor is it desirable.

distribution. Suppose N configurations have been sampled. Furthermore, assume K observables have been measured on each of these configurations and O_i^k is the k-th observable on the i-th configuration. $f(\langle O^1\rangle, \langle O^2\rangle, \ldots, \langle O^k\rangle)$ is a derived observable. One way to estimate the uncertainty of f would be to perform b independent monte carlo computations and take the spread of these as the statistical uncertainty of f. In most cases this would not be practical. Instead, it can be assumed that the sample distributions of the O^k are the best known approximations to their true distributions. According to the bootstrap procedure one resamples from the sample distributions and takes this as an approximation to sampling from the true distributions. M bootstrap samples are generated by drawing N times randomly from the N configurations with replacement and the bootstrap mean is calculated for each observable and for each of the M bootstrap samples by averaging over the N randomly resampled configurations. On the m-th bootstrap sample the bootstrap average of the observables O^k is called $O^{k(m)}$. Out of these one can construct M bootstrap values for f according to

$$f^{(m)} = f(O^{1(m)}, O^{2(m)}, \ldots, O^{K(m)}). \tag{5.10}$$

Then, the statistical uncertainty of f is

$$(\Delta f)^2 = \frac{1}{M}\sum_m f^{(m)2} - \frac{1}{M^2}\left(\sum_m f^{(m)}\right)^2. \tag{5.11}$$

As the number of possible distinct bootstrap samples is very large, M can be chosen very large. In this work usually a value of 2000 is employed. The bootstrap method is used for the estimation of statistical uncertainties throughout this work. [75]

In the presence of autocorrelation the bootstrap method underestimates the uncertainties. This can be avoided by performing a blocking prior to the bootstrap procedure without changing the rest of the method. This means that prior to resampling, L consecutive configurations are combined into blocks. Then, the M bootstrap samples are generated by sampling randomly with replacement N/L blocks instead of sampling individual configurations. The method is expected to be accurate if $L \gtrsim \tau_{\text{int}}$. [102] The correct blocksize can also be estimated by varying L and calculating the resulting bootstrap uncertainty. A good value for L is reached if the uncertainty does not increase by further increasing L. [102]

5.2 Systematic uncertainties

Calculations are necessarily done using finite lattices. The algorithms used in this work guarantee that, up to statistical uncertainties, the results are exact for the given set of parameters and a given lattice size. However, results in the limits of vanishing lattice spacing and infinite lattice volumes can not be directly obtained; both limits imply that the number of degrees of freedoms tend to infinity. Therefore, calculation with different lattice spacings and volumes are extrapolated to the two limits. The interplay between the two limits is illustrated in figure 5.1. [33]

The continuum limit has to be taken along a trajectory in the parameter space leading to a second order critical point at which the correlation length in lattice units diverges. Because of the divergence of the correlation length the details of the action become irrelevant and coninuum

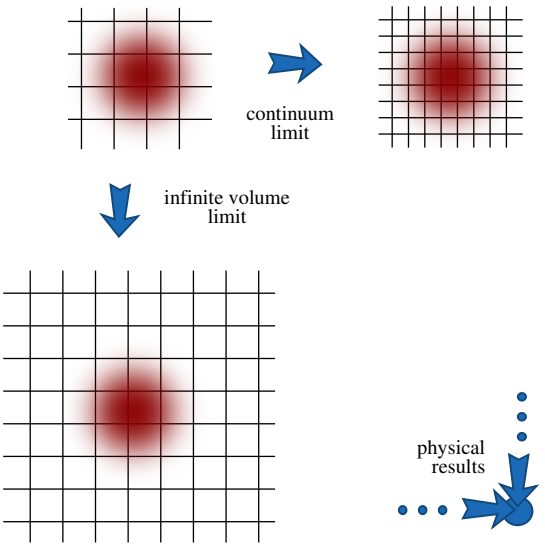

Figure 5.1 *– Overview of the limits necessary in a lattice calculation. Lattice calculations are necessarily done with a finite number of lattice sites. Therefore, both the continuum and the infinite volume limits must be taken. The red blob indicates a typical correlation length.*

physics emerges. It is convenient to choose a trajectory on which $N-1$ observables are constant. Here, N is the number of fundamental parameters of the action. It is common practice to use the gauge coupling β to determine the lattice spacing. Then, the continuum limit lies at $\beta \longrightarrow 0$. [34]

In case of QCD, it is not known beforehand which values for the quark mass parameters are correct at a given β. Therefore, it is useful to perform several calculations with different values for these parameters. Preferably, these parameters are chosen close to the desired trajectory in parameter space. This allows to inter-/extrapolate to this trajectory without performing new calculations. This can be done by introducing fit functions that interpolate or extrapolate between simulations at different parameters. The choice of the fit functions introduces systematic uncertainty that must be estimated. Reasonable choices for a fit functions would be e.g. a Taylor expansion arround the physical point or a fit function based on leading order chiral perturbation theory. [17, 20]

The following sources of systematic uncertainties are important for many lattice calculations:

- Uncertainties originating from the continuum extrapolation.
- Uncertainties originating from the infinite volume extrapolation.
- Uncertainties from the interpolation or extrapolation of simulation parameters.

In this work the Historam method, which was introduced in [17, 20], is used to deal with these uncertainties. To apply this method, one identifies all instances where possible higher orders terms where neglected. For example, if a quantity X has formally leading order a^2 correction, one can determine $X(a^2)$ at different values of a and fit $X(a^2)$ with the ansatz $c_0 + c_1 a^2$. To estimate the effects of even higher order terms, one has to find several equally well justifiable procedures that have the same leading order behavior but differ in the higher orders. In the case

of the continuum limit it is customary e.g. to vary the number of lattice spacings included in the above fits. One then performs analyses with all thinkable combinations of these procedures. The results for a specific quantity will be scattered around a mean which will be taken as the final estimate of the quantity. The spread of the distribution is an estimate of the systematic uncertainty. The distribution can be nicely visualized with a histogram, which lead to the name of the method. [17, 20]

It might happen that not all fits entering the histogram method are working equally well. Some might have an excellent fit quality while others may have a very bad one. Fits with a poor fit quality do not describe the data very well and hence should not have a big influence on the final estimate. It is therefore natural to weight the fits with some measure of fit quality. In this work, two weighting methods have been used. The first method is the fit quality or p-value: In a χ^2 fit, the quantity to be minimized is the quadratic sum of residuals, often called χ^2-value. It can be shown, under reasonable assumptions, that the χ^2-values are distributed according to a χ^2 distribution. A χ^2 distribution is fully specified by the number n_{dof} of degrees of freedoms of the fit. The quality of fit Q is given as

$$Q = 1 - \mathrm{cdf}(n_{\mathrm{dof}}, \chi^2) \tag{5.12}$$

where χ^2 is the quadratic sum of residuals of the fit and cdf is the cumulative distribution function of the χ^2 distribution with n_{dof} degrees of freedom. If the fit function perfectly describes the data, Q is distributed uniformly between 0 and 1. [17, 20] The second is a weighting method based on the Akaike information criterion (AIC). The AIC weight of a fit is is given as

$$w_{\mathrm{AIC}} = \exp\left(-\frac{1}{2}(\chi^2 + 2p)\right) \tag{5.13}$$

where p is the number of paramters of the fit function. [20]

5.3 Spectral decomposition of correlation functions

The following discussion is based on [34].

An important feature of any quantum field theory is its spectrum. Correlation functions can be decomposed in terms of the eigenstates of the Hamiltonian. This decomposition is necessary to extract masses from correlation functions. Also it is required for the derivation of the Feynman-Hellman theorem presented in the next section. The lattice regulated Euclidean path integral involves (anti-)periodic boundary conditions. Hence the euclidean correlation function of the operators A and B with time separation t is

$$\langle B(t)A(0)\rangle_T = \frac{\mathrm{tr}\left[e^{-(T-t)H}Be^{-tH}A\right]}{\mathrm{tr}\left[e^{-TH}\right]}. \tag{5.14}$$

Expanding this expression in terms of the eigenstates $\mid n\rangle$ of the Hamiltonian yields

$$\mathrm{tr}\left[e^{-(T-t)H}Be^{-tH}A\right] = \sum_{n,i,j} e^{-(T-t)E_i}e^{-tE_j}\langle n \mid i\rangle\langle i \mid B \mid j\rangle\langle j \mid A \mid n\rangle \tag{5.15a}$$

$$\mathrm{tr}\left[e^{-TH}\right] = \sum_{n} e^{-TE_n}\langle n \mid n\rangle \tag{5.15b}$$

Using the normalization $\langle i \mid j \rangle = \delta_{ij}$, the above expressions simplify to

$$\mathrm{tr}\left[e^{-(T-t)H} B e^{-tH} A\right] = \sum_{i,j} e^{-(T-t)E_i} e^{-tE_j} \langle i \mid B \mid j \rangle \langle j \mid A \mid i \rangle \tag{5.16a}$$

$$\mathrm{tr}\left[e^{-TH}\right] = \sum_{n} e^{-TE_n} \tag{5.16b}$$

The last expression is the partition function of a grand canonical ensemble with inverse temperature[2] $1/(aN_t)$, spatial volume $a^3 N_t^3$ and chemical potential $\mu = 0$. Correlation functions at zero temperature can be obtained in the limit $T \longrightarrow \infty$. In that limit it can be safely assumed that

$$\mathrm{tr}\left[e^{-(T-t)H} B e^{-tH} A\right] \approx \sum_{j} e^{-(T-t)E_0} e^{-tE_j} \langle 0 \mid B \mid j \rangle \langle j \mid A \mid 0 \rangle, \tag{5.17a}$$

$$\mathrm{tr}\left[e^{-TH}\right] \approx e^{-TE_0}. \tag{5.17b}$$

Therefore,

$$\langle B(t)A(0) \rangle = \lim_{T\to\infty} \langle B(t)A(0) \rangle_T = \sum_{j} e^{-t(E_j - E_0)} \langle 0 \mid B \mid j \rangle \langle j \mid A \mid 0 \rangle. \tag{5.18}$$

The quantities $\Delta E_j = E_j - E_0$ are the measurable energies relative to the vacuum energy. In practice, it is customary to have N_t at least as large or larger then N_s. Therefore, the finite volume effects introduced by the finite spatial volume usually dominate the finite temperature effects caused by the temporal lattice extend. [34]

Eqn. (5.18) can be used to extract the mass M_X of a particle X from euclidean correlation functions of interpolating operators A and B. A and B must be chosen to create and destroy a particle of type X. In practice, it is difficult to find interpolating operators that create or destroy exclusively the particle X. In many cases, it is possible, however, to find operators that create and destroy a multitude of states of which the particle X at rest is the lightest one. In such cases, the late time behavior of eqn. (5.18) is

$$\langle B(t)A(0) \rangle \xrightarrow[t\to\infty]{} e^{-M_X t} \langle 0 \mid B \mid X \rangle \langle X \mid A \mid 0 \rangle \tag{5.19}$$

where $\mid X \rangle$ is the state containing one particle of type X. For finite T, the situation is complicated by the periodicity of the lattice: There is another contribution to the correlator, with the asymptotic behaviour [33]

$$\langle B(t)A(0) \rangle \xrightarrow[T-t\to\infty]{} e^{-M_{\tilde{X}}(T-t)} \langle 0 \mid A^\dagger \mid \tilde{X} \rangle \langle \tilde{X} \mid B^\dagger \mid 0 \rangle \tag{5.20}$$

where $\tilde{X}$ is the lowest lying state that is created/destroyed by the adjoint operators of A and B. [33] For the meson operators used in this thesis the forward and the backward propagating parts are identical and the correlation function $C_X(t)$ can be written as

$$C_X(t) = a_X \cosh\left(-M_X(t - T/2)\right) \tag{5.21}$$

[2] Here there is potential for confusion due to the notation. The inverse temperature is often written as β which is already used as a parameter specifying the gauge coupling. To add to the confusion this β appears in the exponential of the action much like a temperaure appears in the exponential of the hamiltonian

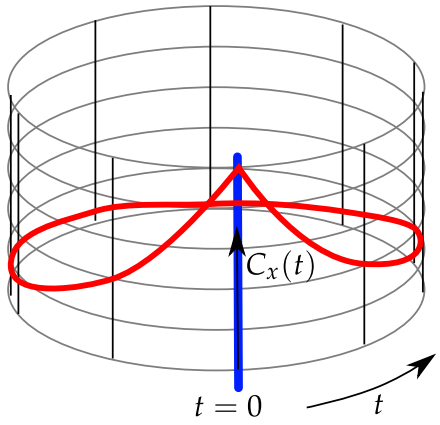

Figure 5.2 *– Illustration of the periodic behaviour of correlation function around.*

In order for only the lightest state to contribute, the correlation function has to be evaluated at a time that is sufficiently late for the forward propagating contribution of the excited states to be suppressed but not so late that the backward propagating excited states become relevant. In the free case, the propagation can wrap multiple times around the temporal direction of the lattice resulting in

$$C_X(t) = a_X \left[e^{-M_X t} + \sum_{n=1}^{\infty} e^{-M_X(nT+t)} + e^{-M_X(T-t)} + \sum_{n=1}^{\infty} e^{-M_X(T+nT-t)} \right]. \tag{5.22}$$

The infinite sums can be factored out leading to the expression

$$C_X(t) = a_X \left[\sum_{n=0}^{\infty} e^{-M_X nT} \right] \left[e^{-M_X t} + e^{-M_X(T-t)} \right] \tag{5.23}$$

An illustration of the behavior of such a correlation function can be found in figure 5.2. The situation is similar for baryons. There, however, the backward propagating states acquire a negative sign. [34] The correlation function shows the same behavior except that the cosh is replaced by a sinh:

$$C_X(t) = a_X \frac{e^{-M_X T/2}}{1 - e^{-M_X T}} \sinh\left(-M_X(t - T/2)\right) \tag{5.24}$$

The forward and backward propagating states are not necessarly the same. [34]. This can be mitigated by instead considering

$$\hat{C}_X(t) = \frac{1}{2}(C_X(t) - C_X(T - t)). \tag{5.25}$$

When calculating the correlation function numerical, the fermion fields have been integrated out. Therefore, it is not possible to put fermionic observables in front of the exponential in the path integral. One can analytically solve the generalized fermionic gaussian integral [34]

$$\int \mathcal{D}\bar{\psi}\mathcal{D}\psi \; \exp(\bar{\psi} D \psi + \bar{\eta}\psi + \bar{\psi}\eta) \propto \det D \exp(-\bar{\eta} D^{-1} \eta). \tag{5.26}$$

From this expression, Wicks theorem follows [34], which states that

$$\langle \bar{\psi}_{i_1} \psi_{j_1} \dots \bar{\psi}_{i_n} \psi_{j_n} \rangle = (-1)^n \langle \sum_\sigma \text{sign}(\sigma) (D^{-1})_{i_1, j_{\sigma(1)}} \dots (D^{-1})_{i_n, j_{\sigma(n)}} \rangle. \tag{5.27}$$

One can use this theorem to express fermionic expectation values as gauge field averages over inverses of the fermion matrix. [34]

5.4 The Feynman Hellmann theorem

The Feynman Hellmann theorem [12–15] relates matrix elements of eigenstates of the Hamiltonian to derivatives of their masses. Here, this theorem is proven for derivatives with respect to quark masses. The derivation is based on the one presented in [104]. For reasons of simplicity, the case of the nucleon is considered, although the theorem holds for all bound states. Throughout the derivation, all quantities are understood to be in lattice units. It is assumed that

$$S_F = \bar{\psi}(m_q \mathbb{1} + M)\psi \tag{5.28}$$

where M does not depend on the quark masses m_q, like in the continuum.

The mass of the ground state of the nucleon is defined, as discussed in the last section, by the late time behavior of correlation functions of nucleon operators. For the purpose of the derivation, the effective mass

$$m_{\text{eff}}(t) = \frac{1}{\delta t} \log \frac{C(t)}{C(t + \delta t)}. \tag{5.29}$$

is used to extract the late time behavior. Here, δt is a small shift in time often taken to be one lattice unit. $C(t)$ is the nucleon two point function

$$C(t) = \langle N(t) \bar{N}(0) \rangle. \tag{5.30}$$

and $\bar{N}$ and N are interpolating operators that create or destroy a state containing a nucleon and exited states. The derivative of the effective mass with respect to the quark mass m_q is

$$\partial_{m_q} m_{\text{eff}}(t) = \frac{1}{\delta t} \left[\frac{\partial_{m_q} C(t)}{C(t)} - \frac{\partial_{m_q} C(t + \delta t)}{C(t + \delta t)} \right]. \tag{5.31}$$

Consequently, it is sufficient to find the derivative of the correlation function.

In the path integral formalism the two point correlation function can be written as

$$C(t) = \langle N(t) \bar{N}(0) \rangle = \frac{1}{Z} \int \mathcal{D}U \mathcal{D}\psi \mathcal{D}\bar{\psi}\, N(t) \bar{N}(0)\, \exp\left(-m_q \sum_x \bar{\psi}(x)\psi(x) - \bar{\psi} M \psi - S_G \right). \tag{5.32}$$

After introducing the shorthand notation

$$Q(t) = \sum_x \bar{\psi}(t, \vec{x})\psi(t, \vec{x}) \tag{5.33}$$

its derivative is

$$\partial_{m_q} C(t) = \sum_{\hat{t}} \left[-\langle N(t) Q(\hat{t}) \bar{N}(0) \rangle + \langle N(t) \bar{N}(0) \rangle \langle Q(\hat{t}) \rangle \right]. \tag{5.34}$$

It consists of one contribution from the derivative of the exponential in the path integral and one contribution from the derivative of the partition function Z. The first is called a connected contribution and the later is call a disconnected contribution.

To relate these expressions to matrix elements their spectral decomposition must be studied. For the connected part it is convenient distinguish several cases: $t > \hat{t} > 0$, $\hat{t} > t$, $t = \hat{t}$ and $\hat{t} = 0$.

The most important case is the first where the spectral decomposition is

$$\langle N(t) Q(\hat{t}) \bar{N}(0) \rangle = \frac{\sum_{i,j,k} e^{-E_i(T-t)} N_{ij} e^{-E_j(t-\hat{t})} M_{jk} e^{-E_k \hat{t}} \bar{N}_{kj}}{\sum_i e^{-E_i T}}. \tag{5.35}$$

For convenience

$$N_{ij} = \langle i \mid N \mid j \rangle \tag{5.36a}$$
$$\bar{N}_{ij} = \langle i \mid \bar{N} \mid j \rangle \tag{5.36b}$$
$$M_{ij} = \langle i \mid \bar{q} q \mid j \rangle \tag{5.36c}$$

where introduced. To take the large T limit, it is useful to distinguish the cases $j = k$ and $j \neq k$ so that the expression becomes

$$\langle N(t) Q(\hat{t}) \bar{N}(0) \rangle = \sum_j N_{0j} e^{-(E_j - E_0)t} M_{jj} N_{j0} + \sum_{j \neq k} N_{0j} e^{-(E_j - E_0)t} M_{jk} e^{-(E_k - E_j)\hat{t}} N_{k0}. \tag{5.37}$$

Upon assuming that in the first term only the ground state in the nucleon channel, with index n and energy E_n, contributes and upon summing over all $\hat{t}$ between 0 and t, the resulting formula is

$$\sum_{\hat{t}=1}^{t-1} \langle N(t) Q(\hat{t}) \bar{N}(0) \rangle = (t-1) N_{0n} M_{nn} N_{n0} e^{-(E_n - E_0)t} + \sum_{\hat{t}=1}^{t-1} \sum_{j \neq k} N_{0j} M_{jk} N_{k0} e^{-(E_j - E_0)t} e^{-(E_k - E_j)\hat{t}}. \tag{5.38}$$

The sum over $\hat{t}$ in the last term is a partial geometric series and upon summation yields

$$\sum_{\hat{t}=1}^{t-1} \langle N(t) \bar{Q}(\hat{t}) \bar{N}(0) \rangle = (t-1) N_{0n} M_{nn} N_{n0} e^{-(E_n - E_0)t} + \sum_{j \neq k} N_{0j} M_{jk} N_{k0} e^{-(E_j - E_0)t} \frac{e^{-(E_k - E_j)} - e^{-(E_k - E_j)t}}{1 - e^{-(E_k - E_j)}}. \tag{5.39}$$

After explicitly applying the symmetry in the sum the result is

$$\sum_{\hat{t}=1}^{t-1}\langle N(t)Q(\hat{t})\bar{N}(0)\rangle = (t-1)N_{0n}M_{nn}N_{n0}e^{-(E_n-E_0)t} - 2\sum_{j,k,E_k>E_j} N_{0j}M_{jk}N_{k0}\left(\frac{e^{-(E_j-E_0)t}}{1-e^{-(E_k-E_j)}} + \frac{e^{-(E_k-E_0)t}}{1-e^{-(E_j-E_k)}}\right). \quad (5.40)$$

This expression is dominated for large t by the ground state and becomes

$$\sum_{\hat{t}=1}^{t-1}\langle N(t)Q(\hat{t})\bar{N}(0)\rangle = (t-1)N_{0n}M_{nn}N_{n0}e^{-(E_n-E_0)t} - Re^{-(E_n-E_0)t} \quad (5.41)$$

where R is a normalization factor which does not depend on t. It is given by

$$R = 2\sum_k \frac{N_{0n}M_{0k}N_{k0}}{1-e^{-(E_k-E_n)}}. \quad (5.42)$$

Now the case $\hat{t} > t$ is considered. Similarly to the previous case, the spectral decomposition in the limit of large T can be calculated to be

$$\sum_{\hat{t}=t-1}^{\infty}\langle N(t)Q(\hat{t})\bar{N}(0)\rangle = \sum_{\hat{t}=t-1}^{\infty}\sum_{j,k} e^{-(E_j-E_0)\hat{t}}e^{-(E_k-E_j)t}M_{0j}N_{jk}\bar{N}_{k0}. \quad (5.43)$$

In contrast to the previous case, the state with index j can be the vacuum. The expression is spitted into the vacuum term with $j = 0$ and the remainder. For the remainder, the geometric series can be summed yielding

$$\sum_{\hat{t}=t-1}^{\infty}\langle N(t)Q(\hat{t})\bar{N}(0)\rangle = \sum_{\hat{t}=t+1}^{\infty}\sum_k e^{-(E_k-E_0)t}M_{00}N_{0k}\bar{N}_{k0} + \sum_{j>0,k}\frac{e^{-(E_j-E_0)}}{1-e^{-(E_j-E_0)}}M_{0j}N_{jk}\bar{N}_{k0}e^{-(E_k-E_0)t}. \quad (5.44)$$

The sum in the first term diverges and has to be regulated by a regulator $\mathcal{T}$ which replaces the ∞ in the above term. The regulated expression becomes

$$(\mathcal{T}-t-1)\sum_k e^{-(E_k-E_0)t}M_{00}N_{0k}\bar{N}_{k0} + \sum_{j>0,k}\frac{e^{-(E_j-E_0)}}{1-e^{-(E_j-E_0)}}M_{0j}N_{jk}\bar{N}_{k0}e^{-(E_k-E_0)t}. \quad (5.45)$$

In the large t limit only the nucleon state with $k = n$ contributes.

The remaining two cases $\hat{t} = 0$ and $\hat{t} = t$ are contact terms. The limit of large T and t with $T \gg t$ is

$$\langle N(t)Q(0)\bar{N}(0)\rangle = e^{-(E_n-E_0)t}\langle 0 \mid N \mid n\rangle\langle n \mid \bar{q}q\bar{N} \mid 0\rangle \quad (5.46a)$$

$$\langle N(t)Q(t)\bar{N}(0)\rangle = e^{-(E_n-E_0)t}\langle 0 \mid N\bar{q}q \mid n\rangle\langle n \mid \bar{N} \mid 0\rangle \quad (5.46b)$$

These are two point functions for the nucleon. They differ from the two point function $\langle N(t)\bar{N}(0)\rangle$ only by that they contain different interpolating operators. Since one of the operator always destroys or creates a nucleon, these two point function always project to the nucleon or its excited states or to vanish.

The disconnected part can be written as the product of the spectral decomposition of a two-point function and a the vacuum matrix element of $\bar{q}q$. More explicitly

$$\langle N(t)\bar{N}(0)\rangle\langle Q(t)\rangle = \left[\frac{\sum_i e^{-E_i(T-t)}N_{ij}e^{-E_j t}\bar{N}_{ji}}{\sum_i e^{-E_i T}}\right]\left[\frac{\sum_i e^{-E_i T}M_{ii}}{\sum_i e^{-E_i T}}\right]. \tag{5.47}$$

Taking the large T limit results in

$$\langle N(t)\bar{N}(0)\rangle\langle\bar{q}(\hat{t})q(\hat{t})\rangle = e^{-(E_n-E_0)t}N_{0n}\bar{N}_{n0}M_{00}. \tag{5.48}$$

The derivative of the effective mass can be calculated from the above ingredients. It is useful to note that all $\exp(-(E_n - E_0)t)$ terms in the expressions (5.41), (5.45), (5.46a), (5.46b), and (5.48) cancel when the they are divided by the nucleon two-point function. In most terms the t-dependence drops out so that these cancel each other in the difference in eqn. (5.31). The only terms that give a non-vanishing contributions are the terms with a prefactor linear in t. They occur in eqs. (5.41) and (5.45). Therefore, it follows that

$$\partial_{m_q} m_{\text{eff}}(t) = \frac{1}{\delta t}\left[\delta t M_{nn} - \delta t M_{00}\right] = \langle n \mid \bar{q}q \mid n\rangle - \langle 0 \mid \bar{q}q \mid 0\rangle \tag{5.49}$$

where the regulator $\mathcal{T}$ dropped out. This is the Feynman-Hellmann theorem.

5.5 Kolmogorov-Smirnov test

The discussion in this section is based on [105]. The Kolmogorov-Smirnov test is used in this work to determine if the χ^2-values from several fits follow a χ^2 distribution. To test this, it is useful to first apply a transformation. For each χ^2-value from a fit one calculates the quality of fit Q. [105] It is defined as

$$Q(\chi^2; n_{\text{dof}}) = 1 - \text{CDF}(\chi^2; n_{\text{dof}}) \tag{5.50}$$

where n_{dof} is the number of degrees of freedom in the fit and CDF is the cumulative distribution function of the χ^2 distribution with n_{dof} degrees of freedom. If all the χ^2-values from the fits where distributed according to the χ^2 distribution, then the distribution of the Q values is a uniform distribution between 0 and 1.

Suppose there are n fits, e.g. to a certain correlation, from n ensembles. Furthermore, let Q_i be the associated fit quality for each fit. The n values Q_i can be considered as samples from a unknown distribution. It can be checked whether the data is compatible with the assumption that this unknown distribution is the uniform distribution between 0 and 1. One convenient recipe is the Kolmogorov- Smirnov test. A illustration how the Kolmogorov-Smirnov test was used can be found in figure 5.3. We calculated the empirical cumulative distribution function of

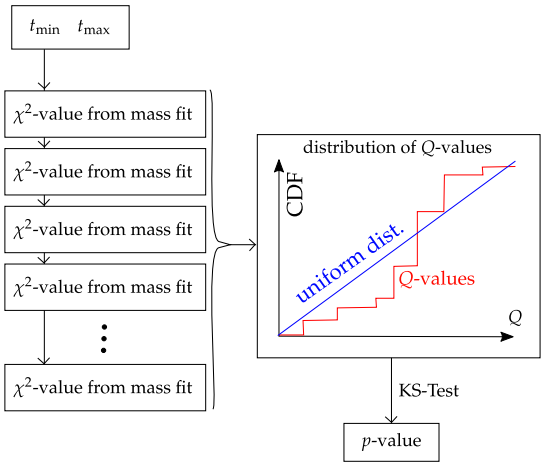

Figure 5.3 *– Schematic illustration of the application of the Kolmogorov-Smirnov test to determine the optimal values of the fitting interval (t_{min}, t_{max}). For any reasonable combination of this interval a mass, e.g. the nucleon mass, is extracted from each ensemble by a fit to the propagator as described in the main text. For each ensemble the resulting χ^2 value is collected and the fit quality is successively calculated. Then, the empirical cumulative distribution function of the fit qualities is determined and compared with the theoretical prediction. The fit range can be used if the resulting p-value of the test is larger than a predefined threshold, e.g.* 0.3.

the Q_i. It is a function of the fit quality Q and starts the point $(0, 0)$ in the $(Q, \mathrm{CDF}(Q))$ plane and ends at $(1, 1)$. It is defined via

$$\underset{\text{emp.}}{\mathrm{CDF}}(Q) := \sum_{Q_i > Q} \frac{1}{N_Q} \tag{5.51}$$

where N_Q is the number of Q-values the empirical cumulative distribution function is calculated of. Under the assumption that the underling distribution is the uniform distribution between 0 and 1, this function has the limit of a linear function between the points $(0, 0)$ and $(1, 1)$ if the number of measurements are taken to infinity. For an finite number of measurements it can be checked whether these are compatible with a underlying uniform distribution. The "distance" D between the empirical cumulative distribution function and the cumulative distribution function $\mathrm{CDF}(Q)$ of the assumed underlying distribution is defined as

$$D := \max \left| \underset{\text{emp.}}{\mathrm{CDF}}(Q) - \mathrm{CDF}(Q) \right|. \tag{5.52}$$

The probability that this value D is larger then the observed D, given that the underlying distribution is truly the uniform distribution, is

$$P(D > D_{\text{observed}}) = Q_{\mathrm{KS}}\left(\sqrt{N_Q} + 0.12 + 0.11 N_Q^{-1/2}\right) \tag{5.53}$$

where

$$Q_{\mathrm{KS}}(\lambda) := \sum_{j=0}^{\infty} (-1)^{j-1} e^{-2j^2\lambda^2}. \tag{5.54}$$

Further information on the Kolmogorov-Smirnov test can be found in [105] and references therein where this discussion is based on.

5.6 Correlated fits

Frequently, the dependence of several depended variables on several other independent variables must be described by a model function which must be fitted to the measured data. Often, both

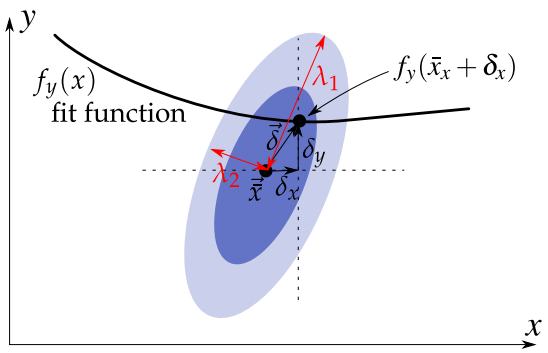

Figure 5.4 *– Schematic illustration of the correlated fit. Here a function $f_y(x)$ is is fitted to data that has an error both in x and y direction. For each datapoint a free fit parameter δ_x is introduced. For this datapoint the fit function is evaluated at $\bar{x} + \delta_x$ where $\bar{x}$ is the mean value of x measured at this datapoint. The vector $\vec{\delta} = (\delta_x, \delta_y)$ with $\delta_y = f(\bar{x} + \delta_x) - \bar{y}$ quantifies the deviation from the datapoint. The contribution of this datapoint to the χ^2 value of the fit is given by $\delta^T C \delta$ if C is the correlation matrix. The blue ellipses indicate the 1σ and 2σ regions. The red lines indicate the size of the eigenvalues of the correlation matrix.*

the independent and the depended variables are measured with finite accuracy, i.e. they have statistical uncertainties. Furthermore, the variables can be correlated. For a proper statistical treatment it is important to take all these uncertainties and correlations into account. In this section the strategy for dealing with such situations is explained. The method described here is frequently employed by the BMW collaboration, for example in [17, 20, 106] For simplicity, the procedure is discussed first in the case of a fit with one depended and one independent variable. Then the generalization to more variables is discussed.

Let $\bar{x}_i$ and $\bar{y}_i$ be the mean values of X and Y on the i-th ensemble. Also, let C_i be the statistical correlation matrix between $\bar{x}_i$ and $\bar{y}_i$. Suppose $f(X)$ predicts Y as a function of X and has several parameters that must be fitted to the available data using a χ^2 minimization. For the χ^2-value to be an indicator of the fit quality, it is necessary that all correlations are fully taken into account. The standard χ^2 routines, as found e.g. in [105], do, however, only deal with the uncertainties of the Y values and can not be used in this setting.

We circumvent this by introducing additional fit parameters $\delta_{x,i}$, one for each ensemble. In the χ^2 routine, we go through all ensembles and evaluate $f(\bar{x}_i + \delta_{x,i})$. Then, we construct $\delta_{y,i} = \bar{y}_i - f(\bar{x}_i + \delta_{x,i})$ Together, $\delta_{x,i}$ and $\delta_{y,i}$ describe the difference between the datapoints and the fit function in the X-Y plane. The situation is depicted in figure 5.4. We combine both values into a vector

$$\vec{\delta}_i = \begin{pmatrix} \delta_{x,i} \\ \delta_{y,i} \end{pmatrix}$$

Then, we calculated the χ^2-value of the fit using

$$\chi^2 = \sum_i \vec{\delta}_i^T C_i^{-1} \vec{\delta}_i$$

where the sum goes over all ensembles. The quadratic form in this expression tells us, how many standard deviations the model function is away from the measured datapoint at the closest point.

The method can be easily generalized to several variables. In that case several fit functions f_j predict the dependent variables Y_j in terms of the independent variables X_j. We introduce parameters $\delta_{x,i,j}$ for each independent variable where i indicates the ensemble and j refers to which independent variable is considered. Similarly, we introduce several $\delta_{y,i,j}$ as differences

between the measurement of the j-th dependent variable and the prediction of the j-th fit function on the i-th ensamble. We construct

$$\vec{\delta}_i = \begin{pmatrix} \delta_{x,i,1} & \delta_{x,i,1} & \dots & \delta_{y,i,1} & \delta_{y,i,1} & \dots \end{pmatrix}^T$$

and calculate

$$\chi^2 = \sum_i \vec{\delta}_i^T C_i^{-1} \vec{\delta}_i$$

where this time C_i^{-1} is the full correlation matrix between all dependent and independent variables. This method is used through the thesis whenever a correlated fit containing several variables measured on the same ensembles is performed.

Chapter 6

The Higgs couplings of nucleons

Nucleons are bound states that consist of quarks, antiquarks and gluons, which bind the quarks together. Their masses are predicted by the standard model of particle physics. [17, 20] According to it, once the electroweak symmetry is broken, fundamental fermions, initially massless, acquire masses by interacting with the background Higgs field. [9] A key property of this mechanism is that masses generated by it are proportional to the strength of the interaction between the external Higgs field and the particles the mass of which is created. [10] This was experimentally confirmed [107] recently. For fundamental fermions that do not interact via the strong interaction, for example electrons, this is the end of the story. Quarks, however, are confined into color neutral states, for example pions or nucleons. Their masses are not solely determined by a Higgs coupling. [108] The details of the complicated interactions of the quarks and gluons inside these bound state are also important for their masses; these interactions carry energy and hence generate masses. [17] Nucleons are often imagined as bound states of valence quarks, e.g. of two up-quarks and one down quark in the case of the proton. In truth, however, quarks of all flavors can be found inside these states, in the form of virtual particles. These quarks couple to the Higgs field proportional to their respective masses and this leads to a coupling of the nucleon to the Higgs field. This coupling, however, is not determined by the nucleon's mass; it is only a fraction of the interaction a fundamental fermion with the same mass would have.

We can determine how much a bound state x couples to the Higgs field via the Higgs coupling of the fermion f by calculating the sigma term $\sigma_{xf} = g_f \frac{\partial m_x}{\partial g_f}$. In this expression g_f is the coupling between the fermion f and the Higgs field. For any fundamental fermion f we find $\sigma_{ff} = m_f$ because $m_f \propto g_f$. For a nucleon N we can therefore substitute the quark-Higgs couplings with the quark masses and write

$$\sigma_{qN} = m_q \frac{\partial m_N}{\partial m_q}. \tag{6.1}$$

The sum $\sum_q \sigma_{qN}$ is smaller then the nucleon's mass, because of the reason laid down above. It is common to define the nucleon quark contents as $f_{qN} = \sigma_{qN}/M_N$.

Each nucleon's mass is given by the expectation value $\langle N \mid H \mid N \rangle$ where $\mid N\rangle$ is a nucleon state at rest, normalized so that $\langle N \mid N \rangle = 1$ and H is the Hamilton of QCD. For all expectation values, here and in the following, a subtraction of the vacuum expectation value is implicitly understood. In [109] a way to decompose this Hamiltonian was suggested. That decomposition has the form

$$H = \sum_q m_q \bar{q} q + O_{\text{rest}}. \tag{6.2}$$

The details of the operator O_{rest} are not important here. It suffices to know that it does not depend on the quark masses. In [109] it was also noted that the expectation value of the trace of the energy momentum tensor θ is

$$\langle N \mid \theta^{\mu}{}_{\mu} \mid N\rangle = \langle N \mid \sum_q m_q \bar{q}q + \gamma_m \sum_q m_q \bar{q}q + \frac{\beta}{g^2} G^2 \mid N\rangle - \langle 0 \mid \ldots \mid 0\rangle = M_N. \tag{6.3}$$

Notably, $\langle N \mid m_q \bar{q}q \mid N\rangle$ and M_N are independent of the renormalization scale. Consequently, M_N^a defined as

$$M_N^a = \langle N \mid \gamma_m \sum_q m_q \bar{q}q + \frac{\beta}{g^2} G^2 \mid N\rangle. \tag{6.4}$$

is also independent from the renomalization scale. [109] Then, from

$$M_N = \langle N \mid \sum_q m_q \bar{q}q + O_{\text{rest}} \mid N\rangle \tag{6.5}$$

follows that $\langle N \mid O_{\text{rest}} \mid N\rangle = M_N^a$. [109] The Feynman-Hellman theorem [12–15] states that $\sigma_{qN} = \langle N \mid m_q \bar{q}q \mid N\rangle$. Therefore, the nucleon masses can be written as [109]

$$M_N = \sum_q \sigma_{qN} + M_N^a. \tag{6.6}$$

The decomposition outlined above is not unique and other proposals exist in the literature. See e.g [109–111]. Also, M_N^a can be broken down further. See [110] for an example of such a calculation. The decomposition outlined in the above paragraph is based solely on properties of operators and not on their matrix elements. This is important since, for example, O_{rest} is independent of the quark mass but M_N^a is not. This can happen because the state $\mid N\rangle$ itself depends on the quark masses. As a consequence, such a decomposition does not capture the complete effect of the of quark masses in one term while keeping the other terms independent of the quark masses. For the same reason, the nucleon mass is not a linear function of the quark masses. Nevertheless, the individual contribution in eqn. (6.6) have real physical meanings and are important for ongoing experiments. The sigma terms σ_{qN} not only tell us how large a nucleon's interaction with the Higgs field, mediated by the quark flavor q, is but also how much a nucleon would interact with certain dark matter candidates if they turn out to exits. [16] Many extensions of the standard model that aim to describe dark matter contain particles that interact with nucleons through scalar quark condensates. One example are WIMPs. In the mentioned theories, the strengths of the spin-independent interactions of the dark matter candidates with nucleons are determined by the quark-dark matter couplings and linear combinations of nucleon sigma terms. The former are properties of the new theories and are to be measured while the latter are predictions of the standard model and should be calculated from it. Direct dark matter detection experiments usually rely on measuring the scattering of the dark matter particles on nuclei and, therefore, need precise values for the sigma terms to relate their findings to parameters of the underlying new theories. [16]

Nucleon sigma terms where calculated before by many authors using different methods. One group of calculations relies on experimental pion nucleon scattering data to calculate the light

sigma terms [112–117]. Earlier determinations of this type preferred a lower value of around 40 MeV while later phenomenological works with improved analysis techniques (s. [115, 117, 118] for a discussion) predict that it might by as high as $\sim$ 60 MeV [115]. The light sigma term can be converted, with the use of chiral perturbation theory and the strange to light quark mass ratio, to values of the strange sigma term [119–121]. Further phenomenological studies of the light and strange sigma terms using various methods, sometimes including published lattice results, have been carried out [122–127]. Several groups have computed the light, strange, and in some instances the charm sigma term on the lattice [128–143] Most lattice calculations favor a lower value of the light sigma term compared to the larger phenomenological values, more in line with the initial phenomenological estimates. The origin of this discrepancy is not fully understood [116].

Here, I present lattice calculations for the up, down, strange, and charm sigma terms. For the up, down, and strange sigma terms I present two calculations. The first is based on a set of gauge configurations which include pion masses down to the physical point. These configuration enabled us to calculate $\sigma_{udN} \approx \sigma_{uN} + \sigma_{dN}$ very precisely but allowed only for a comparatively imprecise determination of σ_{sN}. With this calculation in mind we also derived how σ_{udN}-results can be related to individual up and down sigma terms of the proton and neutron. After discussing that work, I will present a second computation of the same quantities on different gauge configurations. These configurations have significantly reduced statistical uncertainties, compared to the previously used ones. Since they don't include physical pion masses, we could not improve the light sigma term much. For the strange sigma term, on the other hand, these new configurations allowed us to reduce the uncertainty significantly. The analysis strategies differ significant between the two analyses. In the first analysis we performed global fits to Wilson configurations. In the second analysis we splitted the work into two parts so that we where able to leverage the advantages of two datasets. One part was well suited to be carried out on Wilson data. For the other part we used the advantages of a staggered dataset. After discussing this second analysis, I will present a calculation of the charm sigma term from first principles. Then, I explain how heavy quark effective theories [2, 53, 54] can be used to estimate the top and bottom sigma terms. Finally, I present how the results are combined to provide a consistent picture of the nucleon-Higgs interaction.

6.1 General strategy for light and strange sigma terms

Two methods are frequently employed to determine nucleon sigma terms in lattice calculations. One of them, often called "direct method," is based on the direct evaluation of three point functions having the form

$$\langle N(t) \mid \bar{q}q \mid N(0) \rangle. \tag{6.7}$$

These are constructed from nucleon two point functions by inserting a quark antiquark operator pair between the nucleon states. While conceptually simple, it is not simple to use this approach in practice. To evaluate the above expression, many quark field contractions must be evaluated. Some of them are disconnected. In figure 6.1 the quark operators and some contractions for the case $q = u$ are shown. The blue lines represent a connected contribution in which all lines have at most one endpoint at the quark antiquark pair inserted between the nucleon states. These

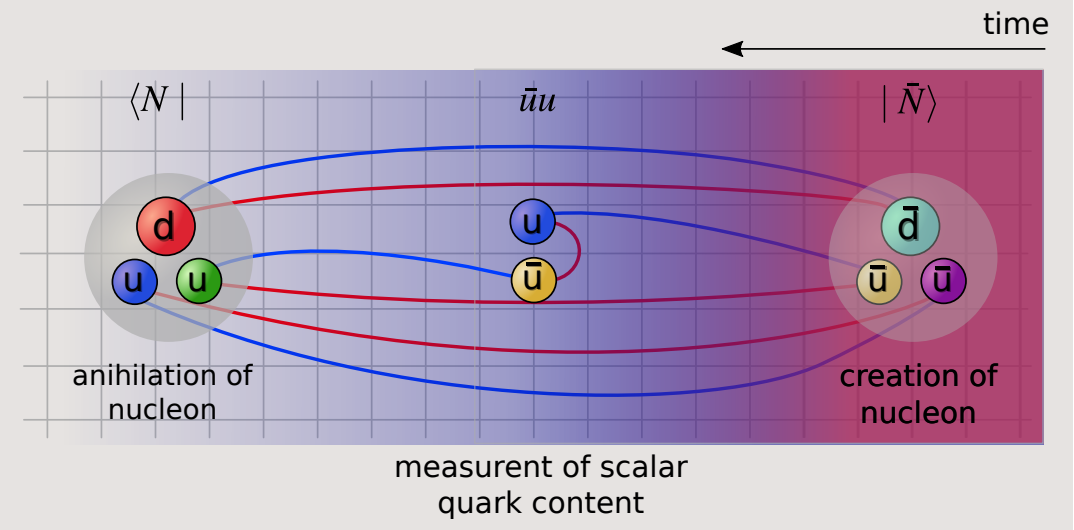

Figure 6.1 – *Sketch of the calculation of the nucleon sigma term. On the right hand side a nucleon is created and on the left hand side a nucleon is annihilated. The nucleon sigma term is measured by including a pair of quark-antiquark operators in between. The insertion of the quark antiquark pair can be achieved either by the Feynman-Hellmann method or by a direct insertion. For the latter case a connected (blue) and a disconnected (red) contribution is indicated. The red shade indicate the contribution of excited states to the two-point function where the blue shade indicates the contribution of the ground state.*

contributions are relatively simple to calculate because all propagators start from a small number of points. Therefore, all necessary propagators can be calculated by inverting the Dirac operator for a few right hand sides. Disconnected contributions (e.g. the red lines) are more difficult to calculate. Since the quark antiquark pair can be inserted at any lattice site, propagators form all lattice points to all lattice points are needed. Calculating them amounts to calculating the the full inverse of the Dirac operator. This is prohibitively expensive in most cases. However, there has been substantial progress using stochastic evaluations of such contributions: This idea is successfully used for nucleon sigma term calculations in [132, 137–143].

We, nevertheless, used a different approach, often called the Feynman-Hellmann method. The Feynman-Hellmann theorem relates changes of energies of eigenstates of the Hamiltonian under variations of the parameters of the theory to matrix elements of these states. According to this theorem, it suffices to calculate derivatives of nucleon masses with respect to quark masses to determine the the nucleon sigma terms. Since masses can be calculated from two point functions, this avoids the calculation of disconnected contributions. The theorem, originally derived in quantum mechanics [12–15], is introduced in section 5.4. Other calculations based on this approach can be found in [123, 126, 127, 129, 131–134, 138, 144]

Before discussing any analysis in detail, I explain the general strategy in the important case of $N_f = 2 + 1$ QCD. Firstly, a parametrization of the nucleon mass on different ensembles is introduced. To this end, and to set the physical point, it is convenient to use proxy quantities for the light an strange quark masses that do not require renormalization. Such quantities can be

readily found by means of chiral perturbation theory [18]:

$$M_\pi^2 = B(m_u + m_d) + \mathcal{O}(m_u^2, m_d^2), \tag{6.8a}$$
$$M_{K^0}^2 = B(m_d + m_s) + \mathcal{O}(m_d^2, m_s^2), \tag{6.8b}$$
$$M_{K^+}^2 = B(m_u + m_s) + \mathcal{O}(m_u^2, m_s^2). \tag{6.8c}$$

The squared pion mass is a proxy for the light quark mass, and a combination of the pion and kaon squared masses is a proxy for the strange quark mass. Specifically,

$$m_{ud} \sim M_\pi^2, \tag{6.9a}$$
$$m_s \sim M_{K_\chi}^2 := M_{K^+}^2 + M_{K^0}^2 - M_\pi^2. \tag{6.9b}$$

The physical values of M_π^2 and $M_{K_\chi}^2$ are known [19]. Since the exact functional dependence of the nucleon mass is not known, a Taylor expansion of M_N around the physical point is used to approximate it. Such a expansion has the form

$$M_N = c_0 + c_1(M_\pi^2 - M_\pi^{(\phi)2}) + c_2(M_{K_\chi}^2 - M_{K_\chi}^{(\phi)2}) + \dots . \tag{6.10}$$

Here and in the following, $M_X^{(\phi)}$ refers to the mass of the particle X at the physical point. For the sake of simplicity, only the first terms in the expansion are shown, although higher terms might be important. This function can be fitted to the numerical results on different gauge ensembles, generated to scatter around the physical point. After fitting, including possible higher order terms, the value of c_0 is an estimator for the nucleon mass at the physical point. Likewise, c_1 and c_2 are estimators for the derivatives of the nucleon mass with respect to the squared pion mass M_π^2 and the squared reduced kaon mass $M_{K_\chi}^2$. They are closely related to the quark mass derivatives of the nucleon mass, because of eqs. (6.9a) and (6.9b). By virtue of the Feymnan-Hellman theorem, c_1 and c_2 are almost proportional to the nucleon sigma terms. These proportionalities would be exact if all higher order corrections to the eqns. (6.8) would vanish, and if a sufficient number of terms in eqn. (6.10) would be included in the fit. The values of c_1 and c_2, with higher order terms in eqn. (6.10) included, sometimes referred to as mesonic sigma terms, are of interest on its own [145].

We used two approaches to calculate the sigma terms:

1. We parametrized the nucleon mass in terms of the quark mass parameters instead of the squared meson masses.
2. We left the parametrization as it is and determined $\partial M_{\text{meson}}^2 / \partial m_{\text{quark}}$ at the physical point to correct for the higher order effects.

Both choices are reasonable and have desirable features. I present two lattice calculations of the light and strange sigma terms, based on two different set of ensembles, each using one of the strategies outline above. The specifics of the different sets of ensembles dictate which of the two approaches is better suited.

6.2 The 2hex analysis for light and stange sigma terms

The analysis described in this section has been published in [146]. It is referred to as "2hex analysis" in this thesis because the action used contains two level of HEX smearing.

The calculation is based on a collection of Wilson gauge ensembles that have been previously used by the BMW collaboration, for example in the calculation of quark masses [66]. Our strategy was to used a fit function to describe the nucleon mass's dependence on the quark masses directly. To that end, we used the renomalization factors already calculated in [66] to define properly renormalized quark masses, and parametrized the nucleon mass in terms of these quark masses. We then fitted the parametrization of the nucleon mass to the lattice data. On one hand, data with a large range of pion masses, including the physical pion mass, was available, so that we where able to determine the slope of the nucleon mass in the light quark mass direction very well. On the other hand, the variation in the reduced kaon mass was relatively small. As a consequence, we could determine the nucleon mass's slope in that direction only with a relatively large uncertainty. After fitting, we used the Feynman-Hellman theorem to read of the sigma terms from the slope of the parametrization.

I will first describe the properties of the gauge ensembles entering this analysis. Then, I will describe how we extracted the baryon, meson, and quark masses form the correlation functions of suitable operators. Afterwards, I will explain what parameterization for the nucleon mass was used. I will then discuss our strategy to estimate the systematic uncertainties. Finally, I will present the results.

6.2.1 The lattice setup of the 2hex analysis

The 2hex dataset is made of of 47 $N_f = 2 + 1$ ensembles, consisting of configurations generated with a Symmanzik improved gauge action and a clover improved fermion action. The gauge fields that enter the fermion action have been smeared by two levels of HEX smearing. On the roughly 13000 gauge configuration that are in the dataset, each propagator was calculated by inverting the Dirac operator with about 40 different sources per configuration. The dataset features 5 different lattice spacing with the coarsest being $a_{\text{coarsest}} \approx 0.116$ fm and the finest being $a_{\text{finest}} \approx 0.054$ fm. The spatial extents of the lattices reach up to 6 fm. The ensembles feature pion masses down to about 120 MeV, going even below the physical point. The configurations have been used for many other projects of the BMW collaboration, e.g. [17, 66]

6.2.2 Extracting masses

We carried out the analysis in a two step procedure. In the first step, we determined the masses of the nucleon, the omega baryon, the pion, the kaon, and the masses of the quarks. Firstly, I describe the extraction of the masses of mesons and baryons. After that, I will discuss the extraction of the quark masses.

To measure the correlation functions, we used standard operators, as described in [17]. To reduce excited state contamination, the quark fields at the source and at the sink where subjected to Gaussian smearing. Details about the operators and the smearing can can be found in [17]. The correlation functions of the operators behave as

$$C(t) = \begin{cases} A \sinh(-m(t - {}^{N_t}/_2])) & \text{for baryons} \\ A \cosh(-m(t - {}^{N_t}/_2])) & \text{for mesons} \end{cases} \tag{6.11}$$

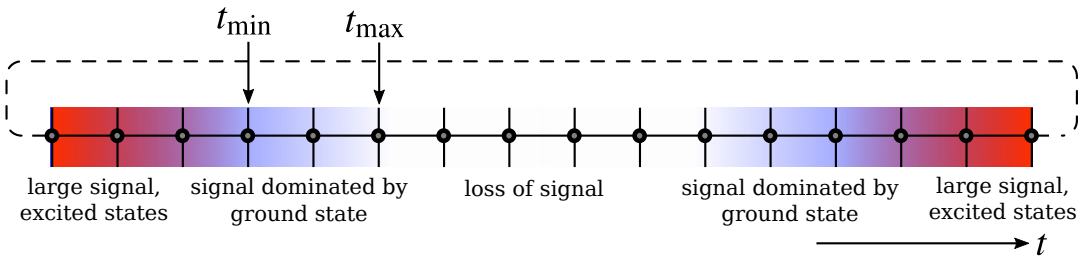

Figure 6.2 – *Regions relevant for the extraction of baryon masses. The blue color represents contribution of the ground state to the correlation function while the red color represents excited state contributions. At small time separations the signal is dominated by excited states. At $t \sim N_t/2$ one typically has a very bad signal to noise ratio. The extraction of the mass must be performed at intermediate values between t_{min} and t_{max}. To use the backward propagating information, the propagator is folded around $N_t/2$.*

for large time separations between the source and the sink, as explained in section 5.3. A is a proportionality constant not of interest here. We folded the measured correlation functions, around their center, to explicitly enforce (anti-)symmetry before extracting m by fitting the above functions to the measured correlation functions. Because the correlation functions contain contributions from excited states at small time separations, we included only datapoints with large enough time separations t in the fit. However, as t gets large, the signal to noise ratio grows and prevents us from extracting masses at very large t. Therefore, we had to find a fit range starting at t_{min} and ending at t_{max} for which the bias on the ground state mass introduced by excited state contributions was small compared to the ground state mass's statistical uncertainty. At the same time, we had to make sure that the signal to noise ratio was still acceptable. The situation is visualized in figure 6.2. We decided if eqn. (6.11) describes the correlation function well, and therefore excited states effects are not statistically significant, by looking at the χ^2-values of the respective fits. If the fit function describes the data well, the χ^2-value of each fit is a sample taken from the χ^2 distribution with as many degrees of freedoms as the difference between the number of datapoints and the number of fit parameter. It is useful to calculate the quality of fit Q, as defined in section 5.5, from the χ^2-value of each fit. Q is for each fit supposed to be a sample draw from a uniform distribution between 0 and 1. If we would have been interested in extracting only one ground state mass from one correlation function, we would have had only one Q value available. In that case it would have been reasonable to find a fit range for which Q is not excessively small. However, since we had several ensembles available, and all these ensembles where statistically uncorrelated, we where able to go beyond this. We checked if the empirical distributions of the Q values where consistent with a uniform distribution. We did this separately for each channel, e.g. the nucleon's or the pion's mass. In doing so, we assumed that the contributions of the excited states in physical units are similar for all ensembles entering the analysis. We varied t_{min} in physical units while retaining a constant $(t_{\mathrm{max}} - t_{\mathrm{min}})/a = 10$ in lattice units. The latter choice was made to ensure that the covariance matrix of the correlation functions in the fit region did not have excessively small eigenvalues that would render the fit unstable. We checked, for each value of t_{min}, if the observed empirical distribution of the Q-values followed the expected uniform distribution. To that end we used a

Kolmogorov-Smirnov test, as explained in section 5.5. As preferred value of $t_{\min}$ we used for each channel a value for which the Kolmogorov-Smirnov test resulted in a p-value bigger then 0.3.

With Wilson fermions, the bare quark masses undergo additive renormalization [33, 66], which is inconvenient for the use in the Feynman-Hellmann theorem. Therefore, we used the ratio-difference quark masses, as defined in [66]. They combine advantages of the PCAC[1] quark masses with advantages of bare quark masses: The ratio-difference quark masses renormalize multiplicatively. Furthermore, the multiplicative renormalization is determined by the non-singlet scalar current renormalization factor Z_S. It can be calculated easier than the renormalization factor of the PCAC quark masses and was available for the dataset considered here. [66] In the following paragraph, first, the PCAC quark masses are defined and their extraction is described. Then, the ratio-difference quark masses are constructed.

The sum of the PCAC quark masses of two flavors q_1 and q_2 is defined as

$$m_{q_1}^{\mathrm{PCAC}} + m_{q_2}^{\mathrm{PCAC}} = \frac{\sum_x \langle \overline{\partial}_\mu \left(A_\mu(x) + a c_A \overline{\partial}_\mu P(x) \right) O(0) \rangle}{\sum_x \langle P(x) O(0) \rangle}. \tag{6.12}$$

$A(x)$ and $P(x)$ are the axial and pseudoscalar current densities constructed from quark flavors q_1 and q_2. The operator O is arbitrary as long as it couples to the pseudoscalar meson with quarks of flavors q_1 and q_2. We choose to use smeared versions of $P(0)$ [66]. The symmetric derivatives $\overline{\partial}$ are defined as

$$\overline{\partial}_\mu \phi(x) := \frac{\phi(x + \hat{\mu}) - \phi(x - \hat{\mu})}{2} \tag{6.13}$$

with all quantities taken in lattice units. [66]. The improvement constant c_A eliminates $\mathcal{O}(a)$ corrections. [66]. The details of the improvement scheme are discussed in detail in [147]. We employed tree-level improvement, i.e. used $c_A = 0 + \mathcal{O}(\alpha_s)$, that leads to corrections of order $\mathcal{O}(\alpha_s a)$ [66]. We extracted $2M_{q_1,q_2}^{\mathrm{PCAC}}(t)$, defined as

$$2M_{q_1,q_2}^{\mathrm{PCAC}}(t) := m_{q_1}^{\mathrm{PCAC}}(t) + m_{q_2}^{\mathrm{PCAC}}(t) = \frac{C_{A4P}(t+1) - C_{A4P}(t-1)}{2C_{PP}(t)}, \tag{6.14}$$

from two correlation functions, $C_{PP}(t)$ and $C_{A4P}(t)$. $C_{PP}(t)$ is the correlation function of two pseudoscalar currents, with a smeared source and a point sink. $C_{A4P}(t)$ is the pseudoscalar to temporal axial vector correlation function, also from a smeared source to a point sink. For more details on the correlation functions see [66]. For moderately large t, eqn. (6.14) plateaus at a constant value. It was this plateau value that we used to define the PCAC quark masses; we fitted a constant to it. The choice of the fitting interval was less crucial compared to the case of hadron masses since the plateaus started very early and the signal did not degrade much over time. Nevertheless, we used the Kolmogorov-Smirnov test to determine a suitable fit interval for thees channels. Finally, we constructed individual quark masses via

$$m_l^{\mathrm{PCAC}} = M_{l,l}^{PCAC}, \tag{6.15a}$$

$$m_s^{\mathrm{PCAC}} = M_{l,s}^{PCAC} - \frac{1}{2} M_{l,l}^{PCAC}, \tag{6.15b}$$

[1] partially conserved axial current

where l is one of the two degenerate light quark flavors. Following [66], we combined these PCAC quark masses with the bare masses m_l^{bare} and m_s^{bare} to calculate the ratio-difference quark masses $m_{l/s}^{\text{rd}}$. The basic idea is the following: On one hand, the bare quark masses are very well suited to calculate the difference

$$d = m_s^{\text{bare}} - m_l^{\text{bare}} \tag{6.16a}$$

in which the additive renormalization cancels. This difference renormalizes only multiplicative, with the renormalization factor Z_S. The PCAC quark masses, on the other hand, are a good starting point to calculate the ratio

$$r = \frac{m_s^{\text{PCAC}}}{m_l^{\text{PCAC}}}. \tag{6.16b}$$

In this ratio the renomalization constant, which is complicated to calculate, drops out. d and r can be combined into unimproved ratio-difference quark masses

$$m_l^{\text{rd,unimp.}} = \frac{d}{r-1} \tag{6.17a}$$

$$m_s^{\text{rd,unimp.}} = \frac{rd}{r-1} \tag{6.17b}$$

These can be $\mathcal{O}(a)$-improved, following [66], by replacing r and d by

$$d^{\text{imp.}} = d\left(1 - \frac{1}{2}b_S d\frac{r+1}{r-1} - \bar{b}_S d\frac{r+2}{r-1} + \mathcal{O}(a^2)\right), \tag{6.18a}$$

$$r^{\text{imp.}} = r\left(1 + (b_A - b_P)d + \mathcal{O}(a^2)\right). \tag{6.18b}$$

Then,

$$m_l^{\text{rd}} = \frac{d^{\text{imp.}}}{r^{\text{imp.}} - 1} \tag{6.19}$$

$$m_s^{\text{rd}} = \frac{r^{\text{imp.}} d^{\text{imp.}}}{r^{\text{imp.}} - 1} \tag{6.20}$$

are the fully $\mathcal{O}(a)$ improved ratio-difference quark masses. In this work we used the tree-level values

$$b_S = 1 + \mathcal{O}(\alpha_s) \tag{6.21a}$$

$$b_A = 1 + \mathcal{O}(\alpha_s) \tag{6.21b}$$

$$b_P = 1 + \mathcal{O}(\alpha_s) \tag{6.21c}$$

$$\bar{b}_S = 0 + \mathcal{O}(\alpha_s^2) \tag{6.21d}$$

$$\bar{b}_A = 0 + \mathcal{O}(\alpha_s^2) \tag{6.21e}$$

$$\bar{b}_P = 0 + \mathcal{O}(\alpha_s^2) \tag{6.21f}$$

for the improvement coefficient so that, formally, $\mathcal{O}(\alpha_a a)$ correction remained. [66]

Table 6.1 *– Values of the integers n_X used in the 2hex anlysis of the sigma terms. The power 2 is used for the pion and reduced kaon mass because the squared mass of those particles are to leading order proportional to the light and strange quark masses.*

X	n_X
Ω	1
π	2
K_χ	2
N	1

6.2.3 The parametrization of the nucleon mass

We introduced a global fit model to describe the nucleon mass in terms of the quark masses. This model is of the form

$$M_X^{n_X} = (1 + g_X^a(a))(1 + g_X^{\mathrm{FV}}(M_\pi, L))M_X^{(\phi)n_X} \times (1 + (c_X^{ud} + g_X^{ud,a}(a))\tilde{m}_{ud} + (c_X^s + g_X^{s,a}(a))\tilde{m}_s + \text{h.o.c}) \quad (6.22)$$

where

$$\tilde{m}_q = \frac{m_q^{\mathrm{rd}}}{aZ_S(1 + g_q^a(a))} - m_q^{(\phi)} \quad (6.23)$$

and X is either π, K_χ, N or Ω. All quantities are to be understood in physical units. Our strategy was to fit the masses of the nucleon, the omega baryon, the pion, and the reduced kaon mass as a function of the quark masses. The physical values $m_q^{(\phi)}$ of the quark masses, which are fit parameters, where not known a priori, but where automatically found by the fit using the data for the pion and reduced kaon masses. The c_X^q are describing the leading order quark mass dependencies of the quantities X. The $g_X^{Y,a}$ are corrections introduced by the finite lattice spacing and took one of the two functional forms

$$g_X^{Y,a}(a) = \text{fit parameter} \times a^2, \quad (6.24a)$$

$$g_X^{Y,a}(a) = \text{fit parameter} \times \alpha_s a. \quad (6.24b)$$

g_X^{FV} parametrized the finite volume corrections to the quantity X with the functional form [148]

$$g_X^{\mathrm{FV}} = \text{fit parameter} \times \sqrt{\frac{M_\pi}{L^3}} \exp(-M_\pi L). \quad (6.25)$$

The integers n_X are tabulated in table 6.1. The renormalization factors Z_S depend on the lattice spacing. They were determined previously in [66] and we did not calculate them again. We fitted all channels simultaneously and could, therefore, not uniquely disentangle the roles of different channels as being responsible for e.g. scale setting or the determination of the physical point. However, we thought off each channel to have a specific role: The omega mass determines the lattice spacing, the squared masses of the pion and reduced kaon determine the values of $m_{ud}^{(\phi)}$ and $m_s^{(\phi)}$, and the fit to the nucleon mass allowed us to extract the sigma terms. We performed, as a crosscheck, a fully independent analysis in which we fitted the pion, reduced kaon, omega, and nucleon mass channels separately in terms of the quark masses. In that way, we neglected a

small correlation between these channels but where able to distinguish the roles the channels played in our analysis. In this secondary analysis, we also calculated the renormalization factors self consistently from the fits. We found the results of this secondary analysis to be in very good agreement with our main results. We concluded that the picture explained above is essentially correct.

6.2.4 Estimation of systematic uncertainties

The following sources of systematic uncertainties where present in this analysis.

i. **Interpolation:** We used eqn. (6.22) to interpolate between different ensembles. It is based on a truncated expansion around the physical point. One can not expect such a truncation to describe the lattice data exactly. In order to estimate the error made we added varying higher order terms to the fit. We included terms proportional to $\tilde{m}_{ud}^2$, $\tilde{m}_{ud}^3$, $\tilde{m}_{ud}\tilde{m}_s$, $\tilde{m}_{ud}^2\tilde{m}_s$ and in the case of the nucleon a term proportional to

$$\tilde{m}_q = \left(\frac{m_q^{PCAC}}{aZ_S(1+g_q^a(a))}\right)^{3/2} - m_q^{(\phi)3/2}. \tag{6.26}$$

These terms appear in a Taylor expansion at higher orders expept for the last term that is inspired by chiral perturbation theory. [116] We also introduced cuts on the pion masses: All ensembles with either $M_\pi^2 > 320\,\text{MeV}$ or $M_\pi^2 > 480\,\text{MeV}$ where removed form the analysis. Furthermore, we estimated effects of even higher orders which could not be resolved directly. We did this by replacing the Taylor expansions by Padé expansions of the same order. They differ from the corresponding Taylor expansions only by terms of higher orders then those which are explicitly present in the fit. To avoid overfitting, we did not add higher order terms to the analysis if the corresponding fit parameter had a relative error larger then 100%. The only exceptions to this rule where next-to-leading order terms in m_{ud} because we found them to be important to describe the light quark mass dependence of the nucleon.

ii. **Finite lattice spacing:** The action used in this work has leading cutoff effects of order $\mathcal{O}(\alpha_s a)$. Because of smearing, these effects are numerically suppressed and the $\mathcal{O}(a^2)$ effects are often dominant [66]. This is taken into account by the two choices in eqn. (6.24). Both choices provide for a reasonable continuum extrapolation. The difference between both choices is an estimate of the uncertainty introduced by said extrapolations. The lattice data is not of enough statistical precision to allow for a separation of both behaviors.

We found that the data can be described well with an ansatz in which the finite lattice spacing corrections are independent of the quark masses, i.e. where the prefactors in $g_X^{q,a}$, $q \in ud, s$ vanish. However, the slopes of the nucleon mass are the actual observables of interest in this work and correction on them are crucial. Therefore, we had to estimate the effect of the finite lattice spacing on these slopes. It turned out that the statistical accuracy of the data was not good enough to directly include the corresponding terms in the fit. To asses the error introduced by assuming these terms to be zero we used the following procedure: For each variation of the fit function we fixed the nucleon mass in the continuum limit to its experimental value. Then, we included one of the above mentioned terms — continuum corrections on the slope in the light or strange quark direction — in the fit. The

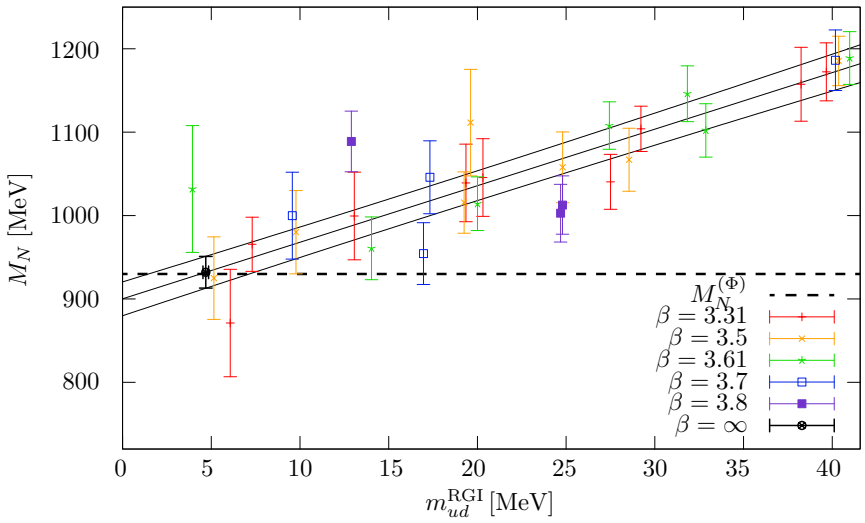

Figure 6.3 *– ud-behavior of an example fit in the 2hex analysis for the sigma terms. On the y axis the mass of the nucleon is shown. On the x axis the average light quark mass is shown. All datapoints are projected to the physical point except for their light quark mass dependence. The color of the datapoints indicate the gauge coupling at which they are obtained. The solid lines indicate the fit and its standard deviation. The dashed line indicates the physical nucleon mass. The black dot indicates the nucleon mass extracted form the fit and its standard deviation. [146]*

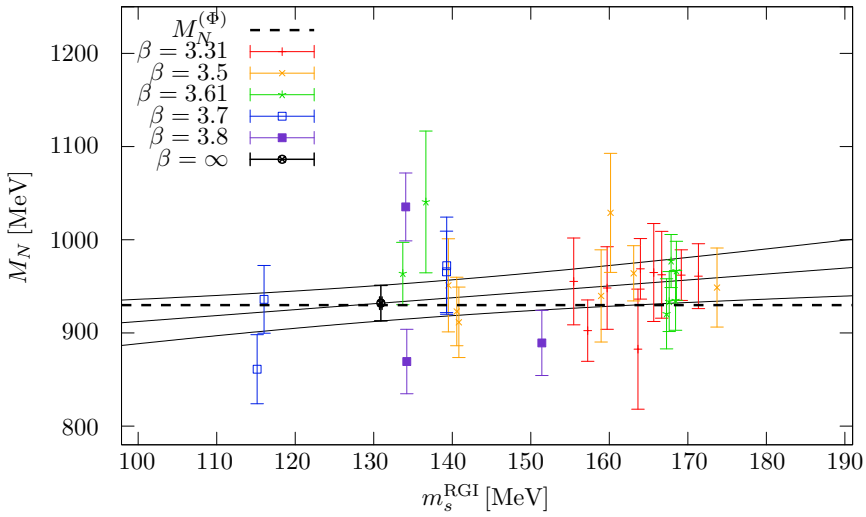

Figure 6.4 *– s-behaviour of an example fit in the 2hex analysis for the sigma terms. On the y axis the mass of the nucleon is shown. On the x axis the average strange quark mass is shown. All datapoints are projected to the physical point except for their strange quark mass dependence. The color of the datapoints indicate the gauge coupling at which they are obtained. The solid lines indicate the fit and its standard deviation. The dashed line indicates the physical nucleon mass. The black dot indicates the nucleon mass extracted form the fit and its standard deviation. [146]*

fixed nucleon mass stabilized the fits enough for them to yield useful results. We estimated the error made by omitting the continuum corrections on the slopes from the main fits by the difference between the values of the sigma term with and without the new terms added. Only for the slope in the light quark direction a lattice spacing dependence could be observed — even with the nucleon mass fixed. The associated difference in the light and strange sigma terms where added to the systematic uncertainties in quadrature.

iii. **Finite volume:** Not only the lattice spacing but also the spatial extend of the lattice is finite and consequently must be extrapolated to the infinite volume limit. A common rule of thumb [17] is that finite volume effects of light hadron masses are negligible if $M_\pi L \gtrsim 4$. We extrapolated away remaining correction using eqn. (6.25).

iv. **Mass extraction ranges:** For the extraction of hadron masses we had to determine the fit ranges. Even after that, small contributions of excited states may have remained. These contributions are exponentially suppressed as the fit range is moved to larger times. If these effects are small, compared to the statistical accuracy of the data, then the results of our analysis has to be independent of the chosen fit range. We estimated remaining contributions of excited state by fitting the correlation functions not only with the initially preferred fit ranges but also with a fit ranges shifted to larger times by one lattice spacing.

We estimated the combined systematic uncertainty with the histogram method [17, 20]: For each possible source of systematic uncertainty we used several valid analysis methods. As each source of systematic uncertainty can be varied independently, the the number of total analyses is the product of the number of possible variations used for the assessment of each of the different contributions to the systematic uncertainty.

Not all of the fits describe the data equally well. To account for this, we weighted each of the contributions to the histograms by a factor that expresses how believable this fit is. For this work, we used three forms of weighting:

- **Flat weights:** Each analysis was weighted the same.
- Q-**weights:** Each analysis was weighted by their respective fit quality Q [105]. This weighting method is especially favorable if some of the fits do not describe the data well. These fits have a low fit quality and are heavily suppressed.
- **AIC-weight:** Each analysis is weighted by its respective AIC weight. [20, 149]. The AIC weight of a given fit is

$$w_{\mathrm{AIC}} = \exp\left(-\frac{1}{2}(\chi^2 + 2p)\right) \tag{6.27}$$

where p is the number of parameters of the fit. This suppresses fits which require a large number of parameters for a good description. [20]

We compared the results of the three methods and found that they agree. We choose to use the AIC weight for our final numbers.

6.2.5 Individual quark contents

Let $f_{u/d}^{n/p}$ be the up or down quark content of the neutron n or proton p. They are defined as

$$f_{u/d}^{p} = m_{u/d}\langle p \mid \bar{u}u/\bar{d}d \mid p\rangle, \tag{6.28a}$$

$$f_{u/d}^{n} = m_{u/d}\langle n \mid \bar{u}u/\bar{d}d \mid n\rangle. \tag{6.28b}$$

Note that $f_u^{p/n} + f_u^{p/n} = f_{udN}$ in the isospin symmetric limit. We derived algebraic relations between the individual quark contents and the light quark content of the nucleon. They read

$$f_{u/d}^{p} = \left(\frac{1}{2} \mp \frac{\delta m}{4m_{ud}}\right) f_{ud}^{p} + \left(\frac{1}{4} \mp \frac{m_{ud}}{2\delta m}\right) \delta m \,\langle p \mid \bar{d}d - \bar{u}u \mid p\rangle \tag{6.29}$$

for the proton p. The corresponding expression for the neutron can be obtained by simply replacing p by n. We splitted the Hamiltonian of QCD into an isospin symmetric Hamiltonian H_{iso} and an isospin splitting part $H_{\delta m}$ defined as

$$H_{\delta m} = \frac{\delta m}{2} \int \mathrm{d}^3x \,(\bar{d}d - \bar{u}u). \tag{6.30}$$

To leading order in δm, the isospin splitting δM_N of the nucleon mass can be expressed as

$$\delta M_N = \frac{\delta m}{2}\langle N \mid \bar{d}d - \bar{u}u \mid N\rangle + \mathcal{O}(\delta m^2). \tag{6.31}$$

We plugged

$$\delta m\langle p \mid \bar{d}d - \bar{u}u \mid p\rangle = \Delta_{\text{QCD}} M_N \tag{6.32}$$

into eqn. (6.29) to arrive at the final formulae

$$f_u^{p/n} = \left(\frac{r}{1+r}\right) f_{ud}^{N} \pm \frac{1}{2}\left(\frac{r}{1-r}\right) \frac{\Delta_{\text{QCD}} M_N}{M_N}, \tag{6.33a}$$

$$f_d^{p/n} = \left(\frac{1}{1+r}\right) f_{ud}^{N} \mp \frac{1}{2}\left(\frac{1}{1-r}\right) \frac{\Delta_{\text{QCD}} M_N}{M_N}. \tag{6.33b}$$

We used the ratio $r = {}^{m_u}/_{m_d}$ to simplify the equations.

A practical application of these formulae requires two inputs: The light quark mass ratio r and the QCD splitting of the nucleon mass. We used the result from [19] for the first quantity. At the time of publication of the calculation described in this section in [146], the result for r described in a latter chapter was not available. For the isospin spiting of the nucleon masses we used the number from [20].

6.2.6 Results and conlcusion

Overall, we carried out 192 fits in the main analysis. On average, those fits had ${}^{\chi^2}/_{n_{\text{dof}}} = 1.4$. The standard analysis, with the nucleon mass not fixed to the physical value, allowed for a determination of the mass of the nucleon. This was a good check for the validity of the analysis. The result that we obtained is

$$M_N = 929(16)(7)\,\text{MeV} \tag{6.34}$$

where the first uncertainty is statistical and the second uncertainty is systematic. The result is in very good agreement with the exeprimental value 938.9 MeV [19] for the isospin average nucleon mass.

For the light and strange quark contents we got

$$f_{udN} = 0.0405(40)(35), \tag{6.35a}$$
$$f_{sN} = 0.113(45)(40), \tag{6.35b}$$

with the same conventions for the uncertainties. We translated our results into nucleon sigma terms using the nucleon mass at the physical point. We found

$$\sigma_{udN} = 38(3)(3)\,\text{MeV}, \tag{6.36a}$$
$$\sigma_{sN} = 105(41)(37)\,\text{MeV}. \tag{6.36b}$$

We determined, using the eqns. (6.33a) and (6.33b), the individual quark contents to be

$$f_u^p = 0.0139(13)(12), \tag{6.37a}$$
$$f_u^n = 0.0116(13)(11), \tag{6.37b}$$
$$f_d^p = 0.0253(28)(24), \tag{6.37c}$$
$$f_d^n = 0.0302(28)(24). \tag{6.37d}$$

The results are in nice agreement with other lattice computations. For details see the discussion at the end of the chapter. For the strange quark contents the uncertainties are relatively large. The reason is the limited lever arm in the strange direction. As can be seen if figure 6.4, the slope of the nucleon mass in the strange quark mass direction is relatively low and the spread of the datapoints is not very large. This situation can be improved on either by increasing the statistical precision of the data or by increasing the lever arm in the strange direction. This is part of our motivation for the 3hex analysis, described in the following section, which implements both improvements.

6.3 The 3hex analysis

The purpose of the this analysis is to improve upon the 2hex analysis described in the last section. The main disadvantages of the 2hex analysis are the limited lever arm in the strange quark mass direction, and the comparatively high statistical uncertainty. Together, they result in a large uncertainty of the strange sigma term. A different data set, called “3hex," on the other hand, provides a larger lever arm and much higher statistical precision. It allows to greatly improve the uncertainty of the strange sigma term. A disadvantage is that no configurations with physical pion masses are present in this dataset. Consequently, an extrapolation to the physical pion mass is limiting the precision on the light quark sigma term to a size comparable to the one obtained in the 2hex analysis, despite the improved precision of the input data.

While we fitted in the 2hex analysis the nucleon mass directly as a function of the quark masses, we used a different strategy in the 3hex case. After determining all the masses on the individual

configurations, in a similar fashion then in the 2hex analysis, we fitted the nucleon mass as a function of the pion and reduced kaon masses. To achieve this, it was not required to determine explicitly the dependence between the pseudoscalar meson masses and the quark masses. Doing so was more difficult then in the 2hex case since the statistical precision on the meson masses is much higher. This initially seemed to be an advantage but it required us to either know the precise form of said dependencies, which we did not, or to use a very high number of terms in a Taylor expansion based fitting ansatz. Since we also had to extrapolate to the physical pion mass, using many terms in a Taylor expansion introduced instabilities to the fit. We circumvented these problems by calculating the relation between the psudoscalar meson masses and the quark masses on a second dataset. This dataset features high precision measurements of the pion and kaon masses on ensembles that very closely bracket the phyiscal point. This enabled us to use, despite of the high precision of the data, a low order Taylor expansion. Since the ensembles in this second dataset where generated with a staggered action, the quark masses appearing in the Lagrangian renormalize only multiplicatively. Therefore, we where able to use them directly. Together, these features of the staggered dataset greatly simplified the calculation compared to a strategy where only Wilson data would have been used.

6.3.1 The lattice setup

This analysis relied a combination of Wilson and staggered ensembles in order to utilize the different strength of both actions.

The Wilson gauge configurations have been generated using the same Symmanzik improved gauge action that was used for the 2hex dataset. The fermion action features three levels of HEX smearing. For the production of the gauge configurations, four non-degenerate quark flavors where used. Details on the configuration can be found in [20]. The ensembles feature a wide range of pion and kaon masses, as can be seen in figure 6.5. The range of covered kaon masses reduces as the pion mass approaches the physical point. To alleviate this, we generated two additional ensembles specifically for this project. These also increased the total range in the reduced kaon masses. One of the new ensembles was generated with u, d and s quarks having degenerate masses. The other was generated with degenerate u and d masses. An overview of the QCD ensembles can be found in table 6.2. For the determination of the finite volume corrections we employed charged ensembles. These are generated with the same QCD action as the neutral ones but also included dynamical QED effects. These charged ensembles are a subset of the charged ensambles from [20] and are listed in table 6.3.

For the staggered part, we employed a set of ensembles generated with a tree level Symmanzik improved gauge action and a fermion action with 4 times stout smeared gauge links. These ensembles are tuned to closely bracket the physical point. The spatial volumes in lattice units where chosen such that the physical volumes of all ensembles are roughly equal and that $M_\pi L \approx 4$. A full list of the ensembles can be found in table 6.4. The action used in these ensambles is detailed in [150, 151]

Table 6.2 – *Neutral 3hex ensembles used for the determination of mesonic light ans strange sigma terms. Numbers are from [20] with an modified determination of the pion mass from [3] and two datapoints specifically generated for this project [3].*

$6/g^2$	am_u	am_d	am_s	$L^3 \times T$	m_π[MeV]	$m_\pi L$	$N_{\text{traj}}/1000$	new
3.2	-0.0686	-0.0674	-0.068	$32^3 \times 64$	413	6.9	1	
3.2	-0.0737	-0.0723	-0.058	$32^3 \times 64$	353	5.9	4	
3.2	-0.0733	-0.0727	-0.058	$32^3 \times 64$	356	5.8	1	
3.2	-0.0776	-0.0764	-0.05	$32^3 \times 64$	294	4.9	4	
3.2	-0.0805	-0.0795	-0.044	$32^3 \times 64$	238	4.0	12	
3.2	-0.0806	-0.0794	-0.033	$32^3 \times 64$	266	4.4	12	
3.2	-0.0686	-0.0674	-0.02	$32^3 \times 64$	488	8.1	4	
3.2	-0.0737	-0.0723	-0.025	$32^3 \times 64$	411	6.8	4	
3.2	-0.0776	-0.0764	-0.029	$32^3 \times 64$	336	5.6	4	
3.2	-0.077	-0.0643	-0.0297	$32^3 \times 64$	438	7.3	4	
3.2	-0.073	-0.0629	-0.0351	$32^3 \times 64$	469	7.8	4	
3.2	-0.077	-0.0669	-0.0391	$32^3 \times 64$	405	6.7	4	
3.3	-0.0486	-0.0474	-0.048	$32^3 \times 64$	422	6.1	1	
3.3	-0.0537	-0.0523	-0.038	$32^3 \times 64$	348	5.1	2	
3.3	-0.0535	-0.0525	-0.038	$32^3 \times 64$	349	5.0	2	
3.3	-0.0576	-0.0564	-0.03	$32^3 \times 64$	275	4.0	12	
3.3	-0.0576	-0.0564	-0.019	$32^3 \times 64$	293	4.2	12	
3.3	-0.0606	-0.0594	-0.024	$48^3 \times 64$	200	4.3	20	
3.4	-0.034	-0.033	-0.0335	$32^3 \times 64$	403	5.0	4	
3.4	-0.0385	-0.0375	-0.0245	$32^3 \times 64$	321	4.0	4	
3.4	-0.0423	-0.0417	-0.0165	$48^3 \times 64$	219	4.1	4	
3.5	-0.0218	-0.0212	-0.0215	$32^3 \times 64$	426	4.4	4	
3.5	-0.0254	-0.0246	-0.0145	$48^3 \times 64$	348	5.4	4	
3.5	-0.0268	-0.0262	-0.0115	$48^3 \times 64$	310	4.8	8	
3.5	-0.0269	-0.0261	-0.0031	$48^3 \times 64$	317	4.9	8	
3.5	-0.0285	-0.0275	-0.0085	$48^3 \times 64$	266	4.1	8	
3.5	-0.0302	-0.0294	-0.0049	$64^3 \times 96$	199	4.1	4	
3.5	-0.027	-0.027	-0.027	$48^3 \times 64$	280	4.4	3	✓
3.5	-0.028	-0.028	+0.009	$48^3 \times 64$	282	4.4	3.5	✓

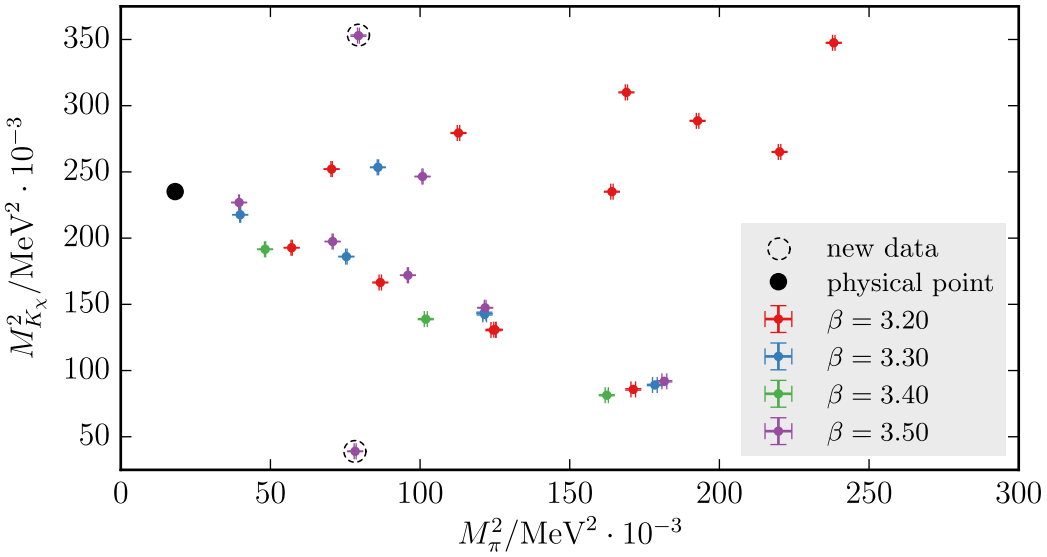

Figure 6.5 – *Landscape of the 3hex dataset in the M_π^2 and $M_{K_\chi}^2$ plane. Different colors correspond to different lattice spacings. The circled points have been generated specifically for this analysis as compared to [20]*

Table 6.3 – *Charged 3hex ensembles that where used to determine the finite volume correction in the determination of the mesonic sigma terms. Numbers are from [3, 20]*

$6/g^2$	am_u	am_d	am_s	$L^3 \times T$	m_π[MeV]	$m_\pi L$	$N_{\mathrm{traj}}/1000$
3.2	-0.0859	-0.0792	-0.0522	$24^3 \times 48$	298	3.7	5
3.2	-0.0859	-0.0792	-0.0522	$32^3 \times 64$	295	4.9	4
3.2	-0.0859	-0.0792	-0.0522	$48^3 \times 96$	295	7.3	4
3.2	-0.0859	-0.0792	-0.0522	$80^3 \times 64$	295	12.2	1

Table 6.4 – *List of 4stout smeared staggered ensembles used for the determination of the mixing matrix J.*

$6/g^2$	am_{ud}	am_s	am_c	$L^3 \times T$	$m_\pi L$	$N_{\text{traj}}/1000$
3.84	0.00151556	0.0431935	0.511843	$64^3 \times 96$	4.1	5.1
3.84	0.00151556	0.04015	.4757775	$64^3 \times 96$	4.1	3.25
3.84	0.00143	.0431935	.511843	$64^3 \times 96$	4.0	3.2
3.84	0.001455	.04075	.4828875	$64^3 \times 96$	4.1	15
3.84	0.001455	.04075	.4665875	$64^3 \times 96$	4.0	3.1
3.84	0.001455	.03913	.4636905	$64^3 \times 96$	4.0	5
3.92	0.001207	0.032	0.3792	$80^3 \times 128$	4.2	10
3.92	0.0012	0.0332856	0.39443436	$80^3 \times 128$	4.2	14.5
4.0126	0.000958973	0.0264999	0.314023	$96^3 \times 144$	4.1	1
4.0126	0.000977	.0264999	0.314023	$96^3 \times 144$	4.2	10
4.0126	0.001002	0.027318	0.323716	$96^3 \times 144$	4.2	2.7

6.3.2 Advanced determination of the fitranges

For each Wilson ensemble several masses had to be extracted. Pion and kaon masses where extracted in a very similar fashion as described in section 6.2.3. We employed an improved procedure to estimate the fit intervals. The statistical uncertainty of the nucleon masses increases as the pion masses get closer to the physical value. That means that the optimal fit range, for which the statistical uncertainty is as small as possible and the systematic excited state effects are subdominant, is, in tendency, earlier for smaller pion masses. To account for this, we devised a strategy to adjust the fitranges based on the statistical uncertainty of the correlation function.

We considered the correlation function $C(t)$ of the nucleon where M is the mass of the nucleon and M' the mass of the first excited state. Including both states, the correlation function takes the form

$$C(t) = c_0(\sinh(-M(t - {}^{N_t}/_2)) + c_1 \sinh(-M'(t - {}^{N_t}/_2))) + \ldots \tag{6.38}$$

Here, "…" indicates even higher excited state contributions, the effect of which we neglected. The presence of the second state in the correlation function introduces a systematic shift to the ground state mass extracted from the correlation function when fitted with an one state ansatz. This is acceptable only if the this shift is smaller then the statistical uncertainty of the extracted mass. Hence, we demanded that the correction by the excited states is smaller then a given fraction r of the statistical uncertainty $\epsilon(t)$ of M. $\epsilon(t)$ can be determined either by fitting the correlation function in the range t to $t + \Delta t$, with Δt being the plateau length or by using the

the effective mass

$$M_{\text{eff}}(t;\Delta t) = -\frac{1}{\Delta t}\log\left(\frac{C(t)}{C(t+\Delta t)}\right) \tag{6.39}$$

Both methods produce similar values for $\epsilon(t)$, although occasionally the two methods resulted in fit ranges differing by at most one lattice spacing. Applying the definition of the effective mass to eqn. (6.38), we arrived at

$$M^{\text{eff}}(t;\Delta t) = \frac{1}{\Delta t}\ln\frac{\sinh(-M(t-{}^{N_t}/_2)) + c_1\sinh(-M'(t-{}^{N_t}/_2))}{\sinh(-M(t+\Delta t-{}^{N_t}/_2)) + c_1\sinh(-M'(t+\Delta t-{}^{N_t}/_2))}. \tag{6.40}$$

If t is small enough for the backward propagating state to be negligible, this expression can be simplified to

$$M^{\text{eff}}(t;\Delta t) = \frac{1}{\Delta t}\ln\frac{\exp(-Mt) + c_1\exp(-M't)}{\exp(-M(t+\Delta t)) + c_1\exp(-M'(t+\Delta t))} \tag{6.41}$$

Upon expanding the inverse of the argument of the logarithm in c_0 we found

$$M^{\text{eff}}(t;\Delta t) = \\ -\frac{1}{\Delta t}\ln\left(\exp(-M\Delta t) + c_1\exp(-(M'-M)t)\exp(-Mt)\cdot(\exp(-(M'-M)\Delta t)-1)\right). \tag{6.42}$$

When Δt is large compared to the decay time of $\exp(-(M'-M)\Delta t)$, the above equation can be written as

$$M^{\text{eff}}(t;\Delta t) = -\frac{1}{\Delta t}\ln\left(\exp(-M\delta t)\left(1 + c_1\exp(-(M'-M)t)\right)\right). \tag{6.43}$$

And with the properties of the logarithm we found

$$M^{\text{eff}}(t) = M - \frac{1}{\Delta t}\ln\left(1 + c_1\exp(-(M'-M)t)\right). \tag{6.44}$$

Assuming that t is big enough for the first excited state to be a small correction, we expanded in this term and arrived at

$$M^{\text{eff}}(t) = M - \frac{c_1}{\Delta t}\exp(-(M'-M)t) + \mathcal{O}\left(\left(\frac{c_1}{\Delta t}\exp(-(M'-M)t)\right)^2\right). \tag{6.45}$$

Demanding that the shift to $M^{\text{eff}}(t)$ due to the excited state is smaller then $r\epsilon(t)$ results in

$$\epsilon(t)r > \frac{c_1}{\Delta t}\exp(-(M'-M)t), \tag{6.46}$$

so that

$$t > -\frac{1}{M'-M}\left(\ln\left(\frac{\epsilon(t)}{\mu}\right) + \ln\frac{r\Delta t\mu}{c_1}\right) \tag{6.47}$$

where μ is an arbitrary constant that makes the argument of the logarithm dimensionless. This condition depends on the uncertainty $\epsilon(t)$ of the effective mass in units of μ, the splitting $M'-M$ and some numerical constant $\log(r\Delta t\mu/c_1)$ which does not depend on time. It is convenient to rephrase the above equation as

$$t > -\frac{\ln\left(\frac{\epsilon(t)}{\mu}\right)}{M'-M} + T \tag{6.48}$$

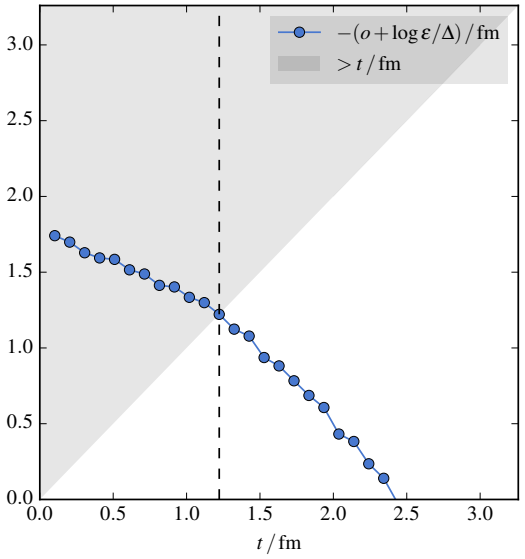

Figure 6.6 *– The condition from eqn. (6.48) on one specific ensemble. The condition is fulfilled when the blue curve is in the white area.*

where T is a constant that has the dimension of time. We evaluated this condition for a wide range of values for T that produce reasonable fit ranges. We have used $T = 0.7, 0.8, 0.9, 1.1$ and set μ equal to the lattice spacing a. For one particular ensemble, the condition from eqn. (6.48) has been visualized in figure 6.6. The effect of this procedure is to shift the starting time fits for ensembles with a low statistical errors to earlier times. We used the procedure to extract the proton mass M_p and the neutron mass M_n. We then calculated the nucleon mass as $M_N = \frac{1}{2}(M_p + M_n)$.

6.3.3 Mesonic sigma terms

In a first step we determined the mesonic sigma terms $\hat{\sigma}_{\pi N}$ and $\hat{\sigma}_{sN}$. These are defined via

$$\hat{\sigma}_{\pi N} = M_\pi^2 \frac{\partial M_N}{\partial M_\pi^2}, \tag{6.49}$$

$$\hat{\sigma}_{K_\chi N} = M_{K_\chi}^2 \frac{\partial M_N}{\partial M_{K_\chi}^2}. \tag{6.50}$$

For this purpose we used the Wilson 3hex configurations described above.

We fitted the lattice data for the nucleon mass to an ansatz of the form

$$M_N(v_i) = M_N^{(\phi)} \prod_i (1 + c_i \Delta v_i)^{t_i} \quad \text{with} \quad \Delta v_i = \left(v_i - v_i^{(\phi)}\right) \tag{6.51}$$

where v_i are variables that the nucleon mass can depend on. $v_i^{(\phi)}$ refers to the values of these variables at the physical point. $M_N^{(\phi)}$ is the measured nucleon mass as found in [9]. The coefficients c_i are parameters that we determined by minimizing the χ^2-value. The parameters t_i are either $+1$ or -1 and correspond in the first case to a term in the Taylor expansion around the physical point and in the second case to a leading order Padé expansion in the variable v_i. If again Taylor expanded, the Padé expansions have the same expansion coefficients as the direct Taylor

Table 6.5 – *The values v_i used in the fitting of the nucleon mass in the 3hex analysis.*

i	meaning	possible t_i values	condition
1	M_π^2	+1	
2	M_{K_χ}	+1/-1	
3	$M_\pi^{\frac{1}{2}} L^{-\frac{3}{2}} e^{-M_\pi L}$	+1	
4	M_π^3	+1	excluded when v_5 is included
5	M_π^4	+1	excluded when v_4 is included
6	$\alpha_s a(M_\pi^2 - M_\pi^{(\phi)2})$	+1	excluded when v_8 and v_9 is included
7	$\alpha_s a(M_{K_\chi}^2 - M_{K_\chi}^{(\phi)}2)$	+1	excluded when v_8 and v_9 is included
8	$a^2(M_\pi^2 - M_\pi^{(\phi)2})$	+1	excluded when v_6 and v_7 is included
9	$a^2(M_{K_\chi}^2 - M_{K_\chi}^{(\phi)}2)$	+1	excluded when v_6 and v_7 is included

expansions but differ in higher order terms. We employed them whenever the effect of higher order terms are not estimated in a different way. In table 6.5 a overview over all variables v_i is given. The first two variables correspond to the leading order pion and kaon mass dependencies of the nucleon. In the case of $v_2 = M_{K_\chi}^2$, the data is sufficiently described by the linear term. We found that including higher order terms leads to coefficients compatible with zero, a deterioration of the fit qualities, and an increases in the uncertainties of the other parameters. We, therefore, estimated the systematic error associated with this fit direction by switching between the Taylor and Padé fit forms. The spread of the data in the $v_1 = M_\pi^2$ direction is sufficient to support a significant curvature. We modeled this curvature either by the next order in the Taylor expansion in M_π^2, by using $v_5 = M_\pi^4$, or by the next order predicted by baryon chiral perturbation theory, $v_3 = M_\pi^3$. [17] $v_3 = M_\pi^{\frac{1}{2}} L^{-\frac{3}{2}} e^{-M_\pi L}$ allows for an estimation of the finite volume effects. [148] The remaining values, v_6-v_9, allow for an estimation of the discretization effects. We fixed the nucleon mass at the physical point to its measured value. Therefore, there are no discretization effects on the nucleon mass at the physical point. Hence, the leading order effects which modify the slopes of the expansion are described by $v_6 = \alpha_s a(M_\pi^2 - M_\pi^{(\phi)2})$ and $v_7 = \alpha_s a(M_{K_\chi}^2 - M_{K_\chi}^{(\phi)2})$. As an alternative, we included $v_8 = a^2(M_\pi^2 - M_\pi^{(\phi)2})$ and $v_9 = a^2(M_{K_\chi}^2 - M_{K_\chi}^{(\phi)2})$ which are formally subleading but are found to be often numerical dominant with the action used as discussed in [66]

The layout of the neutral ensembles (see table 6.2) is such that the extraction of the coefficient c_3 of the finite volume correction Δv_3 is difficult. To improve the reliability of our finite volume corrections, we included the charged ensembles from table 6.3 in the fit. These four ensembles all have the same parameters of the action and differ only in the size of the spatial volume. Hence, they allow for a clean extraction of c_3. These ensembles where generated with an action that includes fully dynamic QED effects. We used the neutron mass M_n instead of the nucleon mass $1/2(M_p + M_n)$ on thees ensembles. Also, instead of the pion and reduced kaon squared masses

we used the connected meson masses $M^2_{\bar{u}u} + M^2_{\bar{u}u}$ and $2M^2_{K_0} - M_{\bar{d}d}$. The quark mass parameters in the QCD+QED action where tuned in such a way that the connected meson masses are equal to the connected meson masses of one of the pure QCD ensambles. For details on the action and the tuning see [20] We verified that c_3 is compatible with the prediction of [148].

The values v_i have uncertainties and these are correlated both with other v_i and with the nucleon masses. We dealt with this in a way closely related to the way described in section 5.6: Some of the v_i are extremely highly correlated, for example $v_1 = M^2_\pi$ and $v_5 = M^4_\pi$. To avoid issues with a singular correlation matrix, we introduced for each ensemble a set of fit parameters δM^2_π and $\delta M^2_{K_\chi}$. We shifted the values of M^2_π and $M^2_{K_\chi}$ measured on the ensembles with these shifts and then calculated form the shifted values v_1-v_9. Then, we calculated the prediction M^{pred}_N for the nucleon mass using eqn. (6.51). and calculated

$$\vec{\delta} = \begin{pmatrix} M^{\text{pred}}_N - M^{\text{meas}}_N \\ \delta M^2_\pi \\ \delta M^2_{K_\chi} \end{pmatrix}$$

where M^{meas}_N is the measured nucleon mass. The contribution of this ensemble to the χ^2 value of the fit is

$$\vec{\delta}^T C^{-1} \vec{\delta}$$

where C is the covariance matrix of the observables M_N, M^2_π and $M^2_{K_\chi}$. In one case, the covariance matrix C was not invertable: For one ensemble the u, d, and s quarks all have degenerate masses. That leads to degenerate values for M^2_π and $M^2_{K_\chi}$ and hence the covariance matrix had one zero eigenvalue. We resolved this issue by adding a regulator ϵ to the diagonal of the covariance matrix rendering it invertable. We then successively reduced ϵ until no change in the fit parameters where detectable.

We estimated the systematic uncertainties introduced by using the expansion in eqn. (6.51) by the following variation of the fit forms:

- By switching on either $v_3 = M^3_\pi$ or $v_4 = M^4_\pi$, we estimated the effect of higher order correction in the M_π direction.
- By using either the Taylor case $t_2 = 1$ or the Padé case $t_2 = -1$, we estimated the effect of higher order correction in the reduced kaon mass direction.
- By modeling the discretization effects either by terms proportional to $\alpha_s a$ or a^2 or by omitting this terms, we estimated the uncertainty of the continuum extrapolation.
- By using a pion mass cut of either 360 MeV order 420 MeV, we estimated the effect of having only data points in a limited range of pion masses.
- By using four different fit ranges for the mass extraction, we estimated the effect of excited state contamination.

In table 6.6 an overview on our variations of terms can be found. All together, we employed 96 different fits for the extraction of the mesonic sigma terms. A representative fit is shown in figure 6.7.

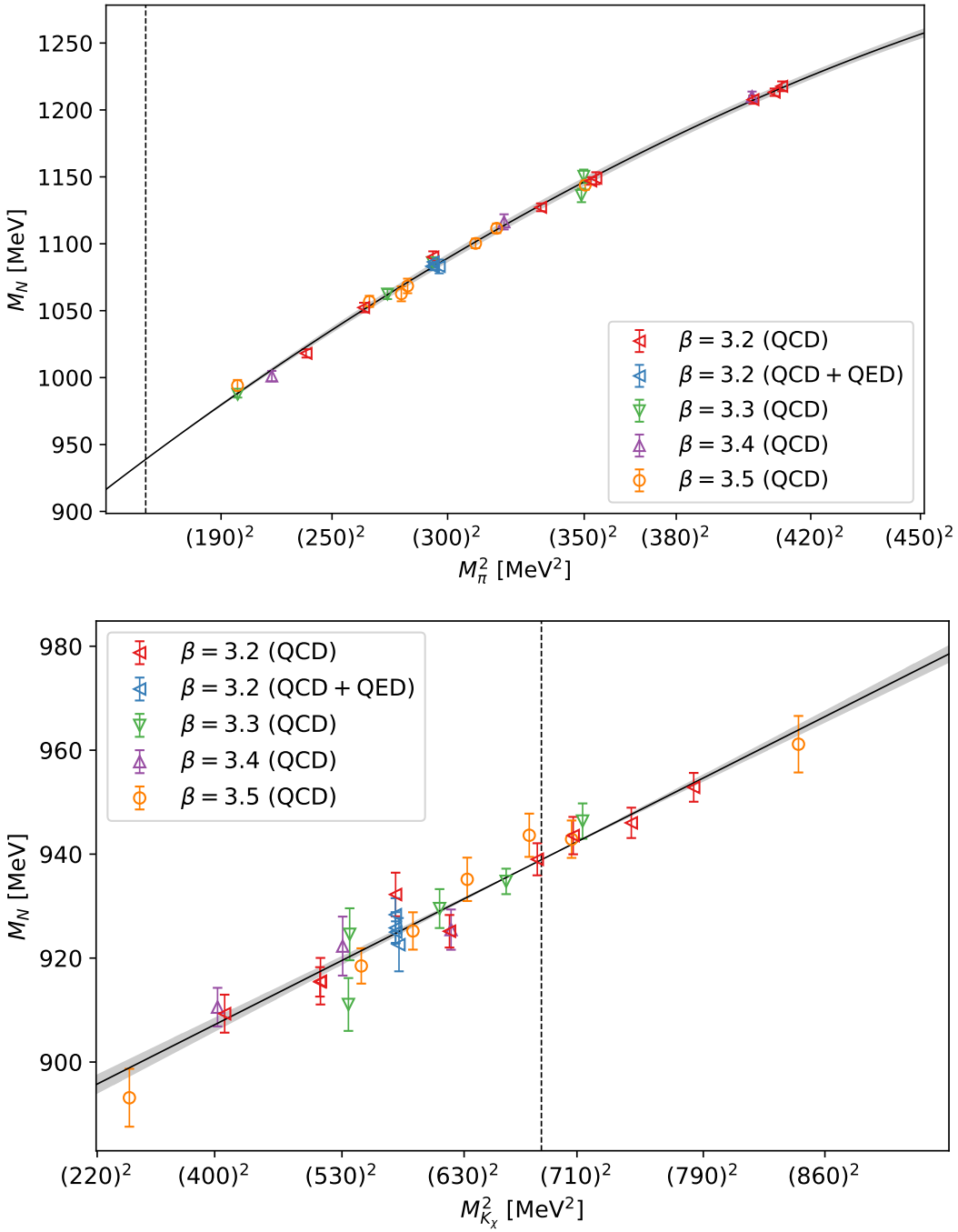

Figure 6.7 – *Two representative fits for the determination of the mesonic sigma terms. In the upper panel the dependence of the nucleon mass on the squared pion mass is shown. In the lower panel the dependence of the nucleon mass on the squared reduced kaon mass is shown. The datapoints have been projected to the physical point except in the squared pion mass or squared reduced kaon mass direction. The dashed line indicates the physical point.*

Table 6.6 – *The variations used to assess the systematic uncertainties of the "mesonic" sigma terms.*

Systematic error	Estimation strategy	N
Higher order terms in pion mass direction	Including either M_π^2 or $M_{K_\chi}^2$ terms in the fit	2
Higher order terms in reduced kaon mass direction	Switching between Taylor to to Padé expansions	2
Finite pion mass range	Different pion mass cuts	2
Discretization effects	Using either $\alpha_s a$ or a^2 or no discretization terms	3
Excited state contamination	Using different fit ranges	4
	Total number of variations:	96

6.3.4 Mixing matrix

We related the "mesonic" sigma terms $\hat{\sigma}_{\pi N}$ and $\hat{\sigma}_{K_\chi N}$ to the true sigma terms σ_{udN} and σ_{sN} via a 2×2 matrix defined by

$$J_{ij} = \frac{m_j}{M_i^2} \frac{\partial M_i^2}{\partial m_j} = \frac{\partial \ln M_i^2}{\partial \ln m_j} \tag{6.52}$$

where $i \in \{ud, s\}$ and $j \in \{\pi, K_\chi\}$. If follows that

$$(\sigma_{udN}, \sigma_{sN})^{\mathrm{T}} = J(\hat{\sigma}_{\pi N}, \hat{\sigma}_{K_\chi N})^{\mathrm{T}}. \tag{6.53}$$

Leading order chiral perturbation theory predicts $J = \mathbb{1}$ [18] (see eqns. (6.9a) and (6.9b)). We determined the correction to this from a set of gauge ensembles generated with a staggered fermion action.

We extracted the pion and kaon masses as well as the pion decay constant on the staggered configurations by fitting a standard staggered cosh-type ansatz with two states to the respective correlation functions. We used two different fitranges, starting from either $t_{\mathrm{min}} = 1.9\,\mathrm{fm}$ or $t_{\mathrm{min}} = 2.3\,\mathrm{fm}$ in physical units and with lengths of 10 lattice spacings. We verified with a Kolmogorov-Smirnov-test that the distribution of the fit qualities are compatible with the expected uniform distribution for both ranges.

As to determine the matrix J, we fitted the values of the three physical observables f_π, M_π^2, and $M_{K_\chi}^2$ as a function of the quark masses. The quark masses them self are not physical observables but parameters of the action. As such they undergo renormalization. We defined the physical values of the quark masses for each gauge coupling independently as the point in the quark mass parameter space at which the squared pion and squared reduced kaon masses acquire their physical values. This defines a mass independent renormalization scheme even though the renormalization factors of this scheme are determined at the physical point.

Around the physical point, each of the before mentioned observables can be Taylor expanded,

resulting in an expression of the type

$$c_0 + c_{1,ud}(m_{ud} - m_{ud}^{(\phi)}[\beta]) + c_{1,s}(m_s - m_s^{(\phi)}[\beta]) + \dots \tag{6.54}$$

Here, rectangular parentheses $[\cdots]$ on a symbol indicate its dependence on the gauge coupling. We expressed the physical light quark mass as $m_{ud}^{(\phi)}[\beta] = m_s^{(\phi)}[\beta]/r[\beta]$ where r is the ratio between the strange and the light quark mass. This ratio is a renormalization scheme and scale independent quantity and the cut-off dependence of it can be written as $r = r_0 + r_1 a^2 + \mathcal{O}(a^4)$, replacing the generic β dependence. We, therefore, reexpressed the Taylor series from eqn. (6.54) as

$$c_0 + c'_{1,ud}\left(\frac{m_{ud} r}{m_s^{(\phi)}[\beta]} - 1\right) + c'_{1,s}\left(\frac{m_s}{m_s^{(\phi)}[\beta]} - 1\right) + \dots \tag{6.55}$$

where $c'_{1,i} = m_i^{(\phi)} c_{1,i}$. We defined

$$\Delta_{ud} = \frac{m_{ud}(r_0 + r_1 a^2)}{m_s^{(\phi)}[\beta]} - 1, \tag{6.56a}$$

$$\Delta_s = \frac{m_s}{m_s^{(\phi)}[\beta]} - 1 \tag{6.56b}$$

and used the expansion from eqn. (6.55) up to quadratic order, including a^2 corrections on the leading terms:

$$c_0 + (c'_{1,ud} + d_{1,ud} a^2)\Delta_{ud} + (c'_{1,s} + d_{1,s} a^2)\Delta_s + c_{2,ud,s}\Delta_{ud}\Delta_s + c_{2,ud}\Delta_{ud}^2 + c_{2,s}\Delta_s^2 \tag{6.57}$$

A feature of our ensembles is that the ratio of the charm to the strange quark mass is constant for all but one ensemble. We generated this one ensemble specifically for this calculation to allow us to disentangle the charm quark mass dependence from the strange quark mass dependence. We added to the above expansion a term depending on the charm to strange quark mass ratio to account for this ensemble resulting in an expansion of the form

$$c_0 + (c'_{1,ud} + d_{1,ud} a^2)\Delta_{ud} + (c'_{1,s} + d_{1,s} a^2)\Delta_s + c_{2,ud,s}\Delta_{ud}\Delta_s + c_{2,ud}\Delta_{ud}^2 + c_{2,s}\Delta_s^2 + c_{c/s}\Delta_{c/s} \tag{6.58}$$

with

$$\Delta_{c/s} = \frac{m_c}{m_s} - \left(\frac{m_c}{m_s}\right)^{(\phi)}. \tag{6.59}$$

We used eqn. (6.58) to fit the squared mass M_π^2 of the pion, the squared reduced kaon mass $M_{K_\chi}^2$, and the value of the pion decay constant f_π as a function of the quark masses. Results of the fits with this function are displayed in figures 6.8, 6.9, and 6.10.

To estimate the systematic uncertainties of our results, we performed a number of different analyses. We varied the following features of our fit functions:

- We used two different values for the starting point of the plateau fits used to extract the pion and kaon masses and the decay constant.
- We found that quadratic terms proportional to Δ_{ud}^2 and Δ_s squared where not statistically significant. To estimate their effect on the results, we either included or excluded them from the fits.

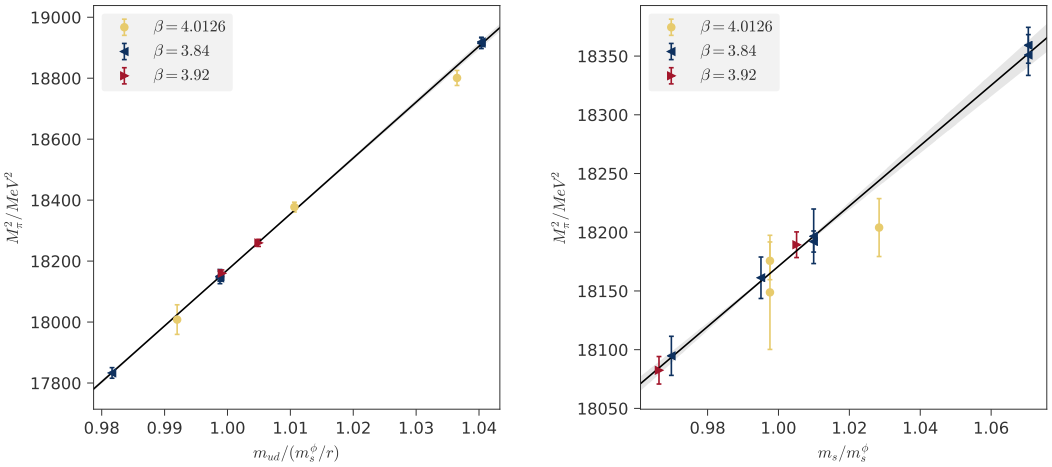

Figure 6.8 – *Dependence of the squared pion mass M_π^2 on the light and strange quark mass as determined from one of many fits. The datapoints are projected to the physical point using the fit function in all but the displayed direction.*

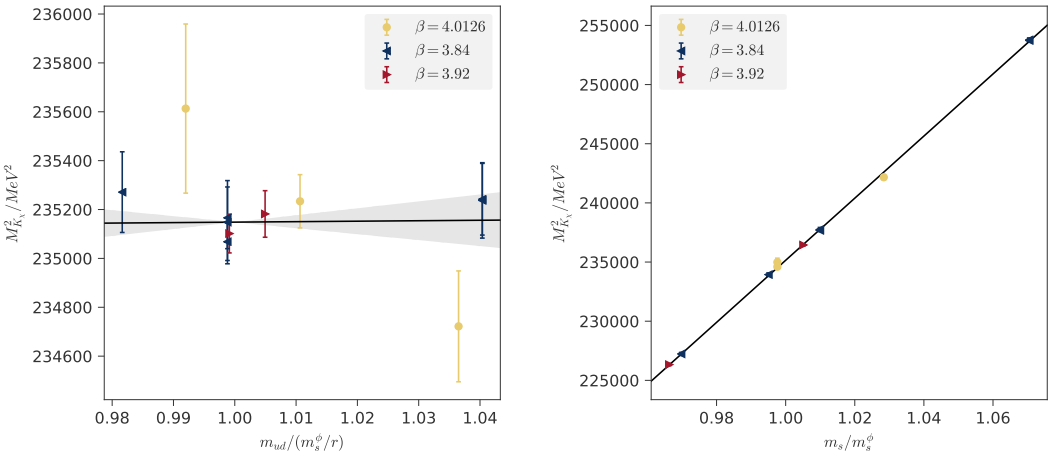

Figure 6.9 – *Dependence of the squared reduced kaon mass $M_{K_\chi}^2$ on the light and strange quark mass as determined from one of many fits. The datapoints are projected to the physical point using the fit function in all but the displayed direction.*

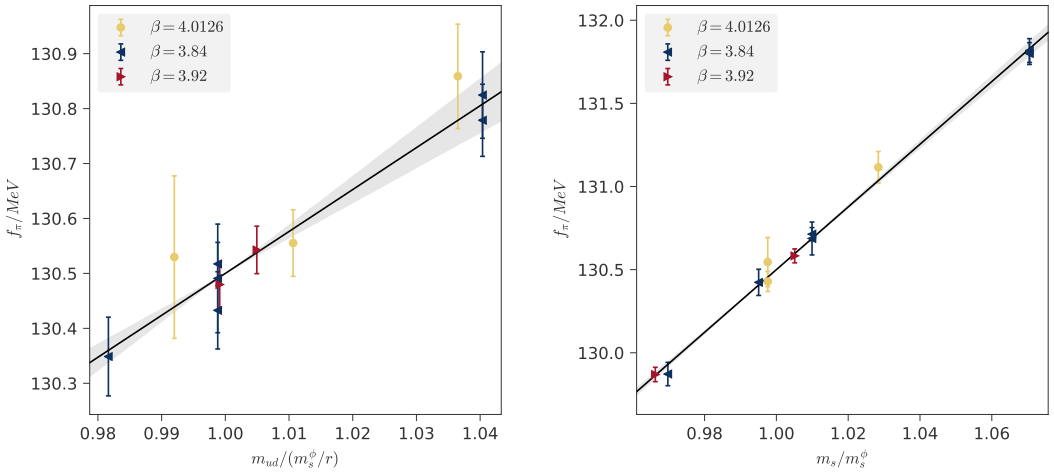

Figure 6.10 – *Dependence of the pion decay constant f_π on the light and strange quark mass as determined from one of many fits. The datapoints are projected to the physical point using the fit function in all but the displayed direction.*

- To estimate the effect of finite lattice spacings we switched the terms proportional to the leading lattice spacing corrections $a^2\Delta_{ud}$ and $a^2\Delta_s$ on or off.

In table 6.7 all variations are summarized.

We performed a completely independent analysis with a different strategy: Instead of fitting the squared masses M_π^2 and $M_{K_\chi}^2$ as a function of the quark masses, in that analysis we fitted the quark masses as the function of M_π^2 and $M_{K_\chi}^2$. Both analysis strategies give equivalent results even on the level of individual fits. For our final analysis we have chosen to use the latter method.

6.3.5 Results for the light and strange sigma terms

Using our results for the mesonic sigma terms $\hat{\sigma}_{udN}$ and $\hat{\sigma}_{sN}$ and for the mixing martix J, we calculated the light and strange quark quark contents. We used, again, the histogram method to calculate the systematic uncertainties. We checked that flat weighting, weighting with the fit quality, and AIC weighting gave consistent results. We quoted as final results the AIC weighted ones. We arrived at

$$f_{udN} = 0.0398(32)(44), \tag{6.60a}$$
$$f_{sN} = 0.0577(46)(33). \tag{6.60b}$$

Table 6.7 – *The variations used to assess the systematic error on the Jacobi matrix relating the "mesonic" sigma terms to the true sigma terms.*

Systematic error	Estimation strategy	N
Excited state contribution to the extracted masses	The fit range used for the mass extraction is varied; the fit is carried out on one aggressive and on one conservative range that differ by a time interval of on lattice unit.	2
Higher order terms	The quadratic terms in Δ_{ud} and Δ_s are either switched on or off	2
Finite lattice spacing	$a^2\Delta_{mud}$ and $a^2\Delta m_s$ terms are either switched on or off independently	4
	Total number of variations:	16

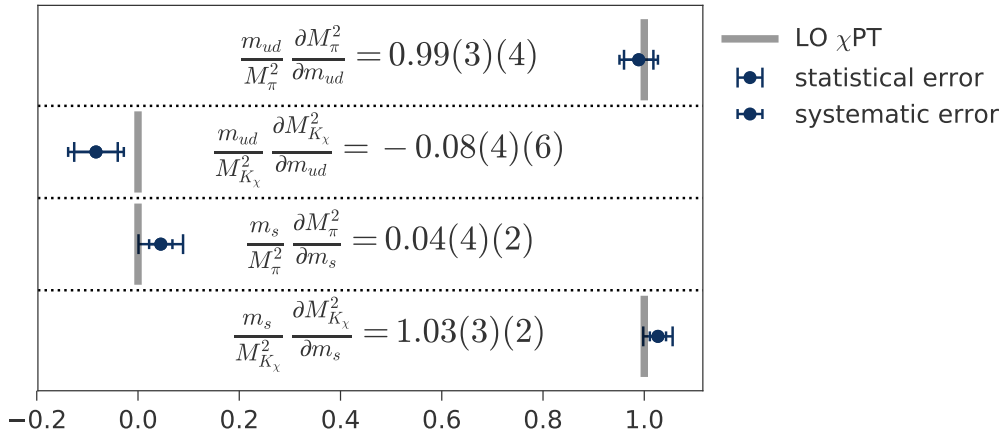

Figure 6.11 – *Results for the mixing matrix J determined with AIC weights. The blue points are the result from the analysis described in the main text. Long errorbars indicate statistical errors and short errorbars indicate systematic errors. The grey lines indicate the predictions of leading order χPT.*

Table 6.8 – *List of 4stout smeared staggered ensembles used for the determination of the charm sigma term. On each configuration the nucleon mass was measured on 64 configuration separated by 10 HMC trajectories.*

$6/g^2$	am_{ud}	am_s	am_c	$L^3 \times T$
3.7	0.00205349	0.05729111	0.509175	$48^3 \times 64$
3.7	0.00205349	0.05729111	0.6788996535	$48^3 \times 64$
3.7	0.00205349	0.05729111	0.848625	$48^3 \times 64$
3.84	0.001455	0.04075	0.362166	$64^3 \times 96$
3.84	0.001455	0.04075	0.4828875	$64^3 \times 96$
3.84	0.001455	0.04075	0.603609	$64^3 \times 96$
3.75	0.00184096226140973	0.0495930491285886	0.440758	$56^3 \times 96$
3.75	0.00184096226140973	0.0495930491285886	0.587677632173775	$56^3 \times 96$
3.75	0.00184096226140973	0.0495930491285886	0.734597	$56^3 \times 96$

The digits in the first parenthesis indicate the statistical uncertainties and the ones in the second parenthesis indicate the systematic uncertainties of our calculations. Using eqns. (6.33a) and (6.33b), we calculated the individual up (u) and down (d) quark contents of the proton (p) and the neutron (n):

$$f_{u,p} = 0.0142(12)(15) \tag{6.61a}$$
$$f_{u,n} = 0.0117(11)(15) \tag{6.61b}$$
$$f_{d,p} = 0.0242(22)(30) \tag{6.61c}$$
$$f_{d,n} = 0.0294(22)(30) \tag{6.61d}$$

6.4 The charm sigma term from the lattice

To determine the charm sigma term, we followed a different strategy then for the light and strange sigma terms. We used a set of nine staggered ensembles, three at each of the values $\beta = 3.75$, $\beta = 3.7753$, and $\beta = 3.84$ of the gauge coupling. An overview over the ensembles can be found in table 6.8.

At each gauge coupling, a "central" ensemble with quark masses very close to the physical point was chosen. For each central ensemble we generated two additional ensembles with all parameters except the charm quark mass chosen the same as for the central ensembles. We used $m_c = {}^3\!/_4 m_c^{\text{central}}$ for one ensemble and $m_c = {}^5\!/_4 m_c^{\text{central}}$ for the other. Here, m_c^{central} is the chram mass of the central ensemble. Using a finite difference formula, we calculated the charm derivative directly from these ensembles.

6.4.1 Extraction of masses

We determined the masses of the nucleons the staggered ensembles in two different ways that are explained below.

Let $O(t)$ be an interpolating operator of a nucleon that is defined such that only products of quark fields located at one timeslice t contribute. Let us call this type of operator local in time. Its correlation function is [152]

$$C_O(t) = \sum_{i=0}^{N_{\text{states}}-1} a_i p_i^{t+1}(\exp(-m_i t) + (-1)^{t+1}\exp(-m_i(N_t - t))) \tag{6.62}$$

where i sums over all contributing states. For each state a_i is a prefactor, m_i is the mass of this state and p_i is the parity which can be either 1 or -1. Due to the the staggered formulation, all operators that are local in time couple to a particle and to its parity partner. It is expected that both couplings are large so that N_{state} must be at least 2 and frequently $p_1 = -1p_0$. It is, however, possible to find operators that are defined on more than one timeslice that get rid of excited state contributions to the correlation function. Such an operator $O'(t)$ has the form

$$O' = \sum_{\tau=0}^{m} b_j \exp(H\tau) O \exp(-H\tau) \tag{6.63}$$

where O is an operator defined only on the t-th timeslice and m is two if only the staggered partity partner is to be eliminated.

The correlation function of such an operator with b_j chosen such that the contributions of the first excited states are heavily suppressed can be calculated from the correlation function $C_O(t)$ of the operator O. The method for doing so was devised in [153, 154] and first applied to Wilson fermion in lattice QCD in [155]. We considered the action of the time evolution operator $U(t)$ on O. We define $O^\tau = U(\tau)OU(-\tau)$. The correlation functions $C_O^{\tau\tau'}(t)$ of two of these operators are

$$C_O^{\tau\tau'}(t) = C_O(t+\tau+\tau') = \sum_{i=0}^{N_{\text{states}}-1} a_i p_i^{t+\tau+\tau'+1}(\exp(-m_i(t+\tau+\tau')) + (-1)^{t+\tau+\tau'+1}\exp(-m_i(N_t - t - \tau - \tau')) \tag{6.64}$$

These operators are linear independent for different values of τ. We assumed that the temporal extent N_t is large enough so that we can safely ignore the backward propagating contributions. We then found

$$C_O^{\tau\tau'}(t) = \sum_{i=0}^{N_{\text{states}}-1} a_i p_i^{\tau+\tau'} \exp(-m_i(\tau+\tau')) p_i^{t+1} \exp(-m_i t). \tag{6.65}$$

We constructed the matrix

$$M(t) = \begin{pmatrix} C_O(t) & C_O(t+1) & \dots & C_O(t+m) \\ C_O(t+1) & C_O(t+2) & \dots & C_O(t+m+1) \\ \vdots & \vdots & \ddots & \vdots \\ C_O(t+m) & C_O(t+m+2) & \dots & C_O(t+2m) \end{pmatrix}. \tag{6.66}$$

This is an correlation matrix of linear independent operators and the standard staggered variational method [156] can be used to analyze it. Thereby, the matrix is decomposed to a form

$$M(t) = S^{\dagger} D(t) S \tag{6.67}$$

with

$$D(t) = \mathrm{diag}(p_0^{t+1} \exp(-m_0 t), p_1^{t+1} \exp(-m_1 t), \ldots, p_m^{t+1} \exp(-m_m t)) \tag{6.68}$$

and

$$S_{ij} = c_i p_i^j \exp(-m_i j) \tag{6.69}$$

with c_i being coefficients such that $c_i^{\dagger} c_i = a_i$. We solved the generalized eigenvalue problem (GEVP)

$$M(t_0)\vec{v}_i(t_0, t_1) = M(t_1)\lambda_i(t_0, t_1)\vec{v}_i(t_0, t_1) \tag{6.70}$$

where t_0 and t_1 had to be chosen in a range where approximately only m states contributed. $\lambda_i(t_0, t_1)$ are the generalized eigenvalues and $\vec{v}_i(t_0, t_1)$ are the generalized eigenvectors. The GEVP can be though of to diagonalize the matrix

$$S^{-1} D^{-1}(t_0) D(t_1) S = S^{-1} \,\mathrm{diag}(p_0^{t_1 - t_0} \exp(-m_0(t_1 - t_0)), \ldots, p_m^{t_1 - t_0} \exp(-m_m(t_1 - t_0)))S. \tag{6.71}$$

If $N_{\mathrm{state}} = m$ and backward propagating contribution can be neglected, the resulting generalized eigendecomposition can be used to extract m correlation functions $C_j(t)$ of operators $O'_j(t)$ of the form written in eqn. (6.63) with the coefficients b_i chosen such that only one mass contributes to each correlation function. These correlation function can found using

$$C'_i(t; t_0, t_1) = \vec{v}_i^{\dagger}(t_0, t_1) M(t) \vec{v}_i(t_0, t_1)$$

where the values of t_0 and t_1 are arbitrary. If these assumptions are not fulfilled, then eqn. (6.4.1) can still be used to obtain correlation functions of interesting operators. In this case the coefficients b_i in eqn. (6.63) are not chosen by this method in a way that all but one exponential in correlation functions $C'_i(t; t_0, t_1)$ are eliminated. Instead, all but one exponentials are heavily suppressed. This allows, nevertheless, to significantly improve the ground state mass extraction.

The method was tested with an artificially generated correlation function of the form as in eqn. (6.62) with $N_{\mathrm{states}} = 6$ and the masses, parities, and prefactors chosen arbitrarily in a reasonable range by hand. In figure 6.12 the effect of using $m = 6$ and $m = 4$ can be seen. We choose for illustrative purposes $t_0 = 3$ and $t_1 = 6$. Here, the effective masses

$$m_i^{\mathrm{eff}}(t; t_0, t_1) = -\frac{1}{2} \log\left(\frac{C'_i(t; t_0, t_1)}{C'_i(t + 2; t_0, t_1)}\right) \tag{6.72}$$

are shown. In the first case all the input masses are reproduced except for a deviation of the effective mass curves at large times. In the second case, the method fails to project out the individual states exactly. However $C'_0(t; t_0, t_1)$ has a significantly reduced overlap with the excited states. The higher $C'_i(t; t_0, t_1)$ have an slight overlap to the ground state and all other states and asymptotically show the same decay as the ground state. Depending on the strength of the overlaps, an reliable mass extraction might or might not be possible. Note that the asymptotic

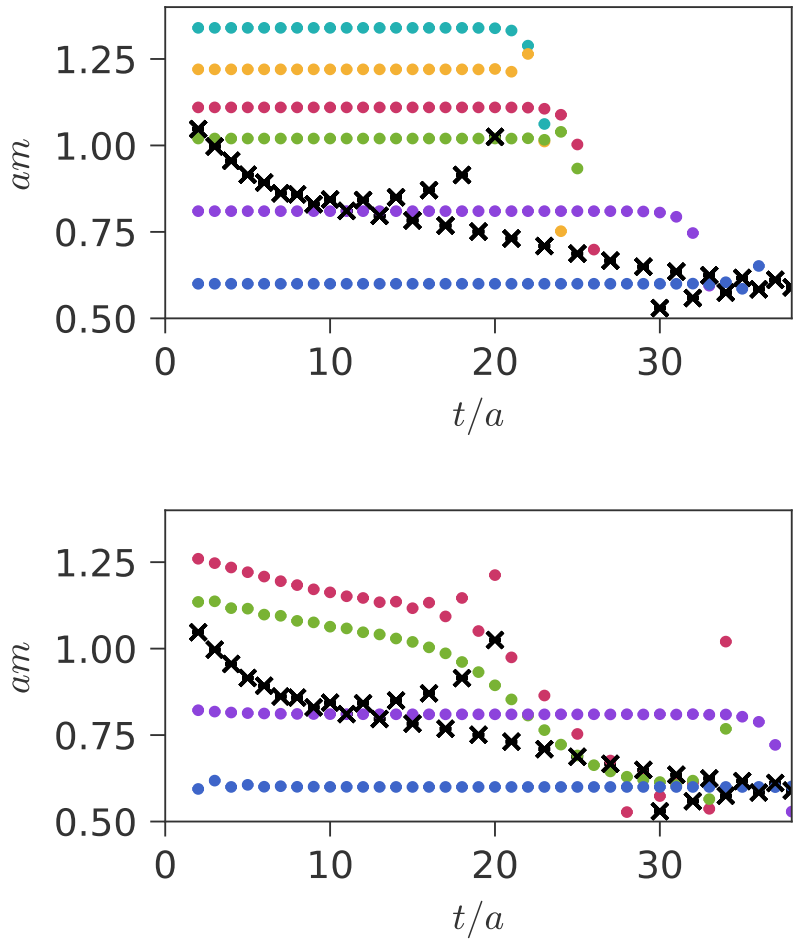

Figure 6.12 – *The GEVP based analysis applied to artificial data. A artificial correlation function with contributions of exactly six states has been generated. This correlation function has been analyzed with the GEVP based method described in the main text. In both panels the colored dots correspond to effective masses of the projected correlation functions $C_i'(t;t_0,t_1)$. The black crosses correspond to the effective mass of the original correlation function $C_O(t)$. In the upper panel the matrix size was taken to be 6×6. On the lower panel the matrix size was 4×4. If the matrix is big enough to accommodate for all states then all energies are reproduced. If the matrix is smaller, the projection to single exponentials is not perfect. The ground state has tiny admixtures of higher states and can be well extracted. The other correlation function have admixtures of the ground state and eventually approach the ground sate mass. A reliable extraction of the masses might or might not be possible. In both cases the effective mass of $C_0'(t;t_0,t_1)$ converges to the ground state mass significantly earlier.*

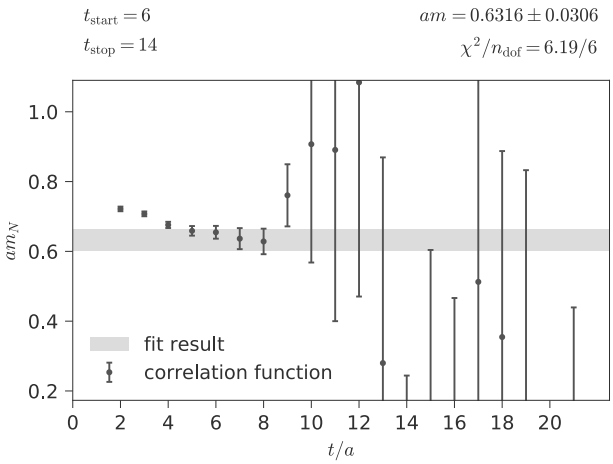

Figure 6.13 – *Fit of the nucleon mass with the GEVP method described in the main text. The matrix size was 2×2. The points with errorbars correspond to the effective mass calculated from projected correlation function $C_0'(t; t_0, t_1)$ with $t_0 = 3$ and $t_1 = 6$. The shaded region indicates the mass extracted with a fit of an one-state exponential ansatz to the correlation function.*

behavior of the $C_0'(t; t_0, t_1)$ calculated with this procedure is the same then the one of the original correlation function $C_O(t)$ but with the excited states contributions heavily suppressed. In practice for the extraction of the nucleon mass it sufficed to use $m = 2$ to eliminate the lowest lying parity partner state. An example of the effective mass of the nucleon on one of our ensembles generated with this method can be found in figure 6.13

The lowest lying parity partner state can also be eliminated from the correlation function by considering a optimized linear combination of the correlation function $C_O(t)$ and the shifted correlation function $C_O(t + 1)$ of the form

$$D_O(t) = C_O(t) + e^{\tilde{m}} C_1(t) \tag{6.73}$$

where $\tilde{m}$ has to be chosen such that the oscillating signal of the parity partner state cancels. To that end we defined the effective mass

$$m^{\mathrm{eff}}(t) = -\log\left(\frac{D_O(t)}{D_O(t+1)}\right) \tag{6.74}$$

and its average between the times t_a and t_b:

$$\bar{m}^{\mathrm{eff}}(t_a, t_b) = \sum_{t=t_a}^{t_b} m^{\mathrm{eff}}(t). \tag{6.75}$$

We minimized

$$\chi^2 = (m^{\mathrm{eff}}(t) - \bar{m}^{\mathrm{eff}}(t_a, t_b))C^{-1}(t, t')(m^{\mathrm{eff}}(t') - \bar{m}^{\mathrm{eff}}(t_a, t_b))$$

to determine $\tilde{m}$. The resulting $D_O(t)$ can be fitted with a standard one-state exponential ansatz.

Both methods described above allow to determine a correlation function that has a reduced contribution of excited states and that can be fitted with a simple exponential ansatz. We have checked that both methods produce results for the charm sigma term that are in very good agreement if all other systematics are treated in the same way. We have chosen to use the second method for our final analysis.

For the calculation of the charm sigma term, we needed not only the nucleon masses but also the differences of nucleon masses on the different ensembles at each gauge coupling. There are three possible differences

$$\Delta^{+} M_N = M_N(m_c = {}^5\!/_4 m_c^{\text{central}}) - M_N(m_c = m_c^{\text{central}}), \tag{6.76a}$$

$$\Delta^{-} M_N = M_N(m_c = m_c^{\text{central}}) - M_N(m_c = {}^3\!/_4 m_c^{\text{central}}), \tag{6.76b}$$

$$\Delta^{+-} M_N = M_N(m_c = {}^5\!/_4 m_c^{\text{central}}) - M_N(m_c = {}^3\!/_4 m_c^{\text{central}}). \tag{6.76c}$$

These fulfill $\Delta^{+-} M_N = \Delta^{+} M_n + \Delta^{-} M_n$ We calculated these differences not from the extracted nucleon masses but we calculated ratios of the optimized correlation functions $D_O(t)$. We fitted these ratios with an exponential ansatz in the same window that was used for the definition of $\tilde{m}$. We choose to t_a in physical units to be either 0.8 fm or 1.0 fm. We choose $t_b/a = t_a/a + 8$ to keep the size of the covariance matrix reasonable.

6.4.2 Calculation of the derivative

We estimated the derivative $m_c \partial M_N / \partial m_c$ from linear combinations of $\Delta^{+} M_n$ and $\Delta^{-} M_n$. Here, we used two different types of linear combinations. We used the difference between the two approaches to estimate the systematic uncertainty introduced by using a finite difference approximation.

First we considered the nucleon mass $M_N(m_c)$ as a function of the charm quark mass. It was natural to apply a finite difference approximation to the derivative of this function. We optimized this finite difference approximation to cancel the leading order correction by using the linear combination

$$\sigma_{cN} = m_c \frac{\partial M_N}{\partial m_c} = 2 \frac{\Delta^{+} M_N + \Delta^{-} M_N}{M_N^{(\phi)}}. \tag{6.77}$$

The systematic error made using this truncation is of order $\mathcal{O}((\delta m_c / m_c)^2) = \mathcal{O}(1/16)$.

As an alternative, we considered the results of heavy quark effective theory. It predicts that the sigma terms of heavy quarks are independent of the quark mass with correction of $\mathcal{O}({}^1\!/_{m_q})$. [2] That implies that to leading order

$$\frac{\partial}{\partial m_c} \frac{\sigma_{cN}(m_c)}{M_N(m_c)} = 0 \quad \text{with} \quad \sigma_{cN}(m_c) = m_c \frac{\partial M_N}{\partial m_c}. \tag{6.78}$$

We can deduce that the nucleon mass as a function of the quark mass has the form

$$M_N(m_c) = M_N^{(\phi)} \left(\frac{m_c}{m_c^{(\phi)}} \right)^{\frac{\sigma_{cN}^{(\phi)}}{M_N^{(\phi)}}}. \tag{6.79}$$

Taylor expanding this in $\sigma_{cN}^{(\phi)}$ leads to

$$M_N(m_c) = M_N^{(\phi)} + \sigma_{cN}^{(\phi)} \log \frac{m_c}{m_c^{(\phi)}} + \sigma_{cN}^{(\phi)2} \log^2 \frac{m_c}{m_c^{(\phi)}} + \mathcal{O}(\sigma_{cN}^{(\phi)3}).$$

Plugging this into eqns. (6.76a) and (6.76b) yields

$$\Delta^+ M_N = \sigma_{cN}^{(\phi)} \log \frac{5}{4} + \sigma_{cN}^{(\phi)2} \log^2 \frac{5}{4}, \tag{6.80a}$$

$$\Delta^- M_N = \sigma_{cN}^{(\phi)} \log \frac{4}{3} - \sigma_{cN}^{(\phi)2} \log^2 \frac{4}{3}. \tag{6.80b}$$

Eliminating the contribution quadratic in $\sigma_{cN}^{(\phi)}$ we found

$$\sigma_{cN} = \frac{1}{\log \frac{5}{4} \log \frac{4}{3} \log \frac{5}{3}} \left(\log^2 \frac{4}{3} \Delta^+ M_N + \log^2 \frac{5}{4} \Delta^- M_N \right). \tag{6.81}$$

Here, the systematic error on σ_{cN} is of order $M_N^{(\phi)} \mathcal{O}\left(\left(\sigma_{cN} / M_N^{(\phi)} \right)^3 \right) = M_N^{(\phi)} \mathcal{O}(3 \times 10^{-4})$.

6.4.3 Error analysis and results

To estimate the systematic uncertainties, we performed 24 different analyses and used the histogram method to combine them. For the uncertainty due to remaining excited state contributions we used two different fit ranges. We estimated the uncertainty associated with the finite difference approximations by using the two different approximations described above. For the scale setting uncertainty, we used either the nucleon mass at the central ensemble or the pion decay constant f_π as the lattice scale. Finally, we had to deal with the uncertainty associated with the discretization artifacts. Here, we choose to use one of the following three continuum extrapolations:

i. A fit constant in a^2 with only the two coarsest lattice spacings included.
ii. A fit constant in a^2 with all lattice spacings included.
iii. A fit linear in a^2 with all lattice spacings included.

An overview of the variations can be found in table 6.9. We arrived at

$$f_{cN} = \frac{\sigma_{cN}}{M_N} = 0.0734(45)(55). \tag{6.82}$$

6.5 Heavy quark sigma terms

The sigma terms of the heavy quarks can be deduced from eqn. (2.7). As a crosscheck, we have applied this formula to the charm sigma term. Using dimensional analysis, we expected the leading order error of this estimation to be of order $\mathcal{O}(\Lambda_{\mathrm{QCD}}^2 / m_c^2) \approx 6\%$. Plugging in the coefficients from table 2.2 and our results for the light and strange quark contents we arrived at

$$f_c = 0.07323(61)(65) \tag{6.83}$$

Table 6.9 – *The variations used to assess the systematic uncertainty on the charm sigma term.*

Systematic error	Estimation strategy	N
Excited state contribution to the extracted masses	The fit range used for the mass extraction is varied	2
Higher order terms in the finite difference approximation	Different linear combinations are used	2
Scale setting	Either f_π or M_N is used	2
Lattice artifacts	Using a fit linear or constant in a^2 for all lattice spacings or a fit constant in a^2 for the two finest lattice spacings	3
	Total number of variations:	24

where the indicated uncertainties come from the statistical and systematic uncertainties of the lattice determinations of the input quark contents. This is in excellent agreement with our full lattice determination. With similar arguments, we find that the uncertainty of the bottom sigma term due to the heavy quark expansion is much smaller, namely of order $\mathcal{O}(\Lambda^2_{\mathrm{QCD}}/m_c^2) \approx 0.6\%$ The uncertainty of the top quark sigma terms is even smaller. Applying again 2.2 we find

$$f_{bN} = 0.0702(7)(9), \tag{6.84}$$

$$f_{tN} = 0.0680(6)(7). \tag{6.85}$$

6.6 Discussion

Having a controlled calculation of all the sigma terms at hand, we can calculate the full nucleon-Higgs-coupling

$$f_{hN} = \sum_q f_{qN} = 0.3095(59)(62) \tag{6.86}$$

where the first uncertainty is statistical and the second is systematic. The uncertainties where calculated by using consistent bootstrap-samples in all lattice calculations as far as this was necessary due to correlations. For the systematic uncertainties, we had to combine all histograms from the uncertainty estimation of the different subresults. We did this by calculating all possible combinations of the entries of the histograms of all subresults. In our final publication [3] we give a C code that can carry out this combination to calculate f_{hN} or any other linear combination of quark contents with a full propagation of all systematic and statistical uncertainties along the line explained above.

In figure 6.14 the magnitude of the individual contributions to Higgs proton coupling, the quark contents f_{qN}, are shown. Together, they determine the strength of the Higgs proton coupling

compared to the coupling that an imaginary fundamental fermion with the mass of the proton would have. The contributions to the Higgs neutron coupling are of the same relative magnitude except for the up and down contributions. In figure 6.15 the differences between the proton and neutron case are illustrated.

In figure 6.16 we compare our results to other determination of the light and strange sigma terms existing in the literature. For the light sigma term, our results are in good agreement with most lattice calculations. In general, lattice calculations seem to favor a lower value of the light sigma term then recent phenomenological determinations. For the strange sigma term, the lattice calculations in general scatter slightly more. Our results tend to be slightly higher then other recent lattice determinations, especially those that are based on a direct calculations of matrix elements. However, our results are well in the range of values covered by the spread of the existing determinations. For the charm sigma term, we compare our result with other determinations in figure 6.17. Our value is compatible with most previous lattice determination but offers a significantly reduced uncertainty. It is in good agreement with determinations based on heavy quark expansions.

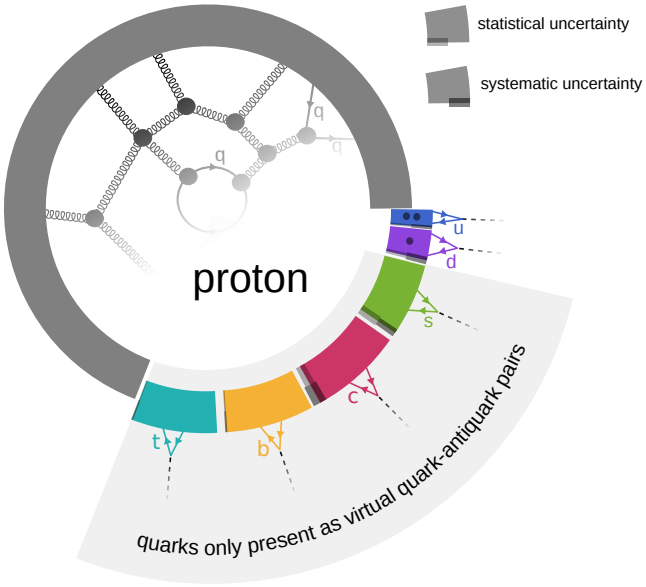

Figure 6.14 – *Contributions of the up, down, strange, charm, bottom, and top quarks to the proton Higgs coupling. The offset parts of the circle correspond to the contribution of the indicated quark flavor to the nucleon Higgs couplig. The individual contributions are shown relative to the mass of the nucleon (full circle).*

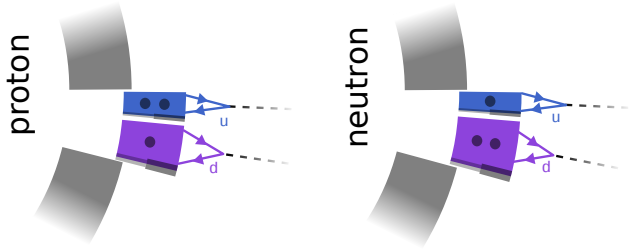

Figure 6.15 – *Difference between the up and down quark contribution to the proton Higgs coupling (left) and the neutron Higgs coupling (right).*

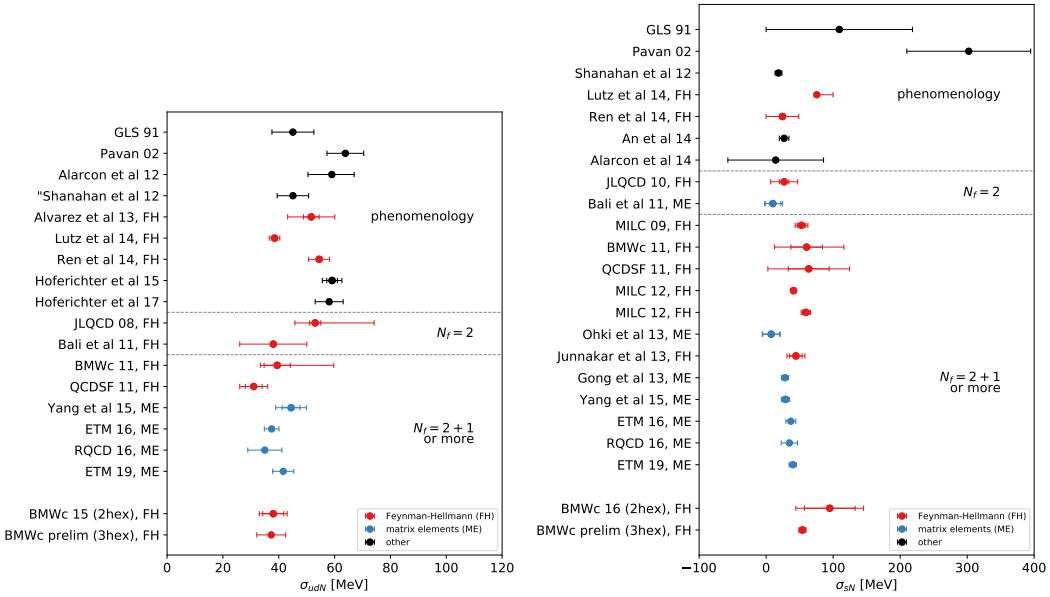

Figure 6.16 – *Comparison between the light and strange sigma terms as determined in this work with previous determinations. The letters "FH" indicate that the calculation have been performed using the* Feynman-Hellman *theorem. The letters "ME" are shorthand for "matrix elements" and indicate lattice computations that where performed using the direct method. The number in the left panel are published in [113] (GLS 91), [114] (Pavan 02), [117] (Alarcon et al 12), [122] (Shanahan et al 12), [123] (Alvarez et al 13), [127] (Lutz et al 14), [126] (Ren et al 14), [115] (Hoferichter et al 15), [118] (Hoferichter et al 17), [144] (JLQCD 08), [132] (Bali et al 11), [134] (BMWc 11), [133] (QCDSF 11), [140] (Yang et al 15), [141] (ETM 16), [142] (RQCD 16), [146] (BMWc 16), [3] (BMWc prelim) and the number in the right panel are published in [113] (GLS 91), [114] (Pavan 02), [122] (Shanahan et al 12), [127] (Lutz et al 14), [126] (Ren et al 14), [124] (An et al 14), [117] (Alarcon et al 14), [131] (JLQCD 10), [132] (Bali et al 11), [129] (MILC 09), [134] (BMWc 11), [133] (QCDSF 11), [135] (MILC 12), [137] (Okhi et al 13), [138] (Junnarkar et al 13), [139] (Gong et al 13), [140] (Yang et al 15), [141] (ETM 16), [142] (RQCD 16), [143] (ETM 19), [146] (BMWc 16), [3] (BMWc prelim).*

Figure 6.17 – *Comparison between the charm sigma term as determined in this work with previous determinations. The letters "FH" indicate that the calculation have been performed using the* Feynman-Hellman *theorem. The letters "ME" are shorthand for "matrix elements" and indicate lattice computations that where performed using the direct method. The letter "HQ" denote calculations based on heavy quark expansions. The shown results are published in the left panel are published in [135] (MILC 12), [139] (χQCD 13), [141] (ETM 16), [142] (RQCD 16), [157] (Hobbs et. al. 17), [16] (Ellis et. al. 18), [143] (ETM 19), [3] (BMWc prelim).*

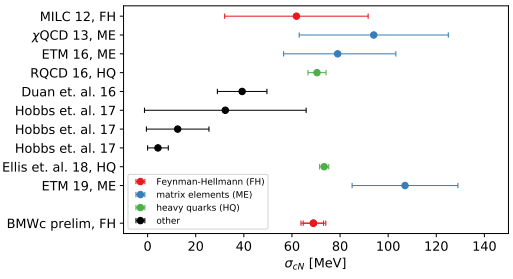

Chapter 7

Light quark mass difference and violations of Dashen's theorem

The following chapter is based on original work published in [106, 158].

The mass difference $\delta m = m_u - m_d$ between the two lightest quarks is, together with the average, an important property of the standard model [9, 19]. It can be determined in lattice calculations if they include non-degenerate light quark masses and electromagnetic effects. The non-degenerate light quark masses are expected to have effects of order $(\delta m/\Lambda_{\mathrm{QCD}})$ on hadron masses, which are about one percent. The electromagnetic effects on hadron masses are predicted to be of order $\mathcal{O}(\alpha)$ with $\alpha \approx 1/137$ being the electromagnetic coupling constant [19]. Both effects are of the same order of magnitude and must be included in a reliable calculation.

δm has been calculated on the lattice many times. The first calculation [159] of this kind was carried out in 1996. It was a quenched calculation which means that the effects of the see quarks where neglected. Later, this quantity was picked up again on the lattice. In [66, 90, 160, 161] the electromagnetic effects where included by employing phenomenological estimates. In [162] for the first time a $N_f = 2$ computation was presented in which electromagnetic effects where calculated in the electroquenched approximation. In that approximation the two light see quarks are dynamic but assumed to have no electric charge. The first calculation in a $N_f = 2 + 1$ setting, also in the electroquenched approximation, was reported in [163]. Since then many other calculation in these settings appeared [164–167]. In [19] these calculations are reviewed in detail.

We present a calculation based on fully dynamic $N_f = 2 + 1$ QCD configurations. We included the electromagnetic corrections, like in the previous studies, in the quenched approximation. The QCD configurations where already used by the BMW collaboration for the determination of the average light quark mass [66, 161]. The BMW collaboration has presented, before the publication of this work, a calculation of hadron mass splittings in full QCD+QED [20]. Although full QED calculation are in principle superior to electroquenched calculations, we nevertheless choose to work in the latter setting. It allowed us to use a dataset featuring pion masses down to the physical point. The dataset used in [20] features only pion masses as low as 195 MeV. Since our calculation is about the light quark masses we find this feature more important. We therefore opted to use the dataset described in [66, 161].

Our calculation is based on $SU(3)$ gauge configurations that where generated with a QCD action featuring degenerate light quarks [66]. We generated $U(1)$ configurations on top of these $SU(3)$ configurations. For that, we assumed that all light sea quarks are degenerate and electrically neutral. When we measured quark propagators, we put different masses for up

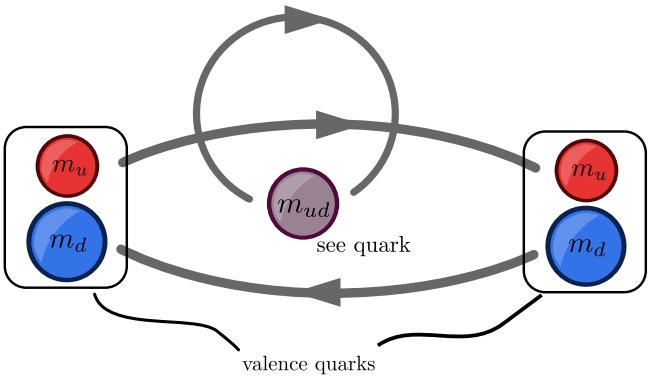

Figure 7.1 – *Effects of the partial quenching. The charged and non-degenrate u and d valence quarks of e.g. a π^+ propagate in a see of uncharged degenrate see quarks. In full QCD+QED also the see quarks would be non-degenerate and charged. Red and blue colors denore positive and negaive charge, the radius is of the quark symbols is proportional to the third root of the corresponding quark mass.*

and down quarks in the fermion matrix. This procedure is called partial quenching. We also took the coupling to the electromagnetic $U(1)$ field into account in these fermion matrices. An illustration of this approach is shown in figure 7.1. Our calculation therefore relies on a partially quenched QCD sector with quenched electromagnetic corrections.

Since δm refers to the difference in the quark mass parameters of the theories' Lagrangian, it requires renormalization. This was addressed in the following way: We replaced δm with the mass splitting ΔM^2 of mesons defined in the partially quenched theory. This mass difference can be related to the quark mass difference by partial quenched chiral perturbation theory [168, 169]. Since the low energy constant appearing in this relation is known, from a calculation based on the same QCD configurations used here, it allows to determine the quark mass difference with small corrections [170].

ΔM^2 must be related to a physical quantity. In this work the mass splitting $\Delta M_K^2 := \frac{1}{2}(M_{K^+}^2 - M_{K^0}^2)$ is used for this purpose. It can be decomposed into two parts within the precision of this work. One part due to the splitting of the light quark masses is proportional to ΔM. The other part is due to the electromagnetic interactions.

Together with δm, we determined another quantity. A well known theorem, Dashen's theorem, states that the isosplin splitting of pions and kaons are the same in the $SU(3)$-flavor symmetric limit. [171] This theorem is violated due to the lack of $SU(3)$ flavor symmetry in nature. The strength of this violation is parametrized by the quantity ε defined as [19]

$$\varepsilon := \frac{\Delta_{\mathrm{QED}} M_K^2 - \Delta_{\mathrm{QED}} M_\pi^2}{\Delta M_\pi^2}. \tag{7.1}$$

To the precision of this calculation $\Delta_{\mathrm{QED}} M_\pi^2$ is equal to ΔM_π^2. [19] Corrections to this identity start at $\mathcal{O}(\delta m^2)$. A direct calculation of the pion mass splitting on the lattice would be much more challenging then the calculation of the kaon mass splitting. This is because for the kaon the valence quarks are of different flavors. For the neutral pion, there are contributions with

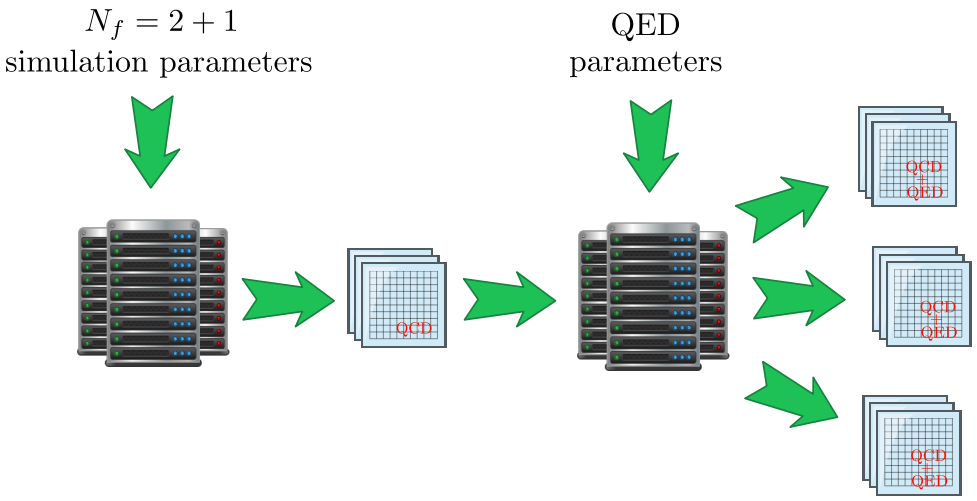

Figure 7.2 *– A visualization of how the gauge configuration used for the determination of the light quark mass difference and the violations of Dashens theorem where generated. In a first step $SU(3)$ gauge configurations where generated with the $N_f = 2 + 1$-QCD parameters. Then using the QED parameters for each QCD gauge configurations QED gauge configurations are produced. (Compter-Icon from* `https://www.iconfinder.com/icons/63466/cloud_computing_data_center_datacenter_hosting_server_servers_icon`*)*

valence quarks of identical flavors. They result in disconnected terms that are difficult to deal with. Fortunately, the pion mass splitting is very well known experimentally. [9]. Hence a lattice determination of $\Delta_{\text{QED}} M_K^2$ is also sufficient to determine ε.

7.1 The lattice setup

The $SU(3)$ gauge configurations where generated with a Symmanzik improved gauge action and a Wilson tree-level improved fermion action. The gauge fields entering the fermion action where smeared with two levels of HEX smearing. The configurations have been used e.g. in [66, 161] and in a determination of the nucleon sigma term [146] described in this thesis.

We generated several $U(1)$ configurations for each $SU(3)$ gauge configuration. The resulting $U(1)$ gauge fields are partially quenched. The procedure is depicted in figure 7.2. We used the non-compact QED_{TL} action We applied no smearing to the $U(1)$ gauge links and the Clover improvement did not include the $U(1)$ links. See also [169] for details on the $U(1)$ configurations and [159, 162, 172] for further explanations of the method. Figure 7.3 depicts the layout of the different fields on the lattice.

We generated two different set of quark propagators for most $SU(3) \times U(1)$ ensembles. For one set we tuned the quark masses in the valence sector so that the bare PCAC (for a definition see e.g. [66]) quark masses, evaluated with the propagators containing the quenched $U(1)$ fields, agree with the bare PCAC masses in the absence of the $U(1)$ fields and with the valence quark masses equal to the see quark masses. For the other set we set the m_u and m_s masses to the same

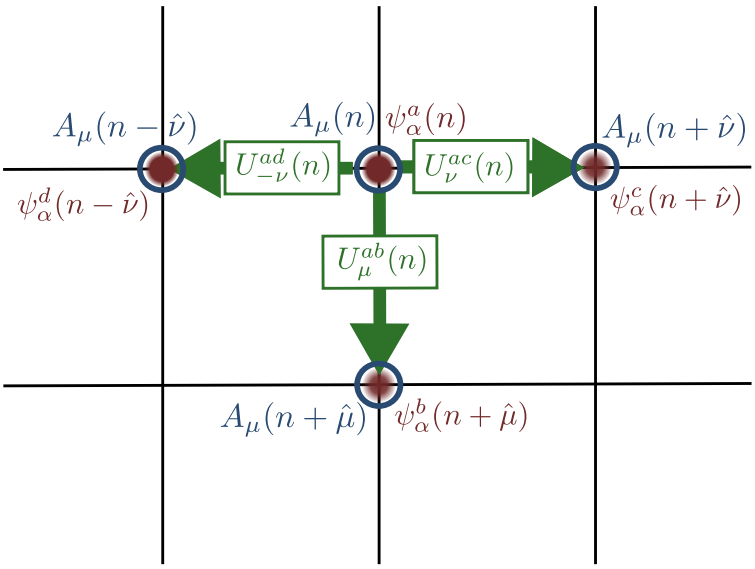

Figure 7.3 *– Layout of the $SU(3) \times U(1)$ gauge fields on a slice of the lattice. The fermion fields (red) reside on each point of the lattice. At each lattice link a $SU(3)$ valued link variable (green) represents the $SU(3)$ gauge fields. The $U(1)$ gauge fields are represented by gauge potentials A_μ (blue) residing at each lattice site.*

value then in the first case. Then m_d was tuned to vary ΔM^2 to bracket the physical point. For one particular ensemble three sets of quark propagators where generated. Two with ΔM^2 close to the physical value and the electromagnetic coupling α twice and four time as large as the physical value. On the third set of propagators we choose $\Delta M^2 \approx 0$ and $\alpha \approx 0$. We extracted masses and mass splitting using the standard ansätze for staggered quarks. See [169] for details.

7.2 Analysis procedure

The action for the valence quarks has 5 free parameters: The strong coupling constant α_s, tuned by the parameter β in the gauge action, the electromagnetic coupling constant α, and the three quark masses m_u, m_d and m_s. β mainly controls the approach to the continuum limit. The physical point is defined at each value of β by the values $(\alpha^{(\phi)}(\beta), m_u^{(\phi)}(\beta), m_d^{(\phi)}(\beta), m_s^{(\phi)}(\beta))$ of the remaining parameters for which four observables acquire their physical value. We used the charged pion mass square $M^2_{\pi^+}$, the squared reduced kaon mass

$$M^2_{K_\chi} := \frac{1}{2}(M^2_{K^+} + M^2_{K^0} - M^2_{\pi^+}), \tag{7.2}$$

the kaon splitting

$$\Delta M^2_K := \frac{1}{2}(M^2_{K^+} - M^2_{K^0}), \tag{7.3}$$

and the electromagnetic coupling α to set the physical point. The last parameter was set directly to its value in the Thompson limit.

ΔM_K^2 is the central quantity in this analysis. Its leading order Taylor expansion in α and δm around the point $\alpha = 0, \delta_m = 0$ is

$$\Delta M_K^2 = C_K(M_{\pi^+}^2, M_{K_\chi}^2, a, L)\alpha + \tilde{D}_K(M_{\pi^+}^2, M_{K_\chi}^2, a)\delta m + \mathcal{O}(\alpha^2, \delta m^2). \tag{7.4}$$

We parametrized the dependence of C_K and $\tilde{D}_K$ on the remaining parameters of the action with the quantities in the brackets. Here, a is the lattice spacing and L is the spatial lattice extend. The QCD contribution $\tilde{D}_K$ and the QED contribution C_K to the kaon mass splitting can be disentangled uniquely only up to the order used here. We used the leading order relation in partially quenched chiral perturbation theory including QED (PQχPT+QED) [168, 169]

$$\Delta M^2 = M_{\bar{u}u}^2 - M_{\bar{d}d}^2 = 2B_2\delta m + \mathcal{O}(m_{ud}\alpha, m_{ud}\delta m, \alpha^2, \alpha\delta m, \delta m^2) \tag{7.5}$$

to replace δm by ΔM^2. The constant B_2 is a low energy constant of PQχPT+QED [168, 169]. The masses $M_{\bar{u}u}$ and $M_{\bar{d}d}$ appearing in this relation are called connected pseudoscalar mesons. These are not physical because the states they correspond to mix in nature to form the π^0 meson. Nevertheless, we can extract their mass in this partially quenched lattice setup unambiguously. We faced no complication with disconnected diagrams because PQχPT+QED [168] predicts that in eqn. (7.5) only the masses calculated from the connected part of the correlation functions of the mesons must be used. We arrived at the expansion

$$\Delta M_K^2 = C_K(M_{\pi^+}^2, M_{K_\chi}^2, a, L)\alpha + D_K(M_{\pi^+}^2, M_{K_\chi}^2, a)\Delta M^2 + \mathcal{O}(\alpha^2, \delta m^2). \tag{7.6}$$

Here D_K plays the role of $\tilde{D}_K$ in eqn. (7.4) and parametrizes the QCD contribution to the kaon mass splitting.

We had to specify how C_K and D_K depend on the indicated parameters. We used Taylor expansions around the physical point to that end. We denoted with $M_{\pi^+}^{(\phi)2}$ and $M_{K_\chi}^{(\phi)2}$ the values of $M_{\pi^+}^2$ and $M_{K_\chi}^2$ at the physical point. The leading order expansion of D_K is

$$D_K(M_{\pi^+}^2, M_{K_\chi}^2, a) = c_0 + c_1(M_{\pi^+}^2 - M_{\pi^+}^{(\phi)2}) + c_2(M_{K_\chi}^2 - M_{K_\chi}^{(\phi)2}) + c_3 f_a(a, \alpha_s) \tag{7.7}$$

where $f(a, \alpha_s)$ is a function that parametrizes the lattice spacing dependence. It is either

$$f(a, \alpha_s) = a^2 \quad \text{or} \quad f(a, \alpha_s) = \alpha_s a. \tag{7.8}$$

The first choice is often numerically dominant while the second choice is the leading behavior determined by the action used. [66] Finite volume corrections to the QCD contribution to the kaon mass splitting are exponentially suppressed in $M_\pi L$ due to the confining property of QCD and therefore negligible compared to the finite volume effects in the QED contribution C_K. We therefore do not include them in eqn. (7.7).

The electromagnetic interaction is a long range interaction and finite volume corrections only decay polynomial in $1/L$ for electromagnetic effects. In the QED$_{\mathrm{TL}}$ formulation, meson masses receive corrections according to [20, 173]

$$\frac{M(L)}{M(\infty)} = 1 - \frac{\alpha\kappa}{M(\infty)L}\left[1 + \frac{1}{M(\infty)L}\left(1 - \frac{\pi}{2\kappa}\frac{T}{L}\right)\right] + \mathcal{O}(\alpha/L^3). \tag{7.9}$$

In that equation, $\varkappa = 2.873\ldots$ is a known constant [20], $M(L)$ is the mass at the spatial lattice extend L, and $M(\infty)$ is the infinite volume mass. This expression does not depend on the inner structure of the mesons up to the $O(1/L^2)$ terms. The terms starting at order $O(1/L^3)$ however do. [20] We corrected all charged meson masses by the leading and next-to-leading order terms in eqn. (7.9) before we performed further fitting. We included the remaining $O(1/L^3)$ corrections, which are structure dependent, by adding a corresponding term to the functional form of C_K with a coefficient determined by the fit. We used the fit function

$$C_K(M^2_{\pi^+}, M^2_{K_\chi}, a, L) = c_0 + c_1(M^2_{\pi^+} - M^{(\phi)2}_{\pi^+}) + c_2(M^2_{K_\chi} - M^{(\phi)2}_{K_\chi}) + c_3 a + c_4 \frac{1}{L^3} \tag{7.10}$$

for C_K. The coefficients c_i are different from the coefficients in eqn. (7.7) although they have the same name for reasons of readability. For C_K, lattice artifacts scale with a.

The above formulae are fitted to the lattice data in fully correlated fits. Figure 7.4 shows the pion and kaon mass dependence of C_K and D_K in the case of one representative fit. The values of the kaon splitting for all ensembles are displayed in figure 7.5. The shaded points indicate the original values, without the application of eqn. (7.9); the solid points show the values corrected by eqn. (7.9). All points are projected to the physical point using eqns. (7.6), (7.7) and (7.10) except in the $1/L$ direction. The solid line and the gray band shows a fit with an $1/L^3$ behavior and its error. The structure dependent corrections starting at order $\mathcal{O}(L^{-3})$ are very small.

We used the physical value of ΔM^2_K, eqn. (7.6), eqn. (7.5), and the value of B_2 from [170] in the $\bar{\text{M}}$S scheme at $\mu = 2\,\text{GeV}$ to extracted from the fit δm, its contribution D_K to the Kaon mass splitting, and the QED contribution C_K to the Kaon mass splitting.

7.3 Estimation of systematic and statistical uncertainties

Our calculation is affected by several systematic uncertainties that we estimated using the histogram method [17]. For that, several equally valid fits have been performed. In table 7.1 all lattice sources of systematic uncertainties and the variation of the fit functions we used to estimate them are shown. In total we performed 128 fit. We combined the results from all of them in histograms: For each observable we prepared one histogram of the results of all analyses. We weighted each entry proportional to its Akaike weight from eqn. (5.13) as described in [20]. We took the central values and the spreads of the histograms as estimators for the central values and the systematic uncertainties. We used a bootstrap method with 2000 samples to estimate the statistical uncertainties. An additional source of systematic uncertainty, which we could not be estimate by using the histogram method, is due to the quenching of QED: The lattice action we used is not in the same universality class as the physical theory because the effects of the electromagnetic interaction on the see quarks is not included. Large N_c counting and the approximate $SU(3)$ flavor symmetry suggest that the quenching error on any electromagnetic mass splittings considered here is of the order of 10% or below. [169] We propagated this 10% error to all final quantities. Consequently, each result has three components of uncertainty: The first component is the statistical uncertainty. The second component is the systematic uncertainty excluding the effects due to partial quenching, and the last component is the uncertainty due to partial quenching. For ϵ, which quantifies the violations of Dashen's theorem, an additional

Table 7.1 *– The systematic lattice uncertainties and their respective estimation strategy. The column with heading N gives the number of variations introduced by this systematic. In the last line the total number of variations of the analysis is indicated.*

Systematic error	Estimation strategy	N
Excited state contribution to the extracted masses	The fit range used for the mass extraction is varied; the fit is carried out on one aggressive and on one conservative range that differ by a time interval of on lattice unit.	2
Scale setting uncertainties	The scale is either set with the Ω^- or the isospin average Ξ baryon.	2
Effects by having data only in a limited pion mass range	All datapoints above 400 MeV or 450 MeV for the scale and above 350 MeV or 400 MeV for the fit to the kaon splitting are removed.	4
Uncertainty of the continuum extrapolation	The continuum extrapolations are performed by an a^2 or an αa term.	2
Higher order corrections to C_K and D_K	The Taylor expansions of these quantities are either used directly or are replace by Padé expansions individually.	4
	Total number of variations:	128

systematic uncertainty must be considered. We assumed that $\Delta_{\mathrm{QED}} M_\pi^2 = \Delta M_\pi^2$. This is true up to $\mathcal{O}(\delta m^2)$ correction. The authors of [19] estimate the size of these correction. According to their estimate $\epsilon_m = \Delta_{\mathrm{QED}} M_\pi^2 / \Delta M_\pi^2 = 0.04(2)$. We included this estimate in our calculation of ϵ and give the uncertainty introduced by it as the fourth uncertainty of ϵ.

7.4 Results and discussion

In table 7.2 our results are compiled. The first set of results are directly related to the quark masses. We calculated the difference δm between the light quark masses in the $\overline{MS}$ scheme at $\mu = 2$ GeV. We used the result for the average light quark mass from [161] to relate that difference to the individual quark masses m_u and m_d. Also, we calculated the ratio m_d/m_u. In particular, this result excludes the $m_u = 0$ solution of the strong CP problem by more then 24 standard deviations. The breaking of the $SU(3)$ flavor symmetry is frequently quantified in the literature by the flavor breaking ratios

$$R = \frac{m_s - m_{ud}}{m_d - m_u} \quad \text{and} \quad Q = \sqrt{\frac{m_s^2 - m_{ud}^2}{m_s^2 - m_{ud}^2}}. \tag{7.11}$$

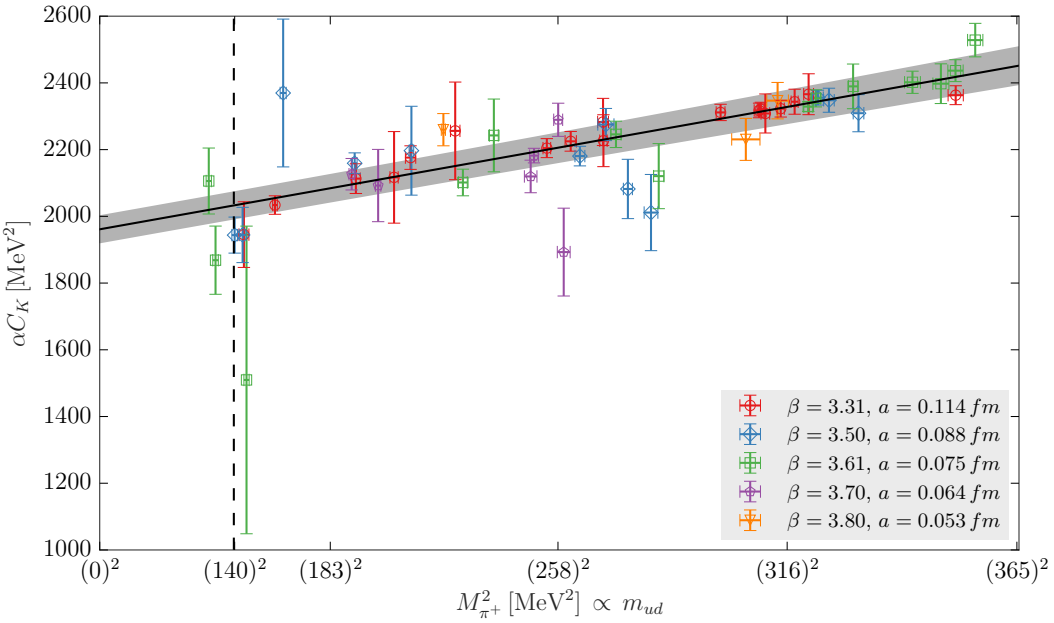

(a) Pion mass dependence of C_K.

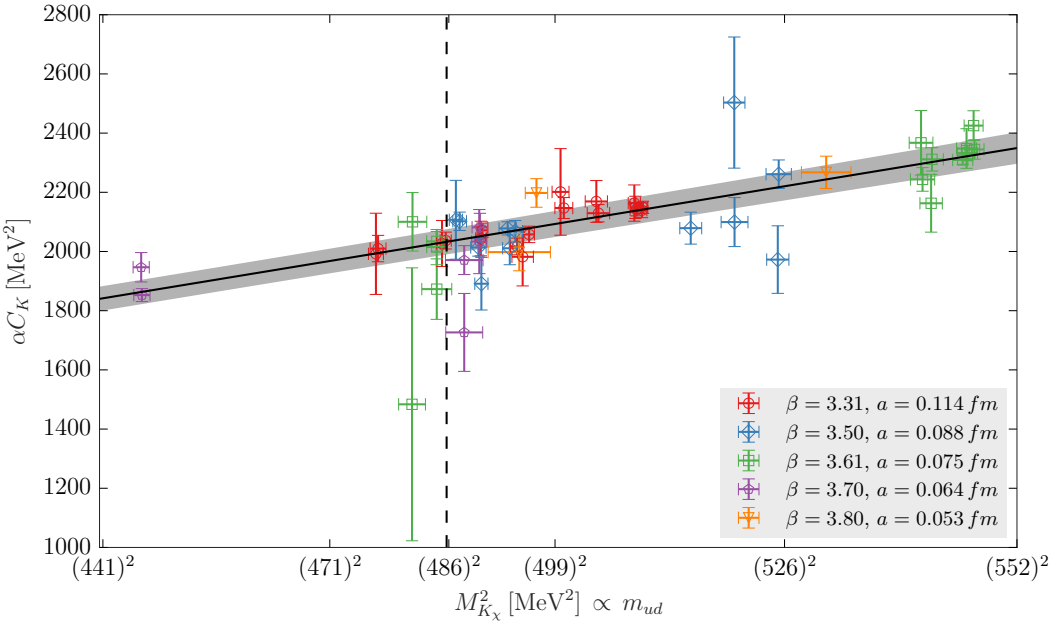

(b) Kaon mass dependence of C_K.

Figure 7.4 *– Pion and Kaon mass dependence of the electromagnetic contribution C_K and the QCD contribution D_K to the Kaon mass splitting. Differnt colors denote different gauge couplings. All datapoints are projected to the physical point usind the respcetive fit function in all directions accept the one shown on the x-axis. The solid line and the grey band indicate the fit function and its error. The dashed lines shows the physical point.*

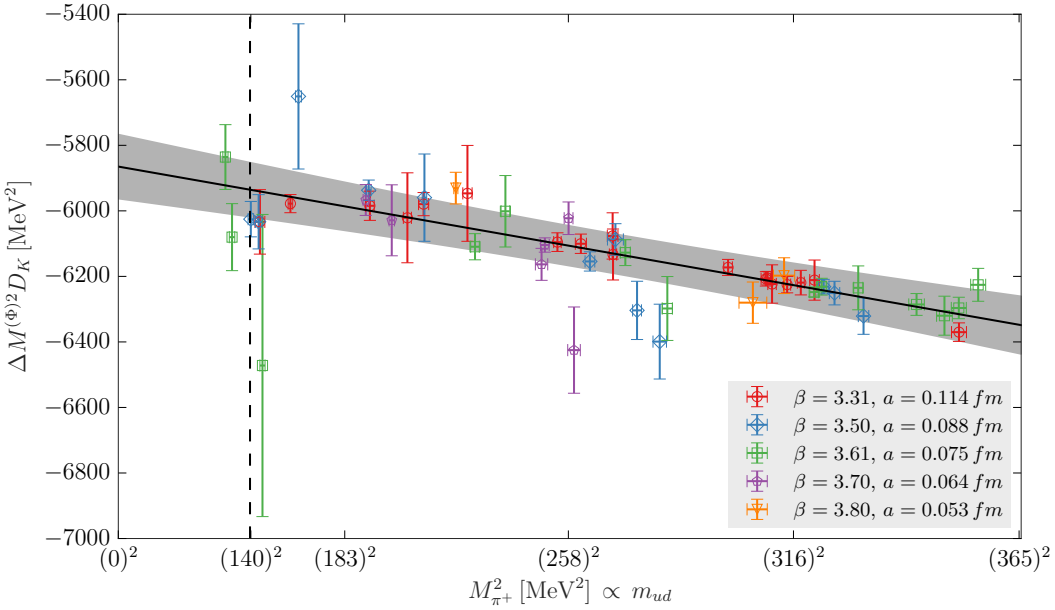

(c) Pion mass dependence of D_K.

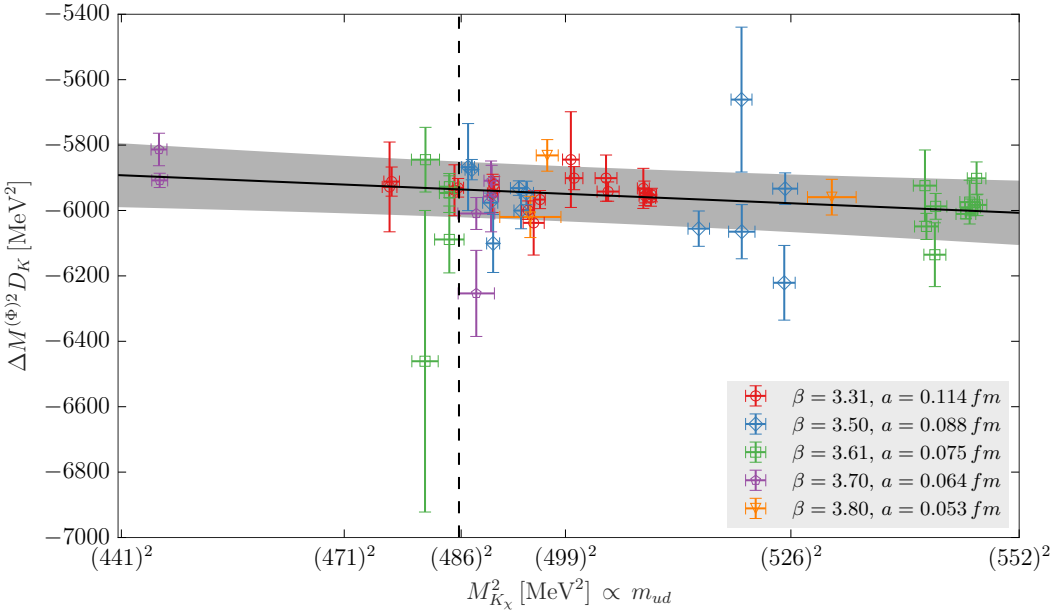

(d) Kaon mass dependence of D_K.

Figure 7.4 *– Pion and Kaon mass dependence of the electromagnetic contribution C_K and the QCD contribution D_K to the Kaon mass splitting. Differnt colors denote different gauge couplings. All datapoints are projected to the physical point usind the respcetive fit function in all directions accept the one shown on the x-axis. The solid line and the grey band indicate the fit function and its error. The dashed lines shows the physical point.*

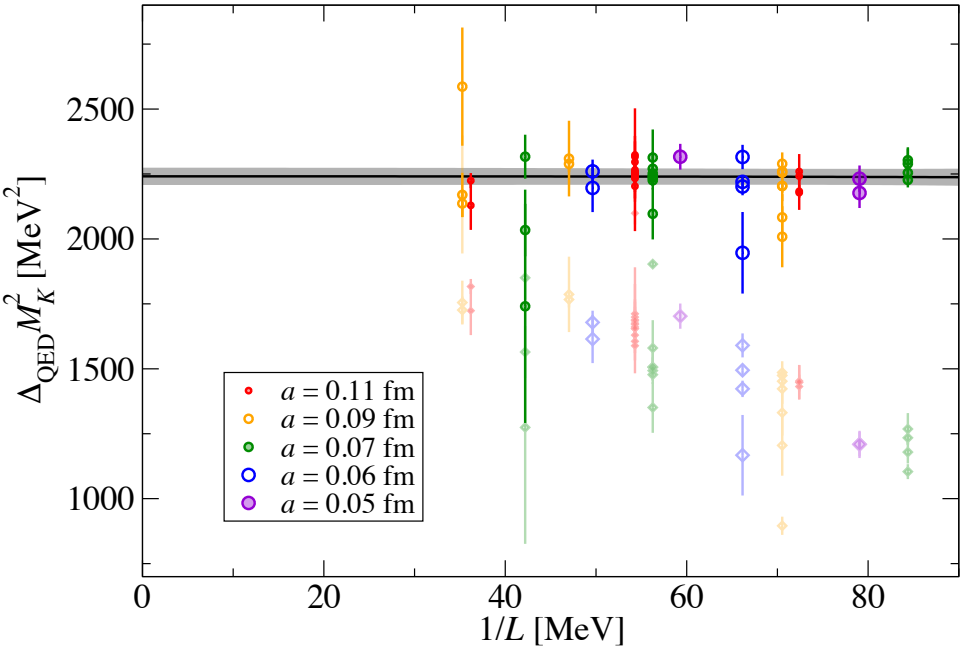

Figure 7.5 *– The Kaon splitting with or without the subtraction of the universal part from eqn. (7.9). The solid points are the datapoints with the correction applied. The faded points show the uncorrected data. The black line and the gray band indicate the $1/L^3$ fit and its statistical error. All datapoints are projected to the physical point except in the finite volume direction. The projection was carried out using a fit of eqns. (7.6), (7.7) and (7.10). [106, 158] to the data. [106]*

Table 7.2 *– Results on the light quark mass difference and on the violations of Dahsen's theorem.*

Observable	Result
Light quark mass difference δm	−2.41(6)(4)(9) MeV
Ratio of light quark masses m_u/m_d	0.485(11)(8)(14)
Mass m_u of the up quark	2.27(6)(5)(4) MeV
Mass m_d of the down quark	4.67(6)(5)(4) MeV
Flavour braking ratio R	38.2(1.1)(0.8)(1.4)
Flavour braking ratio Q	23.4(0.4)(0.3)(0.4)
Violation ϵ of Dahens's theorem[a]	0.77(2)(5)(17)(2)

[a] Fourth error is due to the assumption $\Delta_{\mathrm{QED}} M_\pi^2 = \Delta M_\pi^2$

We also determined these ratios. Finally, we calculated the magnitude of the violation of Dashen's theorem parametrized by ϵ.

Our results are compatible with previous calculations, specifically with those in the FLAG report [19], but offer improved accuracy. The uncertainties on the isospin breaking quantities are dominated by the quenching uncertainty. We therefore conclude that, despite the improvement in the uncertainties offered by this calculation, a study in full QCD + QED would still be desirable.

Chapter 8

Summary and conclusion

The goals of the thesis where to calculate the quark mass dependencies of several observables.

In a first part we determined the nucleon sigma terms and quark contents. We calculated the up, down, strange, and charm quark contents from first principles using lattice QCD. We used a perturbative heavy quark expansion to calculate the bottom and top quark contents. These expansion are expected to be valid for these two quark flavors. We checked their validity also in the case of the charm quark where the errors of the truncated perturbative expansion are expected to be larger then for the top and bottom quarks. We find that our lattice determination is in very good agreement with the perturbative calculation. A key part to our lattice calculation is that we employed several fermion actions in our analysis and leveraged the different advantages they offer for different parts of the calculation.

For the calculation of the sigma terms we employed the Feynman-Hellmann method. Our results are consistent with other lattice determinations. Despite this, we find that recent phenomenological calculation (s. [115]) based on pion-nucleon scattering predict a slightly larger light sigma terms then most lattice calculations, including our own ab-inito calculation. It would be interesting to study the source of this discrepancy.

Our results allow us to calculate the nucleon-Higgs coupling with an error of about 30 %. We believe that our results are of high relevance to direct dark matter detection experiments. It is remarkable that, in the $N_f = 6$ theory, a large fraction of the Higgs nucleon coupling originates from the heavy quark flavors; while they contribute only through quantum fluctuations that are suppressed by their mass, their Higgs coupling is also large, because they are heavy. Both effects almost cancel.

In a second part, we calculated the dependence of the kaon mass splitting on the light quark mass splitting and the electromagnetic charges of the light quarks. We where able to quantify the amount of violation of Dashen's theorem. We used our result to infer the ratio of the light quark masses. The calculation was carried out in a partially quenched setup. While we estimated the error made by using this approximation, it would be interesting to carry out this calculation in a fully dynamic QED+QCD setting.

References

[1] M. E. Peskin and D. V. Schroeder, *Quantum Field Theory*. Westview Press, 1995.

[2] R. J. Hill and M. P. Solon, *Standard Model anatomy of WIMP dark matter direct detection II: QCD analysis and hadronic matrix elements*, *Phys. Rev.* **D91** (2015) 043505, [1409.8290].

[3] "In preparation.".

[4] C.-N. Yang and R. L. Mills, *Conservation of Isotopic Spin and Isotopic Gauge Invariance*, *Phys. Rev.* **96** (1954) 191–195.

[5] D. J. Gross and F. Wilczek, *Ultraviolet Behavior of Nonabelian Gauge Theories*, *Phys. Rev. Lett.* **30** (1973) 1343–1346.

[6] D. J. Gross and F. Wilczek, *Asymptotically Free Gauge Theories - I*, *Phys. Rev.* **D8** (1973) 3633–3652.

[7] D. J. Gross and F. Wilczek, *Asymptotically free gauge theories. II.*, *Phys. Rev.* **D9** (1974) 980–993.

[8] F. Wilczek, *Asymptotic freedom: From paradox to paradigm*, *Proc. Nat. Acad. Sci.* **102** (2005) 8403–8413, [hep-ph/0502113].

[9] Particle Data Group collaboration, M. Tanabashi et al., *Review of Particle Physics*, *Phys. Rev.* **D98** (2018) 030001.

[10] P. W. Higgs, *Broken Symmetries and the Masses of Gauge Bosons*, *Phys. Rev. Lett.* **13** (1964) 508–509.

[11] K. G. Wilson, *Confinement of Quarks*, *Phys. Rev.* **D10** (1974) 2445–2459.

[12] P. Güttinger, *Das Verhalten von Atomen im magnetischen Drehfeld*, *Zeitschrift für Physik* **73** (Mar, 1932) 169–184.

[13] W. Pauli, *Handbuch der Physik*, vol. 24, ch. Principles of Wave Mechanics, p. 162. Springer, 1933.

[14] H. Hellmann, *Einführung in die Quantenchemie*. Franz Deuticke, Leipzig, 1937.

[15] R. P. Feynman, *Forces in Molecules*, *Phys. Rev.* **56** (1939) 340–343.

[16] J. Ellis, N. Nagata and K. A. Olive, *Uncertainties in WIMP Dark Matter Scattering Revisited*, *Eur. Phys. J.* **C78** (2018) 569, [1805.09795].

[17] S. Durr et al., *Ab-Initio Determination of Light Hadron Masses*, *Science* **322** (2008) 1224–1227, [0906.3599].

[18] P. D. B. Collins, A. D. Martin and E. J. Squires, *Particle physics and cosmology*. 1989.

[19] S. Aoki et al., *Review of lattice results concerning low-energy particle physics*, *Eur. Phys. J.* **C74** (2014) 2890, [1310.8555].

[20] S. Borsanyi et al., *Ab initio calculation of the neutron-proton mass difference*, *Science* **347** (2015) 1452–1455, [1406.4088].

[21] S. L. Glashow, *Partial Symmetries of Weak Interactions*, *Nucl. Phys.* **22** (1961) 579–588.

[22] S. Weinberg, *A Model of Leptons*, *Phys. Rev. Lett.* **19** (1967) 1264–1266.

[23] A. Salam, *Elementary Particle Theory*. Almquist and Wiksells, 1969.

[24] S. L. Glashow, J. Iliopoulos and L. Maiani, *Weak Interactions with Lepton-Hadron Symmetry*, *Phys. Rev.* **D2** (1970) 1285–1292.

[25] M. Kobayashi and T. Maskawa, *CP Violation in the Renormalizable Theory of Weak Interaction*, *Prog. Theor. Phys.* **49** (1973) 652–657.

[26] S. M. Carroll, *Lecture notes on general relativity*, gr-qc/9712019.

[27] C. Smeenk, *The elusive higgs mechanism*, *Philosophy of Science* **73** (2006) 487–499.

[28] ATLAS collaboration, G. Aad et al., *Observation of a new particle in the search for the Standard Model Higgs boson with the ATLAS detector at the LHC*, *Phys. Lett.* **B716** (2012) 1–29, [1207.7214].

[29] CMS collaboration, S. Chatrchyan et al., *Observation of a new boson at a mass of 125 GeV with the CMS experiment at the LHC*, *Phys. Lett.* **B716** (2012) 30–61, [1207.7235].

[30] L. Boyle, "Standard model of particle physics, most complete diagram." Wikipedia.

[31] M. Milgrom, *MOND theory*, *Can. J. Phys.* **93** (2015) 107–118, [1404.7661].

[32] T. Marrodán Undagoitia and L. Rauch, *Dark matter direct-detection experiments*, *J. Phys.* **G43** (2016) 013001, [1509.08767].

[33] C. Hoelbling, *Lattice QCD: concepts, techniques and some results*, *Acta Phys. Polon.* **B45** (2014) 2143, [1410.3403].

[34] C. Gattringer and C. B. Lang, *Quantum Chromodynamics on the Lattice - An Introductory Presentation*, vol. 788 of *Lecture Notes in Physics*. Springer, Berlin, Heidelberg, 2010.

[35] P. A. M. Dirac, *The quantum theory of the electron*, *Proc. Roy. Soc. Lond.* **A117** (1928) 610–624.

[36] Y. Nambu and G. Jona-Lasinio, *Dynamical Model of Elementary Particles Based on an Analogy with Superconductivity. 1.*, *Phys. Rev.* **122** (1961) 345–358.

[37] J. S. Bell and R. Jackiw, *A PCAC puzzle: $\pi^0 \to \gamma\gamma$ in the sigma model*, *Nuovo Cim.* **A60** (1969) 47–61.

[38] S. L. Adler, *Axial vector vertex in spinor electrodynamics*, *Phys. Rev.* **177** (1969) 2426–2438.

[39] K. Fujikawa, *Path Integral Measure for Gauge Invariant Fermion Theories*, *Phys. Rev. Lett.* **42** (1979) 1195–1198.

[40] K. Fujikawa, *Path Integral for Gauge Theories with Fermions*, *Phys. Rev.* **D21** (1980) 2848.

[41] S. Weinberg, *The quantum theory of fields. Vol. 2: Modern applications*. Cambridge University Press, 2013.

[42] L. M. Brown, T. Y. Cao, M. Dresden, R. Mills, S. S. Schweber and D. V. Shirkov, *Renormalization: From Lorentz to Landau (and Beyond)*. Springer Science & Business Media, 2012.

[43] T. van Ritbergen, J. A. M. Vermaseren and S. A. Larin, *The Four loop beta function in quantum chromodynamics*, *Phys. Lett.* **B400** (1997) 379–384, [hep-ph/9701390].

[44] M. Czakon, *The Four-loop QCD beta-function and anomalous dimensions*, *Nucl. Phys.* **B710** (2005) 485–498, [hep-ph/0411261].

[45] P. A. Baikov, K. G. Chetyrkin and J. H. Kühn, *Five-Loop Running of the QCD coupling constant*, *Phys. Rev. Lett.* **118** (2017) 082002, [1606.08659].

[46] T. Luthe, A. Maier, P. Marquard and Y. Schröder, *Towards the five-loop Beta function for a general gauge group*, *JHEP* **07** (2016) 127, [1606.08662].

[47] F. Herzog, B. Ruijl, T. Ueda, J. A. M. Vermaseren and A. Vogt, *The five-loop beta function of Yang-Mills theory with fermions*, *JHEP* **02** (2017) 090, [1701.01404].

[48] J. A. M. Vermaseren, S. A. Larin and T. van Ritbergen, *The four loop quark mass anomalous dimension and the invariant quark mass*, *Phys. Lett.* **B405** (1997) 327–333, [hep-ph/9703284].

[49] K. G. Chetyrkin, *Quark mass anomalous dimension to O (alpha-s**4)*, *Phys. Lett.* **B404** (1997) 161–165, [hep-ph/9703278].

[50] G. Rodrigo and A. Santamaria, *QCD matching conditions at thresholds*, *Phys. Lett.* **B313** (1993) 441–446, [hep-ph/9305305].

[51] T. Appelquist and J. Carazzone, *Infrared Singularities and Massive Fields*, *Phys. Rev.* **D11** (1975) 2856.

[52] F. Wilczek, *Decays of Heavy Vector Mesons Into Higgs Particles*, *Phys. Rev. Lett.* **39** (1977) 1304.

[53] M. A. Shifman, A. I. Vainshtein and V. I. Zakharov, *Remarks on Higgs Boson Interactions with Nucleons*, *Phys. Lett.* **78B** (1978) 443–446.

[54] X.-D. Ji, *A QCD analysis of the mass structure of the nucleon*, *Phys. Rev. Lett.* **74** (1995) 1071–1074, [hep-ph/9410274].

[55] M. Creutz, *Confinement and the Critical Dimensionality of Space-Time*, *Phys. Rev. Lett.* **43** (1979) 553–556.

[56] M. Creutz, *Monte Carlo Study of Quantized SU(2) Gauge Theory*, *Phys. Rev.* **D21** (1980) 2308–2315.

[57] M. Luscher and P. Weisz, *On-Shell Improved Lattice Gauge Theories*, *Commun. Math. Phys.* **97** (1985) 59.

[58] K. G. Wilson, *Quarks and Strings on a Lattice*, in *13th International School of Subnuclear Physics: New Phenomena in Subnuclear Physics Erice, Italy, July 11-August 1, 1975*, pp. 69–142, 1975.

[59] H. B. Nielsen and M. Ninomiya, *Absence of Neutrinos on a Lattice. 1. Proof by Homotopy Theory*, *Nucl. Phys.* **B185** (1981) 20.

[60] H. B. Nielsen and M. Ninomiya, *Absence of Neutrinos on a Lattice. 2. Intuitive Topological Proof*, *Nucl. Phys.* **B193** (1981) 173–194.

[61] H. B. Nielsen and M. Ninomiya, *No Go Theorem for Regularizing Chiral Fermions*, *Phys. Lett.* **B105** (1981) 219–223.

[62] B. Sheikholeslami and R. Wohlert, *Improved Continuum Limit Lattice Action for QCD with Wilson Fermions*, *Nucl. Phys.* **B259** (1985) 572.

[63] R. Wohlert, *Improved continuum limit lattice action for quarks*, .

[64] M. Luscher and P. Weisz, *O(a) improvement of the axial current in lattice QCD to one loop order of perturbation theory*, *Nucl. Phys.* **B479** (1996) 429–458, [hep-lat/9606016].

[65] M. Luscher, S. Sint, R. Sommer, P. Weisz and U. Wolff, *Nonperturbative O(a) improvement of lattice QCD*, *Nucl. Phys.* **B491** (1997) 323–343, [hep-lat/9609035].

[66] S. Durr, Z. Fodor, C. Hoelbling, S. D. Katz, S. Krieg, T. Kurth et al., *Lattice QCD at the physical point: Simulation and analysis details*, *JHEP* **08** (2011) 148, [1011.2711].

[67] J. B. Kogut and L. Susskind, *Hamiltonian Formulation of Wilson's Lattice Gauge Theories*, *Phys. Rev.* **D11** (1975) 395–408.

[68] N. Kawamoto and J. Smit, *Effective Lagrangian and Dynamical Symmetry Breaking in Strongly Coupled Lattice QCD*, *Nucl. Phys.* **B192** (1981) 100.

[69] APE collaboration, M. Albanese et al., *Glueball Masses and String Tension in Lattice QCD*, *Phys. Lett.* **B192** (1987) 163–169.

[70] C. Morningstar and M. J. Peardon, *Analytic smearing of SU(3) link variables in lattice QCD*, *Phys. Rev.* **D69** (2004) 054501, [hep-lat/0311018].

[71] A. Hasenfratz and F. Knechtli, *Flavor symmetry and the static potential with hypercubic blocking*, *Phys. Rev.* **D64** (2001) 034504, [hep-lat/0103029].

[72] S. Capitani, S. Durr and C. Hoelbling, *Rationale for UV-filtered clover fermions*, *JHEP* **11** (2006) 028, [hep-lat/0607006].

[73] L. Lellouch, "Including isospin breaking in lattice qcd calculations: Qed (+ qcd) in a finite volume." `http://benasque.org/2015qcd/talks_contr/063_Lellouch.pdf`.

[74] M. Hayakawa and S. Uno, *QED in finite volume and finite size scaling effect on electromagnetic properties of hadrons*, *Prog. Theor. Phys.* **120** (2008) 413–441, [`0804.2044`].

[75] M. E. J. Newman and G. T. Barkema, *Monte Carlo Methods in Statistical Physics.* Oxford University Press, 1999.

[76] D. J. E. Callaway and A. Rahman, *Lattice Gauge Theory in Microcanonical Ensemble*, *Phys. Rev.* **D28** (1983) 1506.

[77] A. D. Kennedy, I. Horvath and S. Sint, *A New exact method for dynamical fermion computations with nonlocal actions*, *Nucl. Phys. Proc. Suppl.* **73** (1999) 834–836, [`hep-lat/9809092`].

[78] E. Y. Remez, *Sur la détermination des polynômes d'approximation de degré donnée*, *Comm. Soc. Math. Kharkov* **10** (1934) .

[79] M. A. Clark, *The Rational Hybrid Monte Carlo Algorithm*, *PoS* **LAT2006** (2006) 004, [`hep-lat/0610048`].

[80] A. Frommer, B. Nockel, S. Gusken, T. Lippert and K. Schilling, *Many masses on one stroke: Economic computation of quark propagators*, *Int. J. Mod. Phys.* **C6** (1995) 627–638, [`hep-lat/9504020`].

[81] D. H. Adams, *On the fourth root prescription for dynamical staggered fermions*, *Phys. Rev.* **D72** (2005) 114512, [`hep-lat/0411030`].

[82] S. Durr and C. Hoelbling, *Scaling tests with dynamical overlap and rooted staggered fermions*, *Phys. Rev.* **D71** (2005) 054501, [`hep-lat/0411022`].

[83] C. Bernard, *Staggered chiral perturbation theory and the fourth-root trick*, *Phys. Rev.* **D73** (2006) 114503, [`hep-lat/0603011`].

[84] C. Bernard, C. E. DeTar, Z. Fu and S. Prelovsek, *Scalar meson spectroscopy with lattice staggered fermions*, *Phys. Rev.* **D76** (2007) 094504, [`0707.2402`].

[85] S. Prelovsek, *Effects of staggered fermions and mixed actions on the scalar correlator*, *Phys. Rev.* **D73** (2006) 014506, [`hep-lat/0510080`].

[86] S. Durr, C. Hoelbling and U. Wenger, *Staggered eigenvalue mimicry*, *Phys. Rev.* **D70** (2004) 094502, [`hep-lat/0406027`].

[87] S. Durr and C. Hoelbling, *Staggered versus overlap fermions: A Study in the Schwinger model with N(f)=0, 1, 2*, *Phys. Rev.* **D69** (2004) 034503, [`hep-lat/0311002`].

[88] HPQCD, UKQCD, MILC, Fermilab Lattice collaboration, C. T. H. Davies et al., *High precision lattice QCD confronts experiment*, *Phys. Rev. Lett.* **92** (2004) 022001, [`hep-lat/0304004`].

[89] C. T. H. Davies, G. P. Lepage, F. Niedermayer and D. Toussaint, *The Quenched continuum limit*, *Nucl. Phys. Proc. Suppl.* **140** (2005) 261–263, [hep-lat/0409039].

[90] MILC collaboration, C. Aubin, C. Bernard, C. E. DeTar, J. Osborn, S. Gottlieb, E. B. Gregory et al., *Light pseudoscalar decay constants, quark masses, and low energy constants from three-flavor lattice QCD*, *Phys. Rev.* **D70** (2004) 114501, [hep-lat/0407028].

[91] HPQCD, UKQCD collaboration, E. Follana, C. T. H. Davies, G. P. Lepage and J. Shigemitsu, *High Precision determination of the pi, K, D and D(s) decay constants from lattice QCD*, *Phys. Rev. Lett.* **100** (2008) 062002, [0706.1726].

[92] MILC collaboration, A. Bazavov et al., *Scaling studies of QCD with the dynamical HISQ action*, *Phys. Rev.* **D82** (2010) 074501, [1004.0342].

[93] MILC collaboration, A. Bazavov et al., *Nonperturbative QCD Simulations with 2+1 Flavors of Improved Staggered Quarks*, *Rev. Mod. Phys.* **82** (2010) 1349–1417, [0903.3598].

[94] J. Giedt, *Power-counting theorem for staggered fermions*, *Nucl. Phys.* **B782** (2007) 134–158, [hep-lat/0606003].

[95] C. Bernard, M. Golterman and Y. Shamir, *Effective field theories for QCD with rooted staggered fermions*, *Phys. Rev.* **D77** (2008) 074505, [0712.2560].

[96] Y. Shamir, *Renormalization-group analysis of the validity of staggered-fermion QCD with the fourth-root recipe*, *Phys. Rev.* **D75** (2007) 054503, [hep-lat/0607007].

[97] C. Bernard, *Order of the chiral and continuum limits in staggered chiral perturbation theory*, *Phys. Rev.* **D71** (2005) 094020, [hep-lat/0412030].

[98] S. Durr and C. Hoelbling, *Lattice fermions with complex mass*, *Phys. Rev.* **D74** (2006) 014513, [hep-lat/0604005].

[99] M. Creutz, *Chiral anomalies and rooted staggered fermions*, *Phys. Lett.* **B649** (2007) 230–234, [hep-lat/0701018].

[100] M. Creutz, *Reply to: 'Comment on: 'Chiral anomalies and rooted staggered fermions'*, *Phys. Lett.* **B649** (2007) 241–242, [0704.2016].

[101] M. Creutz, *SU(3) breaking and the pseudo-scalar spectrum in multi-taste QCD*, *EPJ Web Conf.* **175** (2018) 04001, [1707.08597].

[102] ALPHA collaboration, U. Wolff, *Monte Carlo errors with less errors*, *Comput. Phys. Commun.* **156** (2004) 143–153, [hep-lat/0306017].

[103] B. Efron, *Bootstrap methods: Another look at the jackknife*, *Ann. Statist.* **7** (1979) 1–26.

[104] C. Bouchard, C. C. Chang, T. Kurth, K. Orginos and A. Walker-Loud, *On the Feynman-Hellmann Theorem in Quantum Field Theory and the Calculation of Matrix Elements*, *Phys. Rev.* **D96** (2017) 014504, [1612.06963].

[105] W. H. Press, S. A. Teukolsky, W. T. Vetterling and B. P. Flannery, *Numerical Recepies in C: the art of scientific computing*. Press Syndicate of the University of Camebride, 2nd ed., 1992.

[106] Z. Fodor, C. Hoelbling, S. Krieg, L. Lellouch, T. Lippert, A. Portelli et al., *Up and down quark masses and corrections to Dashen's theorem from lattice QCD and quenched QED*, *Phys. Rev. Lett.* **117** (2016) 082001, [1604.07112].

[107] ATLAS collaboration, T. A. collaboration, *Combined measurements of Higgs boson production and decay using up to 80 fb^{-1} of proton–proton collision data at $\sqrt{s}$ = 13 TeV collected with the ATLAS experiment*, .

[108] H. Fritzsch, M. Gell-Mann and H. Leutwyler, *Advantages of the Color Octet Gluon Picture*, *Phys. Lett.* **B47** (1973) 365–368.

[109] X.-D. Ji, *Breakup of hadron masses and energy - momentum tensor of QCD*, *Phys. Rev.* **D52** (1995) 271–281, [hep-ph/9502213].

[110] Y.-B. Yang, J. Liang, Y.-J. Bi, Y. Chen, T. Draper, K.-F. Liu et al., *Proton Mass Decomposition from the QCD Energy Momentum Tensor*, *Phys. Rev. Lett.* **121** (2018) 212001, [1808.08677].

[111] C. Lorcé, *The origin of the nucleon mass*, in *22nd International Conference on Few-Body Problems in Physics (FB22) Caen, France, July 9-13, 2018*, 2018. 1811.02803.

[112] R. Koch, *A New Determination of the pi N Sigma Term Using Hyperbolic Dispersion Relations in the (nu**2, t) Plane*, *Z. Phys.* **C15** (1982) 161–168.

[113] J. Gasser, H. Leutwyler and M. E. Sainio, *Sigma term update*, *Phys. Lett.* **B253** (1991) 252–259.

[114] M. M. Pavan, I. I. Strakovsky, R. L. Workman and R. A. Arndt, *The Pion nucleon Sigma term is definitely large: Results from a G.W.U. analysis of pi nucleon scattering data*, *PiN Newslett.* **16** (2002) 110–115, [hep-ph/0111066].

[115] M. Hoferichter, J. Ruiz de Elvira, B. Kubis and U.-G. Meißner, *High-Precision Determination of the Pion-Nucleon σ Term from Roy-Steiner Equations*, *Phys. Rev. Lett.* **115** (2015) 092301, [1506.04142].

[116] M. Hoferichter, J. Ruiz de Elvira, B. Kubis and U.-G. Meißner, *Roy–Steiner-equation analysis of pion–nucleon scattering*, *Phys. Rept.* **625** (2016) 1–88, [1510.06039].

[117] J. M. Alarcon, J. Martin Camalich and J. A. Oller, *The chiral representation of the πN scattering amplitude and the pion-nucleon sigma term*, *Phys. Rev.* **D85** (2012) 051503, [1110.3797].

[118] J. Ruiz de Elvira, M. Hoferichter, B. Kubis and U.-G. Meißner, *Extracting the σ-term from low-energy pion-nucleon scattering*, *J. Phys.* **G45** (2018) 024001, [1706.01465].

[119] J. Gasser, *Hadron Masses and Sigma Commutator in the Light of Chiral Perturbation Theory*, *Annals Phys.* **136** (1981) 62.

[120] B. Borasoy and U.-G. Meissner, *Chiral Expansion of Baryon Masses and σ-Terms*, *Annals Phys.* **254** (1997) 192–232, [hep-ph/9607432].

[121] B. Borasoy, *Sigma terms in heavy baryon chiral perturbation theory revisited*, *Eur. Phys. J.* **C8** (1999) 121–130, [hep-ph/9807453].

[122] P. E. Shanahan, A. W. Thomas and R. D. Young, *Sigma terms from an SU(3) chiral extrapolation*, *Phys. Rev.* **D87** (2013) 074503, [1205.5365].

[123] L. Alvarez-Ruso, T. Ledwig, J. Martin Camalich and M. J. Vicente-Vacas, *Nucleon mass and pion-nucleon sigma term from a chiral analysis of lattice QCD data*, *Phys. Rev.* **D88** (2013) 054507, [1304.0483].

[124] C. S. An and B. Saghai, *Pion- and strangeness-baryon σ terms in the extended chiral constituent quark model*, *Phys. Rev.* **D92** (2015) 014002, [1404.2389].

[125] J. M. Alarcon, L. S. Geng, J. Martin Camalich and J. A. Oller, *The strangeness content of the nucleon from effective field theory and phenomenology*, *Phys. Lett.* **B730** (2014) 342–346, [1209.2870].

[126] X.-L. Ren, L.-S. Geng and J. Meng, *Scalar strangeness content of the nucleon and baryon sigma terms*, *Phys. Rev.* **D91** (2015) 051502, [1404.4799].

[127] M. F. M. Lutz, R. Bavontaweepanya, C. Kobdaj and K. Schwarz, *Finite volume effects in the chiral extrapolation of baryon masses*, *Phys. Rev.* **D90** (2014) 054505, [1401.7805].

[128] ETM collaboration, C. Alexandrou, R. Baron, J. Carbonell, V. Drach, P. Guichon, K. Jansen et al., *Low-lying baryon spectrum with two dynamical twisted mass fermions*, *Phys. Rev.* **D80** (2009) 114503, [0910.2419].

[129] MILC collaboration, D. Toussaint and W. Freeman, *The Strange quark condensate in the nucleon in 2+1 flavor QCD*, *Phys. Rev. Lett.* **103** (2009) 122002, [0905.2432].

[130] R. Babich, R. C. Brower, M. A. Clark, G. T. Fleming, J. C. Osborn, C. Rebbi et al., *Exploring strange nucleon form factors on the lattice*, *Phys. Rev.* **D85** (2012) 054510, [1012.0562].

[131] JLQCD collaboration, K. Takeda, S. Aoki, S. Hashimoto, T. Kaneko, J. Noaki and T. Onogi, *Nucleon strange quark content from two-flavor lattice QCD with exact chiral symmetry*, *Phys. Rev.* **D83** (2011) 114506, [1011.1964].

[132] QCDSF collaboration, G. S. Bali et al., *The strange and light quark contributions to the nucleon mass from Lattice QCD*, *Phys. Rev.* **D85** (2012) 054502, [1111.1600].

[133] QCDSF-UKQCD collaboration, R. Horsley, Y. Nakamura, H. Perlt, D. Pleiter, P. E. L. Rakow, G. Schierholz et al., *Hyperon sigma terms for 2+1 quark flavours*, *Phys. Rev.* **D85** (2012) 034506, [1110.4971].

[134] S. Durr et al., *Sigma term and strangeness content of octet baryons*, *Phys. Rev.* **D85** (2012) 014509, [1109.4265].

[135] MILC collaboration, W. Freeman and D. Toussaint, *Intrinsic strangeness and charm of the nucleon using improved staggered fermions*, *Phys. Rev.* **D88** (2013) 054503, [1204.3866].

[136] C. Alexandrou, M. Constantinou, S. Dinter, V. Drach, K. Hadjiyiannakou, K. Jansen et al., *Sigma terms and strangeness content of the nucleon with $Nf = 2 + 1 + 1$ twisted mass fermions*, *PoS* **LATTICE2012** (2012) 163, [1211.4447].

[137] JLQCD collaboration, H. Ohki, K. Takeda, S. Aoki, S. Hashimoto, T. Kaneko, H. Matsufuru et al., *Nucleon strange quark content from $N_f = 2 + 1$ lattice QCD with exact chiral symmetry*, *Phys. Rev.* **D87** (2013) 034509, [1208.4185].

[138] P. Junnarkar and A. Walker-Loud, *Scalar strange content of the nucleon from lattice QCD*, *Phys. Rev.* **D87** (2013) 114510, [1301.1114].

[139] XQCD collaboration, M. Gong et al., *Strangeness and charmness content of the nucleon from overlap fermions on 2+1-flavor domain-wall fermion configurations*, *Phys. Rev.* **D88** (2013) 014503, [1304.1194].

[140] xQCD collaboration, Y.-B. Yang, A. Alexandru, T. Draper, J. Liang and K.-F. Liu, *πN and strangeness sigma terms at the physical point with chiral fermions*, *Phys. Rev.* **D94** (2016) 054503, [1511.09089].

[141] ETM collaboration, A. Abdel-Rehim, C. Alexandrou, M. Constantinou, K. Hadjiyiannakou, K. Jansen, C. Kallidonis et al., *Direct Evaluation of the Quark Content of Nucleons from Lattice QCD at the Physical Point*, *Phys. Rev. Lett.* **116** (2016) 252001, [1601.01624].

[142] RQCD collaboration, G. S. Bali, S. Collins, D. Richtmann, A. Schäfer, W. Söldner and A. Sternbeck, *Direct determinations of the nucleon and pion σ terms at nearly physical quark masses*, *Phys. Rev.* **D93** (2016) 094504, [1603.00827].

[143] C. Alexandrou, S. Bacchio, M. Constantinou, J. Finkenrath, K. Hadjiyiannakou, K. Jansen et al., *The nucleon axial, tensor and scalar charges and σ-terms in lattice QCD*, 1909.00485.

[144] JLQCD collaboration, H. Ohki, H. Fukaya, S. Hashimoto, H. Matsufuru, J. Noaki, T. Onogi et al., *Calculation of the nucleon sigma term and strange quark content with two flavors of dynamical overlap fermions*, *PoS* **LATTICE2008** (2008) 126, [0810.4223].

[145] "Hadronic contributions to new phyiscs (HC2NP) workshop." discussion session, September, 2016.

[146] S. Durr et al., *Lattice computation of the nucleon scalar quark contents at the physical point*, *Phys. Rev. Lett.* **116** (2016) 172001, [1510.08013].

[147] T. Bhattacharya, R. Gupta, W. Lee, S. R. Sharpe and J. M. S. Wu, *Improved bilinears in lattice QCD with non-degenerate quarks*, *Phys. Rev.* **D73** (2006) 034504, [hep-lat/0511014].

[148] G. Colangelo, A. Fuhrer and S. Lanz, *Finite volume effects for nucleon and heavy meson masses*, *Phys. Rev.* **D82** (2010) 034506, [1005.1485].

[149] H. Akaike, *A new look at the statistical model identification*, *IEEE Transactions on Automatic Control* **AC-19** (December, 1974) 716–723.

[150] S. Borsanyi, Z. Fodor, C. Hoelbling, S. D. Katz, S. Krieg and K. K. Szabo, *Full result for the QCD equation of state with 2+1 flavors*, *Phys. Lett.* **B730** (2014) 99–104, [1309.5258].

[151] R. Bellwied, S. Borsanyi, Z. Fodor, S. D. Katz, A. Pasztor, C. Ratti et al., *Fluctuations and correlations in high temperature QCD*, *Phys. Rev.* **D92** (2015) 114505, [1507.04627].

[152] M. F. L. Golterman and J. Smit, *Lattice Baryons With Staggered Fermions*, *Nucl. Phys.* **B255** (1985) 328–340.

[153] Y. Hua and T. Sarkar, *Generalized pencil-of-function method for extracting poles of an em system from its transient respones*, *IEEE transactions on antennas and propagation* **37** (1989) 229–234.

[154] T. K. Sarkar and O. Pereira, *Using the matrix pencil method to estimate the parameters of a sum of complex exponentials*, *IEEE Antennas and Propagation Magazine* **37** (1995) .

[155] C. Aubin and K. Orginos, *A new approach for Delta form factors*, *AIP Conf. Proc.* **1374** (2011) 621–624, [1010.0202].

[156] C. DeTar and S.-H. Lee, *Variational method with staggered fermions*, *Phys. Rev.* **D91** (2015) 034504, [1411.4676].

[157] T. J. Hobbs, M. Alberg and G. A. Miller, *Bayesian analysis of light-front models and the nucleon's charmed sigma term*, *Phys. Rev.* **D96** (2017) 074023, [1707.06711].

[158] L. Varnhorst, S. Durr, Z. Fodor, C. Hoelbling, S. Krieg, L. Lellouch et al., *Up and down quark masses and corrections to Dashen's theorem from lattice QCD and quenched QED*, *PoS* **LATTICE2016** (2017) 200, [1702.00309].

[159] A. Duncan, E. Eichten and H. Thacker, *Electromagnetic splittings and light quark masses in lattice QCD*, *Phys. Rev. Lett.* **76** (1996) 3894–3897, [hep-lat/9602005].

[160] MILC collaboration, A. Bazavov et al., *MILC results for light pseudoscalars*, *PoS* **CD09** (2009) 007, [0910.2966].

[161] S. Durr, Z. Fodor, C. Hoelbling, S. D. Katz, S. Krieg, T. Kurth et al., *Lattice QCD at the physical point: light quark masses*, *Phys. Lett.* **B701** (2011) 265–268, [1011.2403].

[162] T. Blum, T. Doi, M. Hayakawa, T. Izubuchi and N. Yamada, *Determination of light quark masses from the electromagnetic splitting of pseudoscalar meson masses computed with two flavors of domain wall fermions*, *Phys. Rev.* **D76** (2007) 114508, [0708.0484].

[163] MILC collaboration, S. Basak et al., *Electromagnetic splittings of hadrons from improved staggered quarks in full QCD*, *PoS* **LATTICE2008** (2008) 127, [0812.4486].

[164] T. Blum, R. Zhou, T. Doi, M. Hayakawa, T. Izubuchi, S. Uno et al., *Electromagnetic mass splittings of the low lying hadrons and quark masses from 2+1 flavor lattice QCD+QED*, *Phys. Rev.* **D82** (2010) 094508, [1006.1311].

[165] RM123 collaboration, G. M. de Divitiis, R. Frezzotti, V. Lubicz, G. Martinelli, R. Petronzio, G. C. Rossi et al., *Leading isospin breaking effects on the lattice*, *Phys. Rev.* **D87** (2013) 114505, [1303.4896].

[166] R. Horsley et al., *QED effects in the pseudoscalar meson sector*, *JHEP* **04** (2016) 093, [1509.00799].

[167] MILC collaboration, S. Basak et al., *Electromagnetic effects on the light pseudoscalar mesons and determination of m_u/m_d*, *PoS* **LATTICE2015** (2016) 259, [1606.01228].

[168] J. Bijnens and N. Danielsson, *Electromagnetic Corrections in Partially Quenched Chiral Perturbation Theory*, *Phys. Rev.* **D75** (2007) 014505, [hep-lat/0610127].

[169] BUDAPEST-MARSEILLE-WUPPERTAL collaboration, S. Borsanyi et al., *Isospin splittings in the light baryon octet from lattice QCD and QED*, *Phys. Rev. Lett.* **111** (2013) 252001, [1306.2287].

[170] BUDAPEST-MARSEILLE-WUPPERTAL collaboration, S. Dürr et al., *Lattice QCD at the physical point meets SU(2) chiral perturbation theory*, *Phys. Rev.* **D90** (2014) 114504, [1310.3626].

[171] R. F. Dashen, *Chiral SU(3) x SU(3) as a symmetry of the strong interactions*, *Phys. Rev.* **183** (1969) 1245–1260.

[172] BUDAPEST-MARSEILLE-WUPPERTAL collaboration, A. Portelli et al., *Electromagnetic corrections to light hadron masses*, *PoS* **LATTICE2010** (2010) 121, [1011.4189].

[173] Z. Davoudi and M. J. Savage, *Finite-Volume Electromagnetic Corrections to the Masses of Mesons, Baryons and Nuclei*, *Phys. Rev.* **D90** (2014) 054503, [1402.6741].

Erklärung

Hiermit erkläre ich, Lukas Varnhorst, dass ich das Thema

Aspects of quark mass dependence in lattice QCD

selbstständig und ohne fremde Hilfe bearbeitet, nur die angegebenen Quellen und Hilfsmittel benutzt und alle wörtlichen oder inhaltlichen übernommenen Literaturstellen als solche gekennzeichnet habe.

Wuppertal,

Lukas Varnhorst

Translation:

Hereby, I, Lukas Varnhorst, declare that I have worked on the topic

Aspects of quark mass dependence in lattice QCD

with no help from others, that I have used only the indicated refereces and and all citations, direct or indirect, are indicated.

The translation of the declaration has only been included for the convenience of the reader.